Qualitative and quantitative investigation of the cytogenetic effects of densely ionizing radiation in vitro and in vivo

Vom Fachbereich Physik
der Technischen Universität Darmstadt

zur Erlangung des Grades
eines Doktors der Naturwissenschaften
(Dr. rer. nat.)

genehmigte Dissertation von
Dipl.-Phys. Carola Hartel
aus Frankfurt am Main

Darmstadt 2010
D17

Referent: Prof. Dr. M. Durante
Korreferent: Prof. Dr. Dr. h.c. G. Kraft

Tag der Einreichung: 9.2.2010
Tag der Prüfung: 12.5.2010

Abstract

The purpose of this work was to compare the cytogenetic effects of densely and sparsely ionizing radiations in vitro and in vivo. To achieve this, chromosomal aberrations in peripheral blood lymphocytes were exposed in vitro to different doses of X-rays and C-ions with different energies; furthermore, lymphocytes were obtained from prostate-cancer patients before, during and after radiotherapy and analyzed using the multiplex fluorescence in situ hybridization (mFISH) technique. These cancer patients were either treated with C-ion boost irradiation in the course of a conventional photon intensity-modulated radiotherapy (IMRT) or solely with IMRT. Blood samples were taken from each patient before, during, at the end of and one year after the therapy.

In the in vitro experiments, an increase in the relative biological effectiveness (RBE) for the induction of chromosomal aberrations with increasing linear energy transfer (LET) of the C-ions was observed in the investigated energy range (270 MeV/u C-ions, LET=14 keV/µm; 100 MeV/u C-ions, LET=29 keV/µm; extended Bragg peak of C-ions, LET=60–85 keV/µm). The ratio of complex to simple exchanges, the C-ratio, which is discussed as a biomarker for densely ionizing radiation, was calculated and a LET- and dose-dependent increase was found. Likewise, the complexity of complex chromosome aberrations increased with LET and dose.

For prostate-cancer patients, the frequency of chromosomal aberrations found in the peripheral blood lymphocytes increased during the radiotherapy course; but after the C-ion boost, the frequency was lower than in patients treated with comparable doses of IMRT. No significantly increased C-ratio was found in the patients treated with the C-ion boost compared to the patients treated with IMRT. A higher frequency of aberrations was measured in patients who were exposed to an increased target volume. The aberration frequency decreased significantly in two out of 16 patients in the year after therapy.

The study shows that the reduced integral dose applied to normal tissue during the C-ion boost is reflected in a lower chromosomal aberration frequency compared to IMRT. While the in vitro experiments showed an enhanced C-ratio for densely ionizing radiation, no increased C-ratio was observed in the patients' samples after C-ion boost therapy.

As mFISH allows identification of individual chromosomes involved in aberrations, the distribution of breakpoints among individual chromosomes and the frequencies of pairwise chromosomal exchanges were analyzed in addition.

Zusammenfassung

Ziel dieser Arbeit war es, die zytogenetischen Effekte von dicht und dünn ionisierender Strahlung in vitro und in vivo zu vergleichen. Dazu wurden Chromosomenaberrationen in peripheren Blutlymphozyten in vitro mit verschiedenen Dosen Röntgenstrahlung und C-Ionen verschiedener Energien bestrahlt sowie Lymphozyten von Prostatakarzinompatienten vor, während und nach der Strahlentherapie entnommen und mittels mFISH (multiplex fluorescence in situ hybridization) untersucht. Die Prostatakarzinompatienten wurden mit einer Kombination aus C-Ionen Bestrahlung und anschließender intensitätsmodulierter Strahlentherapie (IMRT) oder ausschließlich mit IMRT behandelt.

In den in vitro Experimenten wurde ein Anstieg der relativen biologischen Wirksamkeit (RBE) für Chromosomenaberrationen mit steigendem linearen Energietransfer (LET) innerhalb des untersuchten Energiebereichs gefunden (270 MeV/u C-Ionen, LET=14 keV/µm; 100 MeV/u C-Ionen, LET=29 keV/µm; ausgedehnter C-Ionen Bragg-Peak, LET=60–85 keV/µm). Das Verhältnis von komplexen zu einfachen Chromosomenaustauschen, genannt C-ratio, welches als Biomarker für dicht ionisierende Strahlung diskutiert wird, wurde ermittelt und ein Dosis- und LET-abhängiger Anstieg wurde beobachtet. Ebenso stieg die Komplexität komplexer Chromosomenaberrationen mit Dosis und LET an.

Die Aberrationsrate, die in den Blutlymphozyten von Prostatakarzinompatienten gefunden wurde erhöhte sich im Verlauf der Strahlentherapie. Nach der C-Ionen-Bestrahlung war die Abberationsrate geringer als in Patienten die mit einer vergleichbaren Dosis IMRT bestrahlt wurden. Die C-ratio war in den mit C-Ionen bestrahlten Patienten im Vergleich zu den IMRT Patienten nicht signifikant erhöht. In Patienten, welche mit einem größeren Zielvolumen bestrahlt wurden, war die Aberrationsrate signifikant höher. Im Jahr nach der Therapie wurde ein signifikanter Rückgang der Aberrationsrate in zwei von 16 Patienten beobachtet.

Die Studie zeigt, dass sich die niedrigere integrale Dosis, die bei der Kohlenstoffionen-Therapie im Normalgewebe appliziert wird, durch eine niedrigere Aberrationsrate, verglichen mit IMRT, auswirkt. Während nach in vitro Bestrahlung ein höherer Anteil komplexer Aberrationen nach Bestrahlung mit dicht ionisierender Strahlung gefunden wurde, konnte ein solcher Effekt in vivo in Patienten, die sich einer Kohlenstoffionen-Therapie unterzogen, nicht gezeigt werden.

Da es mit der mFISH Färbung möglich ist alle Chromosomen, die an Ab-

errationen beteiligt sind, zu identifizieren, wurde die Verteilung der Bruchpunkte in den einzelnen Chromosomen sowie die Häufigkeit von Austauschen zwischen allen Chromosomenpaaren untersucht.

Contents

List of Figures

List of Tables

1. Introduction

1.1. Motivation

The purpose of this work was to gain more insight in the cytogenetic effects of densely ionizing radiation and in the application of aberration analysis in biological dosimetry. For this, the chromosomal aberrations induced by densely and sparsely ionizing radiation in vitro and in vivo were analyzed using the high-resolution multiplex fluorescence in situ hybridization (mFISH) staining technique. Biological dosimetry of exposure to densely ionizing radiation becomes increasingly important because of the increasing use of particle therapy for cancer treatment [Kraft and Kraft, 2009; Schulz-Ertner, 2009; Durante and Loeffler, 2010]. In addition, the exposure to galactic cosmic radiation (which includes densely ionizing particles) is one of the major problems for long-term manned space missions [Durante and Cucinotta, 2008].

With the mFISH technique the aberration spectrum can be analyzed with high resolution. For this study, mFISH was essential mainly for two reasons: the search for a cytogenetic signature ("fingerprint") of the heavy ion irradiation, and the analysis of transmissible aberrations. By analyzing LET-dependent changes in the aberration spectrum, information about possible cytogenetic biomarkers is obtained.

Transmissible aberrations are important regarding the late effects of radiation exposure. In tumor therapy, bone marrow, which contains the stem cells, is often unavoidably exposed to radiation. Cytogenetically aberrant stem cells can pass transmissible aberrations to their daughter cells and thus increase the risk of secondary cancers. Progenies of aberrant bone marrow cells can be found in the peripheral blood lymphocytes, and are the reason why a radiation exposure can be detected decades after the exposure by an enhanced yield of transmissible aberrations in the peripheral blood lymphocytes [Kleinerman et al., 1989]. In the present study, mFISH was applied to the lymphocytes of cancer patients undergoing radiotherapy to study the influence of different radiotherapy regimens and to detect changes in the aberration spectrum in the year after therapy. A change in the aberration spectrum towards transmissible aberrations indicates that bone marrow was exposed. When transmissible aberrations are induced in stem cells, these cells produce aberrant progenies which mature to lymphocytes (and other cell types).In contrast, the originally irradiated cells (carrying transmissible and non-transmissible aberrations) decline with time.

For the in vitro experiments, human peripheral blood lymphocytes were exposed to C-ions with different energies to measure dose-effect curves for the induction of chromosomal aberrations. X-ray experiments were performed for comparison. Dose-effect curves are a useful tool for biological dosimetry in case of an accidental, occupational or medical exposure of an individual to sparsely or densely ionizing radiation. For X-rays, wide knowledge about biological dosimetry exists, but the knowledge about densely ionizing radiation is rather limited. The dose-effect curves that were obtained during this work therefore provide a useful extension.

From the dose-effect curves, information on the relative biological effectiveness (RBE) of the different C-ion energies compared to X-rays were obtained. A precise knowledge of the RBE is most important to predict the biological effects of heavy ion irradiation [Kraft, 1999]. The mFISH staining technique allows identifying different aberration types, therefore the frequencies of different aberration types (excess acentric fragments, simple exchanges, complex exchanges) were investigated. The corresponding RBE values for simple and complex exchanges were calculated. The aberration spectrum was analyzed regarding the presence of a biomarker (fingerprint) for densely ionizing radiation (C-ratio: ratio of complex to simple exchanges). All this information can help to gain a better understanding of the formation of cytogenetic damage after exposure to densely and sparsely ionizing radiation.

At present, C-ion therapy is performed in Heidelberg, Germany, and in Chiba and Hyogo, Japan. The Heidelberg ion therapy center (HIT) followed after a pilot project for C-ion therapy at GSI Helmholtzzentrum für Schwerionenforschung (GSI), Darmstadt, Germany. The pilot project started in 1997, mainly with the treatment of tumors in the head- and neck region. A clinical trial with prostate-cancer patients started in 2006. The pilot project yielded very good results [Schulz-Ertner et al., 2003, 2007a,b], which are based on the physical and biological advantages of C-ion beams. The inverse depth-dose profile of C-ions compared to photons allows a higher dose to the tumor, the enhanced RBE of C-ions in the region of the physical dose maximum potentiates the dose to radioresistant tumors [Kraft, 2000b; Kraemer et al., 2003]. But the question was raised whether this extremely good tumor control is followed by an enhanced risk of secondary tumor production.

For the in vivo investigations peripheral blood lymphocytes from prostate-cancer patients treated with IMRT or C-ion boost plus IMRT were obtained before, during and after therapy. In addition to the monitoring of the aberration yields during therapy course, their persistence up to one year after therapy was investigated. The aberration frequencies and aberration patterns were compared for the different therapy regimens.

The prostate-cancer patients were chosen for this study for several reasons. As a main purpose of this work was to study the radiation effects on the surrounding tissue, which is represented by the blood lymphocytes,

it was essential to choose a tumor whose radiotherapy exposes a sufficiently large volume of normal tissue. External beam radiotherapy of prostate cancer unavoidably exposes a large volume of normal tissue to radiation, as the prostate is located in the inner part of the pelvis. Another important point is the estimation of the risk of secondary cancers, arising from irradiated stem cells. External beam radiotherapy of prostate cancer unavoidably exposes the bone marrow in the femur head and the pelvis to the radiation, and therefore prostate-cancer patients were suited for this study. Other reasons, which played a role as well, were of practical nature. Choosing a tumor-type treated in the GSI pilot project made it easy to obtain samples, which were taken in Heidelberg or Darmstadt, and could be transported to the laboratory in short time. For obtaining a blood sample one year after therapy it was advantageous that most patients lived in the area and attended a follow-up care in the Heidelberg University Hospital.

The impact of radiotherapy with different radiation qualities on the tumor control and on possible side effects can be monitored in clinical studies in parallel to the therapy and during a comparably short follow-up time. But late effects of radiotherapy, including secondary cancers, occur many years after the treatment. The comparison of the aberration frequencies between different radiotherapy regimes can predict the relative risk of late effects. Late effects are increasingly important, as modern radiotherapy achieves increasing tumor control rates and longer patient survival. The results obtained in the present study will be applicable for other tumor types as well. C-ion therapy is increasingly used, it is for example also applied to pediatric tumors [Combs et al., 2009], thus it is most important to achieve better information about the risk for late effects of C-ion irradiation. In prostate-cancer patients, which are mostly over 60 years old at the time of diagnosis, secondary cancers, occuring typically many years after the therapy, are of minor importance compared to other therapy-related problems (e.g. rectal bleeding [Ishikawa et al., 2006]).

The aberration analysis with mFISH provides various information including the involvement frequencies of individual chromosomes in aberrations, thus an analysis of the distribution of breaks in the individual chromosomes was performed, although this was not a main goal of the study.

In the following sections of this chapter the physical, biological and medical backgrounds relevant for this work are described. In Section 1.2 the interaction mechanisms of X-rays and charged particles with matter are described, in Section 1.3 the biological effects of ionizing radiation, with special respect to DNA damage, DNA repair and aberration formation are given. Sections 1.4 and 1.5 provide information about prostate cancer and about external beam radiotherapy, the latter with a focus on the radiation qualities relevant for the work presented here, i.e. photons and C-ions.

1.2. Physics of ionizing radiation

The radiation qualities relevant for the application in radiotherapy can be divided into two classes. Electromagnetic radiation like γ-radiation and X-rays and particle radiation like electrons, protons, α-particles and heavy ions. Both types of radiation were used for the work described in this thesis, namely X-rays and C-ion beams. The interaction mechanisms of both radiation qualities with matter are described in the following sections.

1.2.1. Interaction of X-rays with matter

X-rays interact with matter mainly via three different mechanisms: photoelectric effect, Compton scattering and pair production. The contributions of these three effects to the total energy deposition depend on the photon energy and on the target material. The photoelectric effect is the dominant effect for low photon energies. The photon transfers its energy to an atomic electron, ejecting this electron from the atom. The kinetic energy of the emitted electron is equal to the energy of the incident photon minus the binding energy of the electron. The Compton effect is the main mechanism of energy transfer to the target material for intermediate energies. The incident photon transfers a part of its energy to an atomic electron causing its liberation, while the remainder of the original photon's energy is emitted as a new, lower energy photon with an emission direction different from that of the incident photon. Pair production is the dominant process for high photon energies, it becomes possible with photon energies exceeding 1.02 MeV. By interaction with the electric field of a nucleus, the energy of the incident photon is converted into an electron-positron pair. The energy of the initial photon minus the energy necessary to produce the electron-positron pair appears as the kinetic energy of the electron-positron pair and the recoil nucleus.

Macroscopically the intensity loss of electromagnetic radiation in matter can be described by the absorption law

$$I_X = I_0 \cdot e^{-\mu x} \tag{1.1}$$

with the initial intensity I_0, the intensity I_x at the penetration depth x and the absorption coefficient μ, which is a sum of the coefficients of the effects described before.

For low energetic X-rays, the dose deposition in matter follows an exponential decrease, as can be seen for 120 keV X-rays in Figure 1.1. For high energetic photons the electrons are scattered mainly in forward direction, leading to a dose increase (build-up effect) within the first few centimeters of the material followed by an exponential decrease, as shown in Figure 1.1 for ^{60}Co γ-rays and for 18 MeV photons.

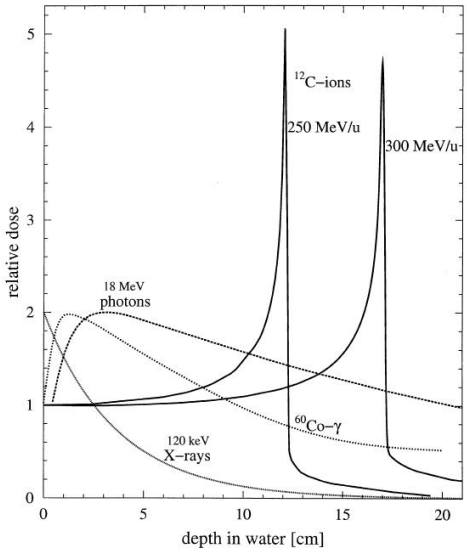

Figure 1.1.: Comparison of the depth-dose profiles of photons and C-ions in water. (This figure is taken from Kraft [2000a]).

1.2.2. Interaction of charged particles with matter

In contrast to X-rays, heavy ions do not deposit most of their energy at the beginning of their way through matter, but on the very end of their track. Heavy ions have, also in contrast to X-rays, a well-defined range in matter which depends on the initial energy of the particles. The peak-shaped dose-deposition curve of heavy ions in matter is called Bragg curve, named after the British physicist and chemist Sir William Henry Bragg (1862 - 1942), who first described the inverse depth dose profile of heavy ions in 1904 [Brown and Suit, 2004]. The depth-dose profiles of C-ions of different energies are shown in Figure 1.1.

An important term describing the energy deposition of a charged particle beam in a target material is the linear energy transfer (LET). The LET of charged particles in a medium is defined as

$$LET_{\Delta} = \left(\frac{dE}{dl}\right)_{\Delta} \tag{1.2}$$

where dl is the distance traversed by the particle and dE is the energy loss due to collisions with electronic energy transfers less than some specified value Δ [ICRU, 1970]. LET_{∞} includes all electrons and equals the energy loss of the ion. The maximum energy transfer that is possible depends on the type and velocity of the incident particle. In the following sections, the use of "LET" without any subscript refers to a LET_{∞}. Figure 1.2 shows the LET as a function of the particle energy for different ions.

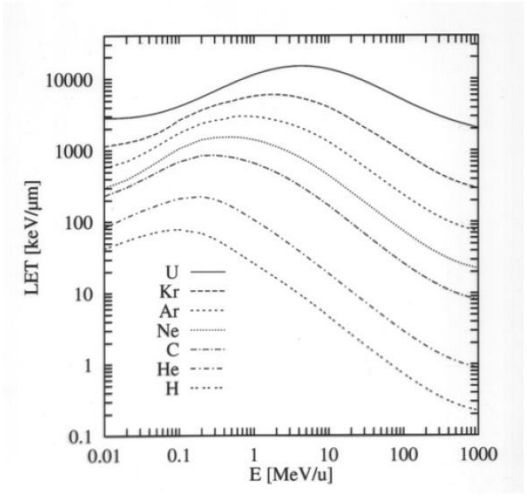

Figure 1.2.: Linear energy transfer (LET) as a function of particle energy for different ions. (This figure is taken from Kraft [2000a]).

Heavy ions deposit their energy in two ways: interaction with the target nuclei and interactions with target electrons. Nuclear stopping is the dominant process for low projectile velocities corresponding to particle energies below about 10 keV/u. For energies used in tumor therapy with particle beams, the electronic stopping, i.e. the interaction of the projectile ions with the target electrons is the main path of energy transfer to the target material (see Kraft et al. [1992] for a review). The Bethe formula, named after Hans Albrecht Bethe (1906 - 2005), a German-American physicist, describes the electronic energy loss per traveled distance of swift charged particles traversing matter:

$$-\frac{dE}{dx} = 4\pi N \frac{Z_{eff}^2 e^4}{m_e c^2 \beta^2} \cdot Z_T \cdot \left[ln\left(\frac{2m_e c^2 \beta^2}{I\,(1-\beta^2)}\right) - \beta^2 \right] \tag{1.3}$$

with N the number of target atoms per volume, Z_{eff} the effective nuclear charge of the projectile, e the elementary charge, m_e the rest mass of the electron, βc the velocity of the projectile, Z_T the nuclear charge of the target material and I the mean ionization potential of the target. For high energies the projectile nuclei have lost all their electrons, $Z_{eff} = Z_P$, for lower energies the effective charge of the projectile nucleus is described by the empirical Barkas formula [Barkas, 1963]

$$Z_{eff} = Z_P \left(1 - e^{-125\beta Z_P^{-2/3}}\right) \tag{1.4}$$

with the effective projectile charge Z_{eff}, the nuclear charge of the projectile Z_P and βc the velocity of the projectile.

The absorbed dose in a target material is defined as the energy deposited per unit mass, measured in units of Gray ($1Gy = 1J/kg$) [ICRU, 1970]. When

a thin target is irradiated with a parallel particle beam, the absorbed dose is given by

$$D\,[Gy] = 1.602 \cdot 10^{-9} \cdot \frac{dE}{dx}\,[keV/\mu m] \cdot F\left[cm^{-2}\right] \cdot \frac{1}{\rho}\left[\frac{cm^3}{g}\right] \tag{1.5}$$

where F is the particle fluence and ρ is the density of the target material. $\frac{dE}{dx}$ is the energy loss, which is equivalent to the LET because all electronic energy transfer processes are taken into account.

On a microscopic scale, the ionization events caused by a projectile particle are arranged along the particle track. Two types of ionization events can be distinguished, ionizations caused by primary collision of the projectile particle with target electrons, and ionizations caused by electrons that received an sufficiently large energy transfer to produce further ionization events themselves (those electrons are called δ-electrons). With decreasing particle energy the distance between the ionization events decreases, therefore ion beams with low energy (and high LET) are densely ionizing, while ion beams with high energy (and low LET) are sparsely ionizing similar to X-rays. The radial dose distribution of a particle track and the track diameter are determined by the primary energy distribution of the electrons and their energy loss. The radial dose distribution within a particle track D(r) is inversely proportional to the squared radial distance i.e. $D(r) \propto 1/r^2$. The maximum radial range of δ-electrons R_{max} increases with the energy of the primary particle and is described by a power law [Kiefer and Straaten, 1986] $R_{max} = 0.05 \cdot E^{1.7}$ where R_{max} is measured in µm and E is the specific energy of the ion in MeV/u.

Figure 1.3 shows simulations of ionization events in water caused by protons and C-ions of different energies on a nanometer scale. It is visible that the density of the ionization events increases with decreasing projectile energy, and is higher for C-ions compared to protons. Many ionization events are located around the center of the particle track, while some high-energetic electrons transfer energy to the outer part of the projectile track (δ-electrons). As described in the following section, the DNA is the sensitive target for radiation in cells and the diameter of a DNA double stand is about 2 nm. Comparsion of the size of the DNA molecule with the distribution of ionization events shown in Figure 1.3 illustrates that the damage induced in a DNA molecule will be much more complex if it is hit by a high-LET ion compared to a low-LET particle. Even for low average doses the locally applied dose in the track center is extremely high for high-LET particles, while other areas remain completely without dose deposition. This high ionization density along the track of a high-LET particle leads to different effects after exposing biological targets to high-LET particle beams compared to X-rays or other low-LET radiation.

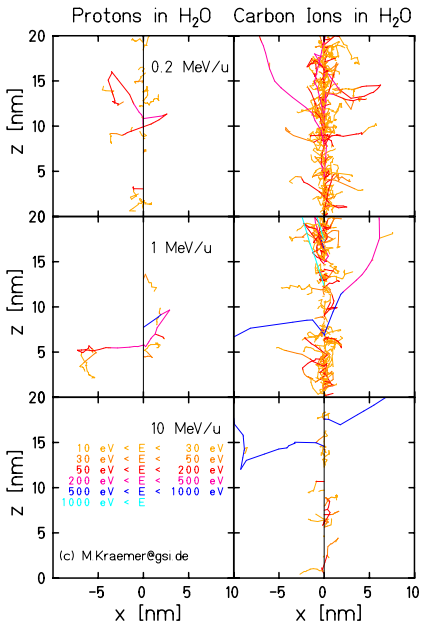

Figure 1.3.: Simulations of ionization events produced by protons and C-ions of different energies in water along a 20 nm track segment. (Courtesy of M. Krämer.)

1.3. Biological effects of ionizing radiation

The understanding of the biological effects of the different types of ionizing radiation is of great importance. Humans are exposed to a variety of ionizing radiation sources including the natural background radiation, radiation for diagnostic and therapeutic purposes, accidental or occupational exposure. In addition, the exposure to ionizing radiation is one of the main topics for manned space missions (e.g. Durante and Cucinotta [2008]; Durante et al. [2007]; Schimmerling et al. [2003]; Kiefer [1999]).

1.3.1. DNA - the target for ionizing radiation

The effect of radiation on cells results mainly from the damage induced in the deoxyribonucleic acid (DNA) molecules, which are contained in the cell nucleus. This was shown in a study by Munro [1970], who irradiated either cell nucleus or cytoplasm only.

The DNA, which encodes the genetic information, consists of two molecule strands which are held together by hydrogen bonding of complimentary base pairs and form the well-known double helix structure, which was first described by Francis Crick and James Watson in 1953 [Watson and Crick, 1953]. Each strand is comprised of subunits, called nucleotides, which are made of sugar, phosphate and one out of the four different bases: adenine (A), thymine (T), cytosine (C) and guanine (G). These bases form complimentary pairs of

A-T and C-G which are the inner part of the double helix structure. The sequence of bases codes the genetic information. Each human cell contains about $3 \cdot 10^9$ nucleotide pairs of DNA [Alberts et al., 2005]. The DNA molecules are associated with proteins and are folded to highly organized structures. The highest grade of chromatin condensation is achieved during metaphase, when the chromatin condenses to form chromosomes which are visible under the microscope. Human cells contain 46 chromosomes, 22 pairs of autosome chromosomes and the sex chromosomes, XX in females and XY in males (a review about the discovery of the number of human chromosomes is given by Harper [2006]). The behavior of the chromosomes during cell division was first described in 1882 by Walter Flemming, who introduced the terms "prophase", "metaphase" and "anaphase" [Obe and Vijayalaxmi, 2007].

During each cell cycle division, a cell undergoes several steps. A schematic illustration of the cell cycle is shown in Figure 1.4. The division of the cycle in four equal portions was made for clarity reasons and does not reflect the actual duration of each phase. One cell cycle generally takes between 12 and 24 hours for most cells in cell culture, thereof the mitotic phase (M-phase) takes typically only one hour. The cell cycle interphase consists of G1-, S- and G2-phase. In G1-phase, biosynthetic activities take place, including the synthesis of enzymes required for DNA replication. DNA synthesis takes place in S-phase, in this phase all DNA is replicated so that each chromosome, which consisted of one chromatid in G1-phase, consists of two sister chromatids when S-phase is finished. In G2-phase, proteins necessary for the following mitotic phase (M-phase) are synthesized. In the M-phase nuclear division and cytoplasmic division take place. During nuclear division the sister chromatids of each chromosome are divided into the two daughter nuclei. After nuclear and cytoplasmic division, the two identical daughter cells that were created can either start cell cycle progression once again, or they can enter a resting phase (G0-phase). Cells can remain in the G0-phase for days, weeks or even years [Alberts et al., 2005]. G0-phase is very common for cells that are differentiated. For example blood lymphocytes, which were used in this work, are normally in G0-phase and they can persist in this phase for several years in the human body.

1.3.2. DNA damage induced by ionizing radiation

Ionizing radiation deposits energy in the cell nucleus either by directly ionizing the target (DNA) molecules or by ionizing other molecules, particularly water, since 80% of a cell is composed of water. If the ionization takes place in water molecules, a large variety of radicals are formed where the OH radical is most important and damages the DNA (this is called "indirect effect" [Hall, 1988]).

Radiation induces several types of DNA damage, which are of different severity regarding their possible repair and consequently the fate of the cell. These lesions are base damages (base loss or base modification), single strand

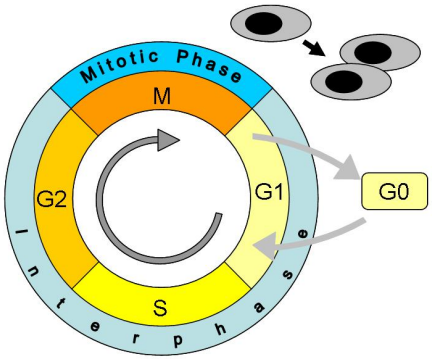

Figure 1.4.: Schematic view of the cell replication cycle.

breaks, double strand breaks and DNA-DNA or DNA-protein cross-links. In addition, several double strand and single strand breaks in close proximity form a so-called clustered lesion. DNA double strand breaks, and especially clustered lesions, are the most severe type of DNA damage induced by ionizing radiation determining the fate of the damaged cell.

1.3.3. DNA repair

During cell cycle, several DNA damage checkpoints exist, which arrest the cell cycle progression to allow repair and to prevent the transmission of DNA damages to daughter cells [Sancar et al., 2004]. For the radiation-induced damage, which is the topic of this thesis, the G1/S checkpoint and the G2/M checkpoint are most relevant. The former prevents the duplication of damage during S-phase by keeping the cell in G1-phase until the damage is repaired, the latter prevents a cell with damaged DNA to undergo mitosis and transfer the damage to daughter cells.

Cells can repair DNA damages via different repair pathways; their use depends on the type of damage and the actual cell cycle stage. The repair pathways are: base excision repair, mismatch repair, nucleotide excision repair and double strand break repair pathways [Sancar et al., 2004; Christmann et al., 2003]. As double strand breaks are the critical damage induced by radiation, especially if they form clustered lesions, the two main pathways to repair double strand breaks, the homologous recombination (HR) and the non-homologous end-joining (NHEJ) are described in the following. NHEJ is an error-prone repair pathway and is the dominant pathway in G0/G1-phase, while HR is error-free and occurs during late S-phase and G2-phase. In HR, the information lost in the broken double strand is retrieved from a homologous DNA double strand. In contrast, the NHEJ reconstitutes the DNA molecule by joining the DNA ends without homology requirements and there-

fore without ensuring sequence restoration in the break region. The NHEJ is mainly responsible for the chromosomal exchanges observed after exposure of cell in G0/G1 cell cycle stage (as it was done in the work presented here) to ionizing radiation.

A third DSB repair pathway, the single strand annealing (SSA), removes the DSB by annealing the DNA segments containing the break with a homologous segment on the same DNA molecule while excising the parts in between. SSA is therefore associated with a loss of information, but does not lead to exchanges between different chromosomes, and can therefore be regarded as a transitional pathway between the error-free HR and the error-prone NHEJ. More details about the different repair pathways can be found in several reviews, e.g. Pfeiffer et al. [2000, 2004]; Christmann et al. [2003]; Sancar et al. [2004]; Wyman and Kanaar [2006]; Kobayashi et al. [2008] and Sasaki [2009].

Misrepair of DNA damage contributes to therapy-induced carcinogenesis [Allan and Travis, 2005]. Translocations are a form of transmissible aberrations and are often found in cancer tissue. The first consistent chromosomal aberration found in human cancer was the Philadelphia chromosome, which causes chronic myeloid leukemia, it was first described in 1960 and was identified as a translocation between chromosomes 9 and 22 in 1973 [Mitelman et al., 2007].

1.3.4. Chromosomal aberrations

As described in the previous section, the repair of DSBs, which have been induced by exposure to ionizing radiation and other physical or chemical agents, can lead to alterations in the DNA molecules which are observable as chromosomal aberrations. Chromosomal aberrations are therefore a useful tool to monitor radiation exposure [Edwards et al., 2005; International Atomic Energy Agency, 2001].

To observe chromosomal aberrations, cells can be arrested in mitosis by the use of colchicine [International Atomic Energy Agency, 2001]. To make the chromosomes suitable for microscopy, the cells are exposed to a hypotonic solution for a defined time and are afterwards fixed (usually with a combination of methanol and acetic acid) and are dropped onto microscopy glass slides. Although chromosomes are visible without staining if a phase contrast microscope is used, they are generally stained before the analysis. Solid staining with a single color, e.g. staining with Giemsa solution allows the analysis of different aberration types, such as polycentric chromosomes, acentric fragments, ring chromosomes and chromatid-type exchanges. Other aberration types such as translocations and insertions are normally not recognizable with Giemsa staining, unless sophisticated banding analysis is performed, e.g. G-banding. For G-banding, the metaphases are treated with pepsin and then stained with Giemsa solution, yielding a strong staining of A-T rich regions and a light staining of C-G rich regions, resulting in a unique banding pattern

of each chromosome pair. However, the analysis of chromosomal aberrations by G-banding is very time-consuming. The development of fluorescence in situ hybridization (FISH), which uses DNA probes labeled with fluorescence colors that bind specifically to a pair of homologue chromosomes, made it possible to visualize translocations and insertions without the sophisticated banding technique. While it was first only possible to stain one or two pairs of chromosomes at once, the multiplex FISH (mFISH) brought further improvement as it allows to identify all chromosome pairs at once and is therefore suited to identify complex chromosomal rearrangements in addition to the other aberration types [Speicher et al., 1996; Kearney, 2006]. The mFISH technique uses combinations of fluorescence colors to assign a unique artificial color to each chromosome pair. Examples of metaphase spreads stained with Giemsa, 2-color FISH and mFISH are given in Figure 1.5. Figure 1.6 shows the difference in aberration recognition for single-color staining and mFISH. The same aberrant metaphase is displayed in Figure 1.6 (a) in DAPI (4',6-Diamidino-2-phenylindol) staining which allows to detect one non-transmissible aberration, and in Figure 1.6 (b) in mFISH staining where two transmissible aberrations are visible in addition to the non-transmissible exchange.

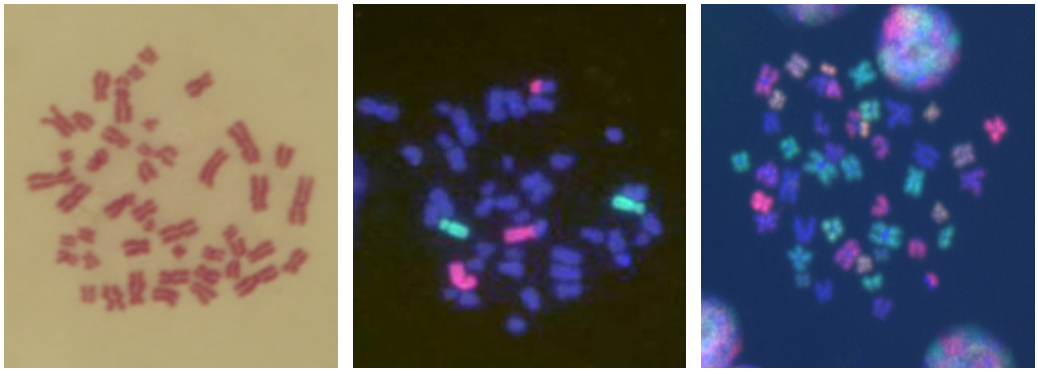

(a) (b) (c)

Figure 1.5.: Examples of different chromosome staining techniques. (a) Giemsa stained metaphase, (b) 2-color FISH stained metaphase (courtesy C. Fournier), (c) mFISH stained metaphase (three-color display is shown).

Chromosomal aberrations are classified according to different scoring systems. They can be divided into different groups according to their complexity (i.e. distinguishing terminal deletions, simple exchanges and complex exchanges), their completeness (i.e. distinguishing complete aberrations, incomplete rejoined aberrations and one-way aberrations [Cornforth, 2001]) and according to their transmissibility to daughter cells. The aberration scoring criteria and classification systems used in the present study are described in more detail in Section 2.6. The choice of a classification system depends on the applied staining and on the question that is to be answered. While the in-

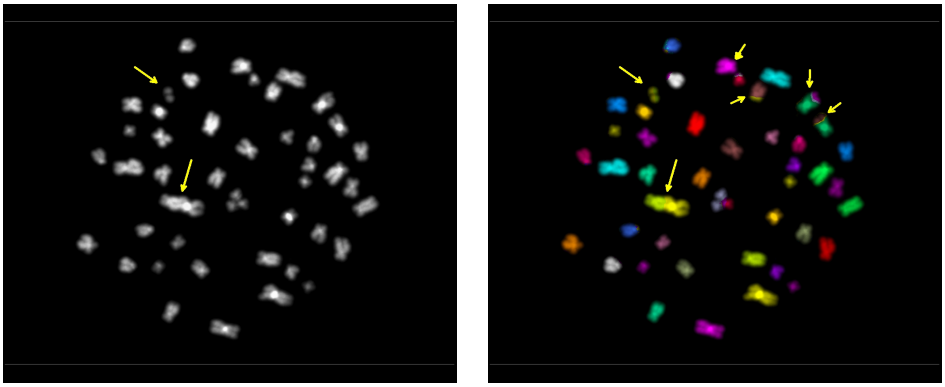

(a) (b)

Figure 1.6.: mFISH stained human peripheral blood lymphocyte carrying aberrations. (a) DAPI image, which is comparable to solid staining. Only non-transmissible aberrations are recognizable, here a dicentric chromosome with an accompanying acentric fragment. (b) mFISH staining reveals that in addition two transmissible exchanges are present in this cell.

vestigation of a special type of aberration (e.g. complex exchanges, insertions) might be of interest for the identification of a possible fingerprint of densely ionizing radiation [Testard et al., 1997; Anderson et al., 2003; George et al., 2003b; Johannes et al., 2004], transmissible aberrations are most relevant for the question of long-term effects of radiation exposure, as they can be passed to daughter cells and may induce cancer [Mitelman et al., 2007].

1.3.5. Relative biological effectiveness of densely ionizing radiation

When biological endpoints like cell inactivation or aberration formation are investigated after cell exposure to sparsely and densely ionizing radiation, the outcome is often different regarding the physical doses necessary to produce the same biological effect, e.g. the induction of a defined number of aberrations per cell. The relative biological effectiveness (RBE) is used to describe the effectiveness of a test radiation compared to a reference radiation. As reference radiation generally γ-rays or X-rays are chosen (the latter are used in the present study). The RBE is defined as

$$RBE = \frac{D_{X-ray}}{D_{test-radiation}}|_{isoeffect} \tag{1.6}$$

with the X-ray dose D_{X-ray} and the dose of the test-irradiation $D_{test-radiation}$ that produce the same biological effect. To achieve RBE values, it is necessary to generate dose-effect curves for the radiation qualities under consideration. The RBE values depend on the effect level under consideration,

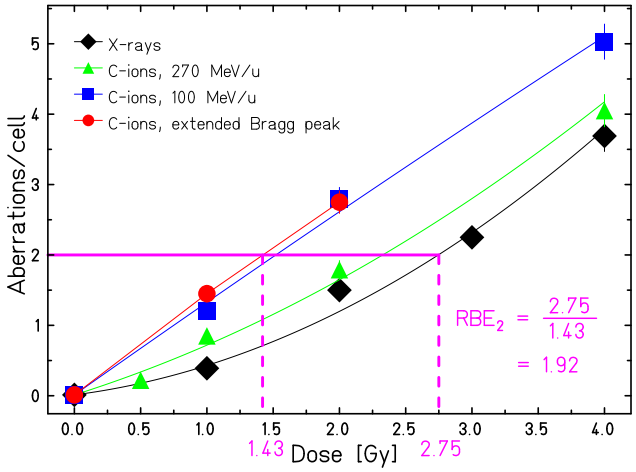

Figure 1.7.: Dose-effect curves for the induction of chromosomal aberrations in peripheral blood lymphocytes by X-rays and C-ions with an energy of 270 MeV/u, 100 MeV/u and extended Bragg peak C-ions. Aberrations were scored on mFISH stained slides. Lines indicate how the relative biological effectiveness (RBE) is determined. The RBE for the induction of 2 aberrations per cell by extended Bragg peak C-ions is calculated in this example.

e.g. 10% clonogenic cell survival, 1% clonogenic cell survial, induction of 0.5 aberrations per cell. Maximum RBE values are achieved when the initial slopes α of the dose-effect curves are compared, i.e. $RBE_{max} = RBE_{\alpha} = \alpha_{test-radiation}/\alpha_{x-ray}$. Figure 1.7 illustrates how the RBE is determined from a set of dose-effect curves. In the example, the RBE for the induction of 2 aberrations per cell by extended Bragg peak C-ions is determined. The X-ray dose necessary to produce 2 aberrations per cell is 2.75 Gy, the extended Bragg peak C-ion dose necessary to produce the same effect is 1.43 Gy. Thus, the RBE for the induction of 2 aberration per cell by extended Bragg peak C-ions is 1.92.

RBE-LET dependencies were studied for more than half a century now, and although the main focus was cell inactivation at the beginning [Barendsen et al., 1960, 1963], the first RBE data for the formation of chromosomal aberration were published only a few years later by Skarsgard et al. [1967]. RBE values depend on many factors, mainly on the LET and on the atomic number of the projectile particles, on the biological endpoint of interest and on the radiosensitivity of the investigated biological system, e.g. cell line or tissue (for details see Kraft [1999]). Figure 1.8 shows the RBE-LET dependence for the induction of one aberration per cell in lymphocytes by C-, Fe, and Xe-ions with different energy. The RBE for induced aberrations depends for high-LET radiation also on the sampling time. High-LET radiation induces a cell cycle delay of heavily damaged cells leading to an underestimation of the RBE if only one sampling time is used [Ritter et al., 2000, 2002a].

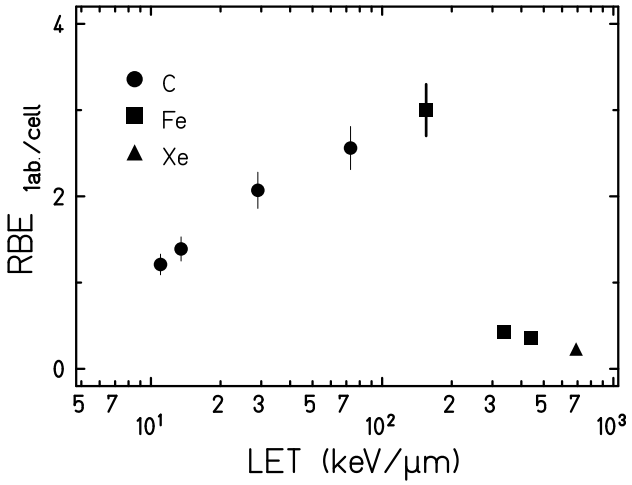

Figure 1.8.: RBE-LET dependence for one aberration per cell induced by C-, Fe- and Xe-ions in lymphocytes. Aberrations were scored in solid stained first cycle metaphases after 48h incubation. (Courtesy R. Lee, unpublished data.)

The RBE is a crucial point regarding the tumor therapy with heavy ion beams, and precise models that determine RBE values are necessary for treatment planning [Kraemer et al., 2003]. A high RBE in the tumor region ensures tumor cell inactivation, especially if a radioresistant tumor is treated. On the other hand it is favorable to choose treatment conditions so that the RBE in the beam entrance channel is low, especially for deep-seated tumors where a large volume of normal tissue is located in front of the tumor, which may contain sensitive structures such as brain stem, nerves, bone marrow or inner organs. This requirements make C-ions suited for the therapy of deep-seated radioresistant tumors, as they show a high RBE in the region of maximal dose deposition, i.e. in the Bragg peak region. Heavier ions, e.g. high energy iron ions, show an elevated RBE in the plateau region in front of the Bragg peak while the RBE drops below 1 in the region of the Bragg peak (so called overkill-effect) [Kraft, 1999]. The high RBE values of high-energetic iron ions are important for space research as iron ions are found in the galactic cosmic radiation. In contrast, light ions such as protons show an elevated RBE only in the last micrometers of their range.

The present study determines the RBE for the induction of different types of chromosomal aberrations in human peripheral blood lymphocytes irradiated with C-ions of different energies. The energies were chosen such that they cover the energy range applied in tumor therapy with C-ions.

1.3.6. Influence of radiation quality on aberration spectrum

As described in the previous section, the biological effectiveness for the induction of aberrations depends on the radiation quality. But in addition to a change in the aberration yield, the different local dose distribution may also be reflected in a change in the aberration spectrum. A biomarker or "fingerprint" for exposure to densely ionizing radiation is suggested in several studies. The most promising biomarker candidate is the fraction of complex exchanges (C-ratio, ratio of complex to simple exchanges). An elevated C-ratio is found after in vitro cell exposure to densely ionizing radiation compared to photons in several studies applying different staining methods (e.g. Testard et al. [1997]; Wu et al. [2003]; George et al. [2003b]; Johannes et al. [2004]). However, other studies did not confirm these findings for in vivo exposure [George et al., 2003b; Durante et al., 2004; Rithidech et al., 2007]. Other biomarkers were proposed as well, e.g. insertions [Anderson et al., 2000], ratios of intra-arm to inter-arm intrachanges and intra-arm intrachanges to interchanges [Bauchinger and Schmid, 1998; Brenner et al., 2001]. Thus, from the current state of knowledge no definite conclusion can be drawn whether there is a suitable biomarker for densely ionizing radiation exposure in vitro and in vivo. Increasing research in the field of densely ionizing radiation and the application of new staining methods could help to clarify this issue.

The search for a biomarker for densely ionizing radiation is of importance as humans are exposed to a variety of densely and sparsely ionizing radiations, e.g. occupationally, accidentally or for medical purposes. In case an overexposure occurs, the dose to which an individual was exposed can be estimated using biological dosimetry [International Atomic Energy Agency, 2001], but it would be desirable to gain information about the radiation quality in parallel by the use of a specific biomarker.

In the work described here, the mFISH method was applied to score aberrations in human peripheral blood lymphocytes exposed to X-rays and C-ions in vitro and in vivo. In parallel to the analysis of the aberration yield, the aberration spectrum was determined to search for possible biomarkers for the exposure to C-ions in vitro and in vivo.

1.3.7. Chromosome territories

DNA is not randomly distributed in the cell nucleus, but occupies distinct micrometer-scale territories during interphase (mFISH stained interphase nuclei give an impression of the distinct chromosome regions, as can be seen in Figures 1.5 (c) and 2.4 (h)). A detailed review about the discovery of chromosome territories and the present knowledge about nuclear architecture is given by Cremer and Cremer [2006a,b]. The territories of individual chromosomes in the cell nucleus are believed to follow regular patterns, i.e. chromosomes that occupy neighboring territories in one cell are expected to be neighbors

also in other cells, at least within the same tissue and organism. If this is true, the relative positioning of chromosomes in the interphase nucleus should be reflected in the induced chromosomal exchanges when the cells are exposed to ionizing radiation, i.e. neighboring chromosomes are expected to form exchanges more frequent than distant chromosomes. When mFISH analysis is performed, the information about the exchange rates between individual chromosomes can be obtained. To address the question of interphase positioning of chromosomes, data about the exchange frequencies were collected for all analyzed metaphases during the work described here.

1.4. Prostate cancer

Prostate cancer is the most frequent cancer in males, with an incidence of about 58.000 cases per year in Germany. With a total of 230.000 cancer incidences in males, prostate cancer therefore represents a 25 % fraction of all cancer incidences in men in the German population (data published by Robert Koch Institut, Berlin, Germany[1]). Prostate cancer occurs mainly in elderly man. About 90% of the patients are 60 years or older at the time of diagnosis, the mean age at time of diagnosis is about 70 years. Therefore, albeit it is the most common cancer diagnosed in men, it is in Germany the 6th-most-common cause of death in men, and the second-most common cause of cancer-related deaths in men after bronchial carcinoma (data published by Statistisches Bundesamt Deutschland[2]). The treatment of prostate cancer is therefore one of the main topics in cancer therapy. Several therapeutic strategies exist for prostate cancer treatment including radiotherapy, surgery, hormonal therapy and chemotherapy. Prostate cancer is generally a slow-growing tumor and therapy can cure the cancer or delay its growth.

The prostate-cancer patients in the study presented here were treated with photon IMRT or a combination of C-ion boost and IMRT. After the therapeutic potential of heavy ions for locally advanced prostate cancer was investigated [Nikoghosyan et al., 2004], the clinical trial started in 2006. A treatment plan for the IMRT and C-ion boost irradiation is shown in Figure 1.9. A homogeneous high dose in the target volume is achieved with both radiation qualities. However, the dose decrease at the edges of the target volume is steeper in the case of C-ion boost, leading to a better sparing of sensitive organs close to the tumor, as can be seen in the treatment plan for the rectum. The dose to the femur heads is comparable for both treatment conditions. The total volume of irradiated normal tissue is much lower in the case of C-ion boost, as only two beam ports are necessary to achieve the high homogeneous tumor dose, while seven irradiation fields are used for the

[1] www.rki.de
[2] www.destatis.de

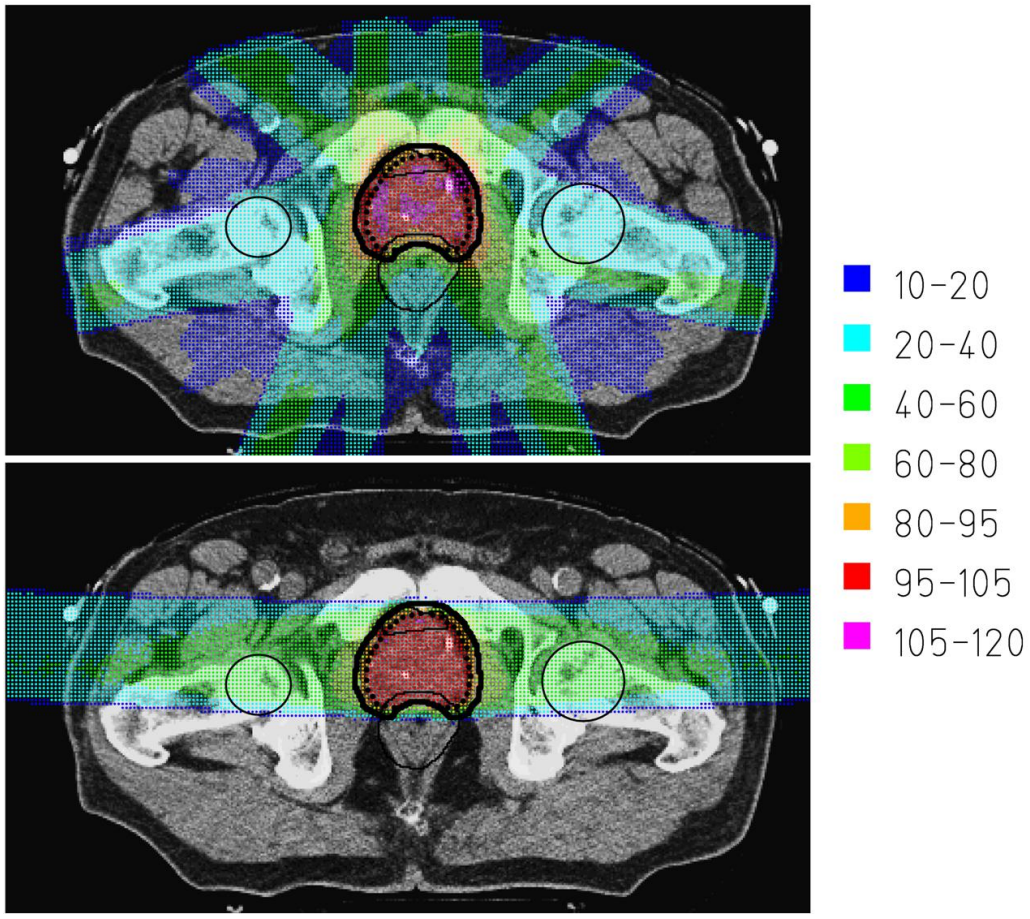

Figure 1.9.: Treatment plans for prostate radiotherapy with IMRT (7 coplanar fields, upper panel, 30 fractions, à 2 Gy) and a C-ion boost (2 fields, lower panel, 6 fractions, à 3 GyE). Shown is in grayscale the computed tomogram overlaid by the prescribed dose percentage in color. The thick contour represents the clinical target volume, the dashed contour the gross tumor volume, and the thinner contours rectum, as well as the femoral head as organs at risk. (Data courtesy of A. Nikoghosyan/ J. Debus, Heidelberg University Hospital.)

IMRT. Details about external beam radiotherapy with photons and charged particles are provided in the following section.

Possible side effects of prostate cancer treatment using external beam radiotherapy are diarrhea, rectal bleeding, urinary incontinence and impotence. Side effects occur within a few weeks after beginning of therapy and often resolve without treatment within several months. Late effects of external beam radiotherapy for prostate cancer include rectal/bowel, urinary and sexual symptoms and a slightly higher risk of developing second solid tumors [Brenner et al., 2000; Bostrom and Soloway, 2007; Mueller et al., 2007]. The risk of developing secondary tumors is expected to depend on the applied radiotherapy, as the dose-distribution in the normal tissue varies with radiotherapy technique [Hall and Wuu, 2003; Hall, 2006].

1.5. External beam radiotherapy

Treating cancer patients is one of the main tasks in modern medicine. Cancer is the second most common cause of death after cardiovascular diseases in the developed countries. The first application of ionizing radiation for therapy of malignant tissue was performed shortly after the discovery of X-rays by W.C. Röntgen in 1895. Because their nature and their biological interaction were not known at that time, X-rays were first used on a very empirical basis. The first therapeutic application is reported by Prof. Freund in Vienna who irradiated and removed a hairy mole on the forearm of a patient [Hall, 1988].

1.5.1. Fractionation

For a curative treatment of solid tumors, high doses of about 60 Gy are applied in the target volume. These doses are fractionated, typically in 30 daily fractions of about 2 Gy at five days per week. Fractionation allows cells in the surrounding normal tissue, which is unavoidably exposed to some dose during therapy, to recover. And it enables reoxygenation of hypoxic areas in the tumor. As hypoxic cells are very radioresistant, reoxygenation of hypoxic areas improves radiation-induced cell inactivation [Hall, 1988].

1.5.2. Photon irradiation

Photon radiotherapy is the most widely used type of external beam radiotherapy. According to the location of the tumor, photons with different energies are applied, as the shape of the depth-dose profile depends on the photon energy (see Figure 1.1). For deep-seated tumors like prostate cancer photons from megavolt accelerators are used. Modern types of photon therapy are the 3D-conformal radiotherapy and intensity modulated radiation therapy (IMRT). In both cases the patient is irradiated from several sides, for each

irradiation field an absorber is placed between accelerator and patient which has a hole that shapes the beam according to the size and geometry of the tumor. In the case of IMRT, in addition to the 3D-conformal application the applied dose is varied within each field.

1.5.3. Proton irradiation

Tumor therapy with accelerated protons was first performed from 1954 to 1957 in Berkeley, USA. Since this time, the use of accelerated proton beams for tumor therapy spread widely. A list of facilities using proton beams or other charged particle beams can be found at the homepage of the "Particle Therapy Co-Operative Group" (PTCOG)[3]. Proton beams show an inverted depth-dose profile compared to photons and are therefore suited for the treatment of deep-seated tumors. In contrast to heavier ions, protons have the disadvantage of higher range straggling and lateral scattering. Also in contrast to heavier ions, protons show an enhanced relative biological effectiveness restricted to the last micrometers of range only, so that for treatment planning an overall RBE of 1.1 is used.

Proton therapy is used for a variety of different tumor sites including prostate cancer, which is the topic of the work presented here. The first clinical trial using a proton boost irradiation together with X-ray treatment for therapy of prostate cancer was published in 1979 [Shipley et al., 1979] and good tumor control was achieved without severe side or late effects. Several other studies followed, for a review on the role of proton therapy in the treatment of prostate cancer see Efstathiou et al. [2009].

1.5.4. Irradiation with accelerated C-ions

Tumor therapy with ions heavier than protons was started in Berkeley, USA, in 1957 using Helium ions. Heavier ions followed from 1975 on including carbon, neon and argon ions [Castro et al., 1980]. Several tumor sites were treated. Therapy with heavy ions was terminated in Berkeley in 1992; two years later started in Chiba, Japan, tumor therapy with C-ions. In 1997 tumor therapy with C-ions began at GSI Helmholtzzentrum für Schwerionenforschung, Darmstadt, Germany, and in 2002 a facility in Hyogo, Japan, began tumor therapy with C-ions. The GSI pilot project was terminated in 2008, over 440 patients were treated at GSI. Recently, in November 2009, the first patient was treated at the HIT ion therapy facility in Heidelberg, Germany.

Physical and biological advantages of C-ions

Carbon ions show an inverse depth-dose profile compared to photons, that makes them suited for the treatment of deep-seated tumors (see Figure 1.1).

[3] http://ptcog.web.psi.ch/

Compared to protons, which show a similar inverted depth-dose profile, Carbon ions show less range straggling and lateral scattering. A recently published review by Weber and Kraft [2009] compares the properties of C-ion and proton beams regarding their application in radiotherapy. In addition to the physical advantages, C-ions have the biological advantage of an enhanced relative biological effectiveness in the region of the maximal physical dose deposition, i.e. in the Bragg maximum. This enhanced effectiveness makes C-ions specially suited for the therapy of radioresistant deep-seated tumors.

Facilities using C-ion beams for tumor therapy

Today, three facilities worldwide use C-ion beams for tumor therapy, these are in Heidelberg, Germany and in Hyogo and Chiba, Japan. Because of the good results from C-ion therapy several new facilities were build and will start operation soon, others are in planning. The HIT facility in Heidelberg, located at the Heidelberg University Hospital started patient therapy with C-ions recently. About 1300 patients per year will be treated at HIT. The HIT facility uses the raster scanning technique, which was first used for C-ion therapy at GSI and is described in the following section. Other centers will follow in Marburg and Kiel, Germany, in Wiener Neustadt, Austria, in Pavia, Italy and in Lanzhou, China.

Technical realization of C-ion therapy at GSI

Tumor therapy with C-ions was carried out at GSI as a pilot project from 1997 to 2008. The tumor treatment with accelerated C-ion beams at GSI used active beam shaping. For this, the target volume is divided into small volume elements (voxels) and each is irradiated with a pencil like beam. The range variation is achieved with an energy variation of the accelerator. The lateral beam movement is realized using perpendicular magnets that deflect the beam and move it from spot to spot [Haberer et al., 1993]. This setup avoids the use of absorbers between beam exit window and patient body, which cause range straggling, lateral scattering and nuclear fragmentation of the initial beam. Especially avoiding the production of neutrons in the absorber material is important, as they can cause secondary cancer in the treated patient [Brenner and Hall, 2008]. In addition, the active scanning system allows defining the number of particles individually for every voxel, this ensures the achievement of a homogeneous biological effective dose within the tumor volume. This makes treatment planning a complex task, as the number of particles must be assigned individually to each voxel [Kraemer et al., 2000; Kraemer and Scholz, 2000]. GSI was the first facility that used a raster scanning system for C-ions; a similar scanning system is used for proton therapy at the Paul Scherrer Institute (PSI) in Switzerland. The HIT facility in Heidelberg, which started patient therapy recently, also uses the raster scanning technique and

active energy variation.

Nuclear fragmentation takes place whenever heavy ion beams traverse matter, and the fragmentation processes must be taken into account for tumor treatment, especially when a deep-seated tumor is treated. The fragments have different ranges leading to a broadening of the Bragg peak [Schardt et al., 1996]. But the fragments also offer a unique possibility for quality control. Stripping of one or two neutrons from the ^{12}C-ion projectiles leads to positron-emitting ^{11}C-ions and ^{10}C-ions. The photon pair that is created by annihilation of the positron can be measured using positron emission tomography (PET) technique [Schardt, 2007]. The observed distribution of annihilation processes inside the patient is compared to a calculated distribution, and if deviations are detected the treatment plan can be corrected for the following fractions.

Clinical results of C-ion therapy

C-ion beam therapy achieved good results for the treatment of several solid tumors. At GSI, mainly patients with tumors in the head and neck region were treated [Schulz-Ertner et al., 2004, 2007a,b]. Patients with a variety of tumors were treated at NIRS, Chiba, Japan, the clinical results are summarized in a publication by Tsujii et al. [2007]. A recent publication by Schulz-Ertner [2009] reviewed the clinical experience with particle therapy in adults. This review summarized clinical outcome, mostly 5-year local control, of the therapy of different solid tumors with protons, C-ions and other heavy ions, sometimes in combination with photon radiotherapy. For C-ion therapy of prostate cancer, the results obtained in Japan indicate a good tumor control with limited rectal morbidity and a good quality of life 12 months after the treatment [Ishikawa et al., 2006; Wakatsuki et al., 2008].

1.5.5. Comparing different radiation qualities and fractionation schemes

As described in Section 1.3.5, accelerated ions have an altered relative biological effectiveness compared to photons. Tumor therapy with accelerated C-ions takes advantage of the high RBE in the target region. However, the RBE and its variation over the target volume must be taken into account for treatment planning. As the RBE is not a constant weighting factor but varies with applied dose, treatment planning becomes a skillful task [Kraemer et al., 2000].

To take into account the RBE when a biological target is exposed to high-LET radiation, the physical dose (measured in Gray [Gy]) has to be replaced by the biological equivalent dose (in Gray equivalent [GyE]) that is defined as

$$D_{biol} = D_{phys} \cdot RBE \tag{1.7}$$

where the RBE value depends on the specific biological material exposed, the biological endpoint of interest and the level of the biological alteration. In addition, the RBE depends in a complex way on many physical parameters such as particle energy, atomic number and LET. The two dose concepts, physical dose and biological equivalent dose, are substantially different and in case of high-LET irradiation it must be carefully determined whether the biological equivalent dose or the physical dose applied by high-LET particle beams is compared to a photon dose. In the study presented here, both dose concepts are used. The physical dose is used in the in vitro studies, where it is the intention to investigate the different biological effects of both radiation qualities. In the patient therapy study, the biological equivalent dose is used.

Another factor that makes the comparison of therapeutically applied doses more complex is the dose fractionation. As pointed out in Section 1.5.1, radiotherapy is generally applied in daily fractions of 2 Gy on five days per week. However, other fractionation schemes are used, in the study presented here a C-ion boost irradiation with 3 GyE per fraction on 6 consecutive days is performed. As the biological outcome depends on the dose fractionation, this must be taken into account when total doses delivered in different fractionation schemes are compared.

2. Materials and Methods

2.1. Blood donors

2.1.1. Patients

Blood samples from patients treated with C-ions and IMRT were obtained to analyze the aberration yield in the peripheral blood lymphocytes. Twenty-two patients with prostate cancer entered the study. The study was approved by the local ethic commission and all patients signed an informed consent form. The mean age of the patients at the beginning of therapy was 66 years (ranging from 54 to 74 years). The patients were divided in three groups according to their treatment. Thirteen patients received C-ion boost irradiation followed by conventional photon IMRT (referred to as C-ion + IMRT patients in the following). Six patients with a similar planning target volume were irradiated with photon IMRT only (called IMRT patients here). Three patients with a larger planning target volume (PTV) which included the pelvic lymph nodes were included in the study. These patients were solely treated with photon IMRT as well (patients are called IMRT* here).

Table 2.1 provides details about each patient regarding applied radiotherapy, age, tumor characterization (using TNM staging and Gleason score) and prostate specific antigen (PSA) level at the time of diagnosis. The tumor stage is given using the TNM staging system, which is used to characterize the actual state of solid tumors. It describes the extent of cancer in a patient's body. It is a universal system applicable to all solid tumors. T describes the size of the tumor and whether it has invaded nearby tissue, N describes the involvement of regional lymph nodes and M describes distant metastasis. The number behind the letter increases with increasing cancer spreading. Local tumors were staged between T1a and T3 for the patients in this study. No patient in this study had known cancer spreading to lymph nodes or distant metastasis. The Gleason system is used to grade prostate cancer cells according to the microscopic appearance of the tissue, which was obtained by biopsy or surgery. Two Gleason grades that range from 1 to 5 are added to obtain the Gleason score (or Gleason sum) ranging from 2 to 10. Lower Gleason scores describe well-differentiated less aggressive tumor tissue that closely resembles normal prostate tissue; high Gleason scores describe poorly-differentiated more aggressive tumor tissue that does not have recognizable glands. The Gleason score ranged from 6 to 9 in the patients of this study.

Patient	Therapy	Age	TNM Stage	GS	PSA [ng/ml]
01	C + IMRT	66	T1c N0 M0	8	14.0
02	C + IMRT	71	T3 N0 M0	9	14.9
03	IMRT*	61	T1c N0 M0	8	19.6
04	C + IMRT	70	T2b N0 M0	7	11.0
05	C + IMRT	59	T1c N0 M0	7	10.9
06	C + IMRT	66	T2a N0 M0	7	16.9
07	IMRT	73	T2c Nx Mx	7	10.1
08	C + IMRT	69	T2a N0 M0	7	13.8
09	C + IMRT	69	T2c N0 M0	8	17.2
10	C + IMRT	57	T2b N0 M0	8	12.4
11	IMRT*	73	T2 N0 M0	8	24.0
12	C + IMRT	72	T1c N0 M0	7	12.9
13	IMRT*	54	T1c N0 M0	8	5.8
14	IMRT	60	T1a N0 M0	6	18.0
15	C + IMRT	74	T2b N0 M0	8	11.0
16	IMRT	59	T1c N0 M0	6	13.0
17	C + IMRT	55	T2c N0 M0	7	10.7
18	C + IMRT	68	T1c N0 M0	7	10.8
19	C + IMRT	73	T2a N0 M0	7	11.0
20	IMRT	65	T1c N0 M0	7	10.4
21	IMRT	59	T1c Nx M0	7	4.0
22	IMRT	73	T1c Nx M0	6	7.5

Table 2.1.: Patients in this study characterized by the applied radiotherapy, the patient's age at the beginning of radiotherapy, the cancer staging by TNM classification of malignant tumors, the Gleason grading system (GS) for prostate cancer and the level of PSA in the blood serum at the time of diagnosis.

The PSA level is the most important serum marker for prostate cancer and is widely used for prostate cancer screening [Schroeder et al., 2009; Andriole et al., 2009]. The upper limit of normal is in most cases chosen between 2.5–4 ng/ml [Ito et al., 2001; Hernandez and Thompson, 2004; Schroeder et al., 2009; Andriole et al., 2009]. However, the PSA level in apparently healthy men increases with age [Stenman et al., 2000; Chun et al., 2007]. The level of PSA in the blood serum ranged from 4–24 ng/ml at the time of diagnosis in the patients of this study.

Tables 2.2 and 2.3 provide information about the irradiation of the three patient groups. As shown in Table 2.2 the planning target volume (PTV) is larger than the gross tumor volume (GTV) as it includes larger safety margins and for some patients it includes the pelvic lymph nodes (the patient group called IMRT* here). The doses applied to the GTV and PTV are given

Patient group	n	GTV [cm^3] mean (range)	PTV [cm^3] mean (range)
C-ion + IMRT	13	64 (50-90)	119 (92-151)
IMRT	6	60 (42-79)	108 (74-174)
IMRT*	3	40 (22-70)	936 (722-1247))
all patients	22	60 (22-90)	227 (74-1247)

Table 2.2.: Volumes of the gross tumor volume (GTV) and planning target volume (PTV) for the three patient groups. The remarkably large PTV for the IMRT* patient group includes the pelvic lymph nodes, in contrast to the PTV of the two other groups.

Patient group	n	Dose to GTV [Gy or GyE] mean (range)	Dose to PTV [Gy or GyE] mean (range)
C-ion + IMRT	13	78 (78-78)	60 (60-60)
IMRT	6	75.9 (74.6-76.7)	69.3 (66-70)
IMRT*	3	76 (76-76)	50.7 (50-51)
all patients	22	77.2 (74.6-78)	61 (50-70)

Table 2.3.: Radiotherapeutic doses applied to the gross tumor volume (GTV) and planning target volume (PTV) for the three patient groups.

in Table 2.3 for the three patient groups. The patients receiving a C-ion boost were treated with 18 GyE C-ion boost to the GTV in daily fractions of 3 GyE on six consecutive days, followed by 60 Gy IMRT to the PTV in daily fractions of 2 Gy on five days per week. The total dose to the GTV was 78 GyE for this patient group. Patients treated solely with photon IMRT (patient groups IMRT and IMRT*) received a total dose to the GTV of 74.6–76.7 Gy in daily fractions of 2–2.24 Gy (five fractions per week). The PTV was exposed to a total dose of 50–70 Gy delivered in daily fractions of 1.5–2.2 Gy (five fractions per week). No patient was treated with chemotherapy before or during the radiotherapy course. Some patients (16 of 22 patients) received a hormonotherapy.

The C-ion boost irradiation was carried out at the SIS accelerator of the GSI Helmholtzzentrum für Schwerionenforschung in Darmstadt using the raster scanning technique, that is described by Haberer et al. [1993]. The initial energy of the C-ion beam was 280–370 MeV/u. The IMRT was performed at the Department of Radiation Oncology at the Heidelberg University Hospital.

From each patient four blood samples (about 8 ml each) during the time of therapy and follow-up were obtained, the first one before therapy, one during, one at the end and one one year after the end of therapy. Samples one year after therapy were taken up to now from 16 patients. Figure 2.1 shows the work

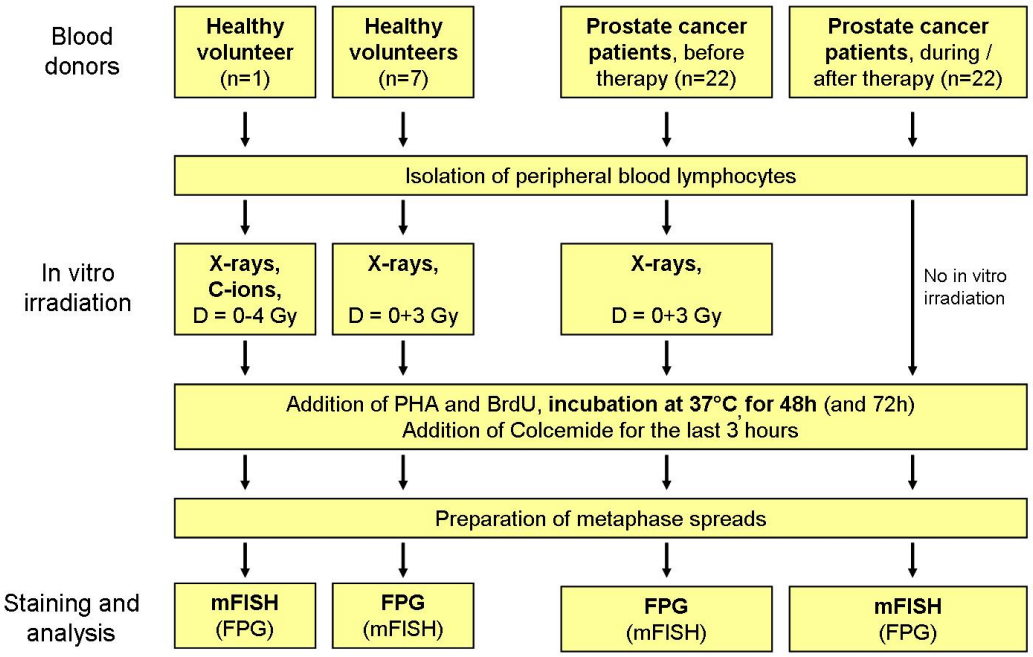

Figure 2.1.: Workflow of the blood samples obtained from healthy volunteers and from patients. The staining method shown in parentheses was performed in parallel, but in the case of mFISH for selected samples only.

flow of the patients' blood samples and samples of healthy volunteers. The handling of the blood samples and the isolation of lymphocytes is described in Section 2.2. The sample obtained before therapy was divided into two samples and one was irradiated in vitro with a dose of 3 Gy X-rays to determine the individual radiosensitivity of each patient. The in vitro irradiation procedure with X-rays is described in Section 2.3.1.

2.1.2. Healthy volunteers

Blood samples from healthy volunteers were taken for two purposes, for comparison with the in vitro irradiated lymphocytes obtained from the prostate-cancer patients before therapy and to generate dose-effect curves for irradiation with X-rays and C-ions. To compare the radiosensitivity of the patients and healthy volunteers ten blood samples from seven healthy donors (males and females, mean age 46 years, range 27–56 years) were taken and exposed in vitro to 3 Gy of X-rays. Additionally, several blood samples from one healthy volunteer (female, 49 years old, non-smoker) were irradiated with X-rays and C-ions of different energies to obtain dose-effect curves. Samples from the same donor were used for all experiments to avoid inter-individual variations in the radiation response. The workflow of the blood samples obtained from healthy volunteers is shown in Figure 2.1.

2.2. Isolation of lymphocytes

Isolation of peripheral blood lymphocytes was performed with samples obtained from prostate-cancer patients and from healthy volunteers. About 8 ml of venous blood were drawn into a Vacutainer® CPT™ cell preparation tube by venipuncture (see Figure 2.2 (a)). Blood samples from patients which were taken at the Heidelberg University Hospital were carried to GSI for lymphocyte isolation, the time between blood drawing and isolation of lymphocytes was shorter than three hours. The cell preparation tubes were centrifuged at room temperature at 1700 g (n = 48.33/s) for 20 min. After centrifugation, the red blood cells are below the gel barrier on the bottom of the tube. Above the gel barrier and density gradient fluid is the layer of lymphocytes and monocytes and on top is the blood plasma (see Figure 2.2 (b)). The plasma was removed with a pipette and the layer of lymphocytes and monocytes was transferred to a sterile 10 ml centrifuge tube. Sterile phosphate buffered saline solution (PBS) was added, cells were resuspended and centrifuged for 10 min at 390 g (n = 25/s). Afterwards, the PBS was removed and the cells were resuspended in RPMI 1640 cell culture medium, supplemented with 20% fetal calf serum (FCS), 2 mM L-glutamine, 100U/ml penicillin and 100 µg/ml streptomycin [Lee et al., 2005], referred to as complete medium. For in vitro irradiation, the cells were transferred into appropriate irradiation containers. Immediately after exposure the cells were reseeded in a final concentration of about $0.5 \cdot 10^6$/ml complete medium, to which 1% phytohemagglutinin and 15 µg/ml 5-bromo-2-deoxyuridine (BrdU) were added. Cells were then incubated for 48 hours and 72 hours at 37°C, 95% relative humidity and an atmosphere of 5% CO_2 in air in the dark to avoid photolysis of BrdU.

2.3. In vitro irradiation

In vitro irradiation was carried out with peripheral blood lymphocytes of patients obtained before therapy, from a group of healthy volunteers to compare with the patients' results and with lymphocytes from one healthy volunteer to achieve dose-effect curves. The isolated peripheral blood lymphocytes from the patients and the group of healthy volunteers were exposed to a dose of 3 Gy X-rays. The isolated peripheral blood lymphocytes from one healthy volunteer were exposed to X-rays, C-ions with energies of 270 MeV/u and 100 MeV/u and as well in an extended Bragg peak C-ions with doses from 0 to 4 Gy.

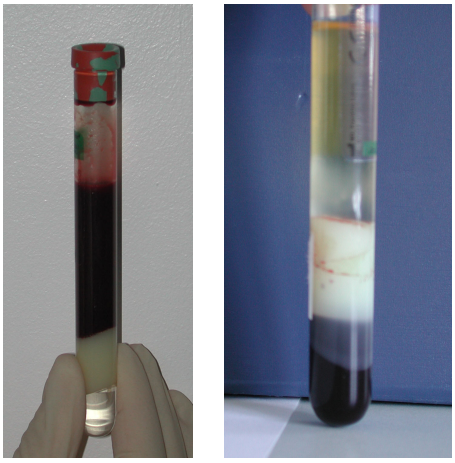

(a) (b)

Figure 2.2.: Blood sample (about 8 ml of venous blood) in a Vacutainer® cell preparation tube. (a) Blood sample before centrifugation, the whole blood being above the gradient fluid and polyester gel barrier. (b) After centrifugation, the blood sample is separated in its components. The blood plasma is on the top (yellow liquid), below are the lymphocytes and monocytes (opaque light yellow liquid above the white gel barrier). The red blood cells are below the gel barrier at the bottom of the glass tube.

2.3.1. X-ray irradiation

X-ray irradiation was carried out at a X-ray machine (Seifert, Ahrensberg, Germany) operated at 250 kV and 16 mA and that included 1 mm Cu- and 1 mm Al-filtering. The dose-rate was about 1.2 Gy/min. The dose applied to the sample was measured using a PTW-SN4 dosimeter (PTW Freiburg, Germany) which was placed in a specially designed plastic holder directly below the biological sample. The irradiation was carried out at room temperature. Isolated peripheral blood lymphocytes were exposed to X-rays in 25 cm^2 cell culture flasks or in specially designed cell containers, which were used for the exposure to 270 MeV/u and 100 MeV/u C-ions (see Section 2.3.2).

2.3.2. C-ion irradiation

Samples from one healthy donor (female, non-smoker) were irradiated with different doses of accelerated C-ions to generate dose-effect curves for the induction of chromosomal aberrations. These experiments were carried out with three different C-ion energies. The irradiation was performed at the heavy ion synchrotron SIS at GSI, Darmstadt, Germany, using the intensity controlled raster scanning technique and active beam energy variation [Haberer et al., 1993]. The irradiation facility was the same as for the treatment of tumor

Energy	LET at sample position
270 MeV/u	14 keV/µm
100 MeV/u	29 keV/µm
Extended Bragg peak	60–85 keV/µm

Table 2.4.: Energies and LET values of the C-ion beams used for in vitro irradiation of the isolated peripheral blood lymphocytes.

Beam energy	Dose	Fluence	Particles/nucleus
270 MeV/u	0.5 Gy	$2.22 \cdot 10^7/cm^2$	5.55
270 MeV/u	1 Gy	$4.44 \cdot 10^7/cm^2$	11.1
270 MeV/u	2 Gy	$8.88 \cdot 10^7/cm^2$	22.2
270 MeV/u	4 Gy	$1.77 \cdot 10^8/cm^2$	44.4
100 MeV/u	1 Gy	$2.14 \cdot 10^7/cm^2$	5.36
100 MeV/u	2 Gy	$4.29 \cdot 10^7/cm^2$	10.7
100 MeV/u	4 Gy	$8.57 \cdot 10^7/cm^2$	21.4
Ext. Bragg peak	1 Gy	$8.61 \cdot 10^6/cm^2$	2.15
Ext. Bragg peak	2 Gy	$1.72 \cdot 10^7/cm^2$	4.30

Table 2.5.: C-ion doses and corresponding particle fluences applied for in vitro irradiation of peripheral blood lymphocytes. The particle traversals per cell nucleus were calculated assuming a cell nucleus area of $25\mu m^2$ [Anderson et al., 2000]. Ext = extended.

patients with C-ions.

Cells were irradiated with monoenergetic 270 MeV/u C-ions, monoenergetic 100 MeV/u C-ions and 25 mm extended Bragg peak C-ions. The corresponding linear energy transfer (LET) values are given in Table 2.4.

For the irradiation with monoenergetic C-ions the cell suspension was loaded into specially designed polyethylene holders with a 2 mm thick well for the cell suspension (about 5 ml cell suspension per well) and 1 mm plastic between the cells and the radiation source [Lee et al., 2005; Ritter et al., 2002a]. For irradiation with the extended Bragg peak C-ions the cell suspension was filled in 5 ml plastic centrifuge tubes which were placed in a plastic block with cavities for the centrifuge tubes [Nasonova and Ritter, 2004]. All irradiations were carried out at room temperature.

Table 2.5 shows details about the in vitro irradiation. Cell samples irradiated with 270 MeV/u C-ions and 100 MeV/u C-ions were exposed to doses up to 4 Gy and samples exposed to extended Bragg peak C-ions received doses up to 2 Gy. The corresponding particle fluences were calculated using Equation 1.5, and the particle traversals per cell nucleus were derived assuming a cell nucleus area of 25 µm^2 [Anderson et al., 2000].

2.4. Cell fixation and preparation of metaphase spreads

Cells were arrested in mitosis by adding colcemid (20 µl/ml medium, stock solution 10 µg/ml) 3 hours prior to cell fixation. Colcemid inhibits the formation of the spindle fibers which separate the chromatids during mitosis and therefore leads to an accumulation of cells in mitosis. Then, metaphase spreads were prepared according to standard protocols [International Atomic Energy Agency, 2001]. For this the cell suspension was centrifuged for 6 min at 200 g (n = 16.6/s), the medium was poured away and the cell pellet was resuspended in the remaining medium (about 100 - 200 µl). Hypotonic KCl solution (0.075 M) preheated to 37 °C was added carefully. After 8 min in the hypotonic solution the cells were centrifuged again for 8 min at 290 g (n = 20/s). The supernatant was removed and the pellet was resuspended. A freshly prepared fixation solution made of methanol and acetic acid (3:1) was added. After 30 min at room temperature the suspension was centrifuged, the supernatant was removed and the pellet was resuspended in methanol/acetic acid. After renewed centrifugation the cells were resuspended in an appropriate volume of methanol/acetic acid fixation solution for the preparation of chromosome spreads. The chromosome spreads were prepared by dropping about 20 µl of cell suspension on wet microscope slides. The quality of the spreading and the appropriate cell density in the dropping suspension were examined under a phase contrast microscope. Slides were left overnight at room temperature to assure complete drying. Afterwards, slides were stained using FPG technique or were frozen at -20 °C for storage until mFISH hybridization.

2.5. Staining of metaphase spreads

The microscopy slides with the metaphase spreads were stained using fluorescence plus Giemsa (FPG) staining or multiplex fluorescence in situ hybridization (mFISH).

2.5.1. Fluorescence plus Giemsa staining

FPG staining enables to differentiate between first, second and later cell cycle after addition of 5-bromo-2-deoxyuridine (BrdU) to the cell culture. BrdU is an analogue of thymidine, which is incorporated in the DNA during replication in the S-phase. The procedure of the FPG staining was first described by Perry and Wolff [1974] and was used here with minor modifications [Ritter et al., 1996]. The microscope slides were incubated in 5 µg/ml Hoechst 33258 in ultrapure water for 1 h at room temperature in the dark, washed and air-dried. Afterwards, a buffer solution (19.45 ml Na_2HPO_4 (0.2 M) + 0.55 ml citric acid (0.1 M)) was dropped on each slide which was then covered

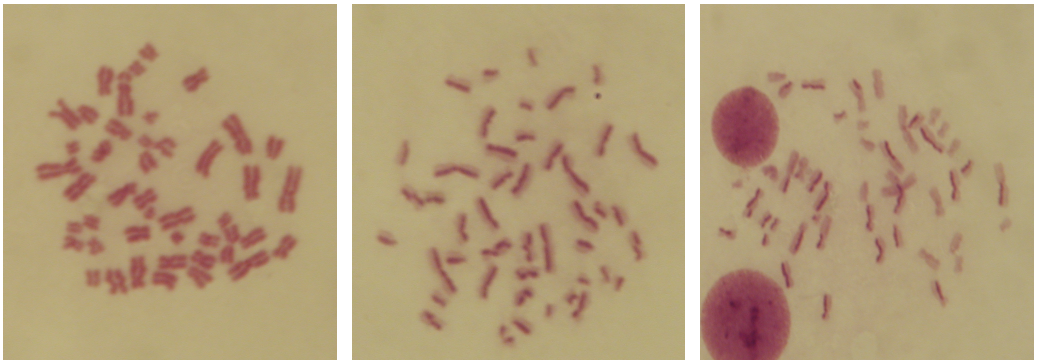

(a) (b) (c)

Figure 2.3.: Examples of FPG-stained metaphases. (a) First cycle, (b) second cycle and (c) third cycle metaphase.

with a cover glass. The samples were irradiated for 1 h with a low-pressure UV lamp ($\lambda = 360$ nm). Next, the slides were incubated in 2xSSC (saline-sodium citrate) buffer for 30 min at 55℃, washed in ultrapure water, air-dried and stored overnight. Finally, the microscope slides were stained with 5 % Giemsa solution in phosphate buffer (one part 0.067 M Na_2HPO_4 and one part 0.067 M KH_2PO_4) for 10 min, washed, dried overnight and embedded in Eukitt. Examples of metaphases stained with FPG-technique are shown in Figure 2.3.

2.5.2. Multiplex fluorescence in situ hybridization

Multiplex fluorescence in situ hybridization (mFISH) analysis was performed to yield detailed information about radiation-induced chromosomal aberrations in peripheral blood lymphocytes. For the mFISH analysis, slides were hybridized using the 24XCyte mFISH kit (Metasystems, Altlussheim, Germany) according to the protocol recommended by the manufacturer with minor modifications. The slides were pretreated with a pepsin solution (250 µl 0.2% pepsin stock solution in 50 ml 0.01 N HCl at 37℃ for one min) to digest remaining cytoplasmic proteins. After washing in PBS, the slides were incubated in 2xSSC at 70℃ for 30 min, followed by denaturation in 0.07 N NaOH for 1 min, washing and dehydration in ethanol. An appropriate volume (7µl for a 18x18 mm cover slip) of 24XCyte DNA probe was denatured meanwhile by incubating for 5 min at 75℃ and 30 min at 37℃. The denatured probe was then pipetted on the prepared microscope slide and covered with a glass cover slip (18x18 mm). The slide was incubated in a humidified chamber at 37℃ for three days. Afterwards, the remaining hybridization probe was washed off and the detection of the biotin-labeled probe was performed according to the manufacturer's protocol. Finally, all DNA material was counterstained

Fluorochrome	Excitation maximum	Emission maximum
DAPI	345 nm	455 nm
DEAC	426 nm	480 nm
FITC	495 nm	521 nm
SpO	559 nm	588 nm
TR	595 nm	651 nm
Cy5	649 nm	670 nm

Table 2.6.: Excitation and emission wavelengths of the fluorochromes used in the 24XCyte mFISH probe kit (Metasystems). The fluorochromes are 4',6-Diamidino-2-phenylindol (DAPI), 7-Diethylaminocoumarin-3-carboxylic acid (DEAC), Fluorescein (FITC), Spectrum Orange™ (SpO), Texas Red® (TR) and Cy™5 (Cy5).

using 4',6-Diamidino-2-phenylindol (DAPI) and the slide was covered with a glass cover slip. The chromosome spreads were analyzed using an Olympus BX61 microscope (Olympus, Tokyo, Japan) equipped with six-position slider holding filter sets specific for the applied fluorochromes. The used fluorochromes are Fluorescein (FITC), 7-Diethylaminocoumarin-3-carboxylic acid (DEAC), Spectrum Orange™ (SpO), Texas Red® (TR) Cy™5 (Cy5) and 4',6-Diamidino-2-phenylindol (DAPI). The excitation and emission wavelengths of the applied fluorochromes are listed in Table 2.6. Images of the metaphases were captured with a charge coupled device camera and karyotypes were constructed using the Isis/mFISH software (Metasystems).

When FPG analysis revealed that the fraction of first mitosis (M1) was less than 90%, the slide was destained and a FPG staining was performed to exclude second or third cycle mitoses. For FPG staining after mFISH, the DAPI was washed off and the FPG staining protocol was applied (see Section 2.5.1 for details). The last step of the FPG protocol, i.e. the staining with Giemsa solution, was substituted by DAPI staining. Afterwards the metaphases were relocated, examined and only first division cells were used for the analysis.

2.6. Scoring of chromosomal aberrations

For the analysis of patients' samples obtained before therapy the scoring of dicentrics on FPG stained slides was used. mFISH analysis of these samples was carried out in parallel, but only for selected patients. The samples from patients obtained during, at the end of and one year after therapy were analyzed with mFISH for all patients, as well as the samples for the in vitro dose-response curves. FPG analysis of samples obtained from the patients during and after therapy was performed in parallel.

2.6.1. Aberration scoring on FPG stained slides

FPG stained slides were analyzed regarding the cell cylce number after irradiation as described in Ritter et al. [1996] to identify first (M1) and second or later metaphases. Examples of FPG stained metaphase are shown in Figure 2.3. Aberration analysis was restricted to M1 cells. For patients' samples obtained during and after radiotherapy, aberrations in 200 M1 cells were analyzed and for in vitro irradiated samples in at least 100 M1 cells. For the aberration analysis, the scoring of dicentrics was chosen, as described by the International Atomic Energy Agency [2001]. Aberration scoring on FPG stained slides was carried out by Dr. Elena Nasonova.

2.6.2. Aberration scoring on mFISH stained slides

Analysis of mFISH stained metaphases was performed in at least 100 cells per sample. An example of the six individual images captured from each metaphase is given in Figure 2.4 (a) to (f). These six images are stored as an image stack and processed together. The background is subtracted and the chromosomes are separated automatically or by hand depending on the quality of the metaphase spread. After processing, the chromosomes are sorted in a karyogramm. An artificial color is assigned to each combination of fluorescent colors and these artificial colored chromosomes is displayed in the karyogramm. An example of a metaphase spread in artificial colors is given in Figure 2.4 (h), an example of a karyogramm in artificial colors is given in Figure 2.5 (a). In the karyogramm display, small colored circles and squares under each chromosome pair indicate the artificial color and the fluorochrome color(s) that characterize the specific chromosome.

To check each chromosome for the presence of chromosomal aberrations, a single color gallery showing the artificial color, the five specific fluorescence colors, an intensity profile of these five specific fluorescence colors along the chromosome axis and an inverted black and white image of the DAPI staining is used. Changes in the color spectrum within one chromosome show the exchange of DNA material between heterologous chromosomes. The origin of the inserted or exchanged chromosome part is determined by its specific fluorescent color signal(s). In most cases an exchange is also visible by a change in the artificial color assigned to the chromosome, but as small exchanges do not always result in a changing artificial color, the single color gallery is used for the analysis. The chromosome structure is investigated using the inverted DAPI image to determine the presence or absence of centromeres. Ring chromosomes are also identified on the basis of the DAPI image. Examples of the single color galleries are given in Figure 2.5 (b) to (d) for different chromosomes. Figure 2.6 (a) shows a karyotype carrying a dicentric chromosome and an acentric fragment. Figures 2.6 (b) and (c) show the single color galleries for both aberrant chromosomes, from the specific colors visible follows that

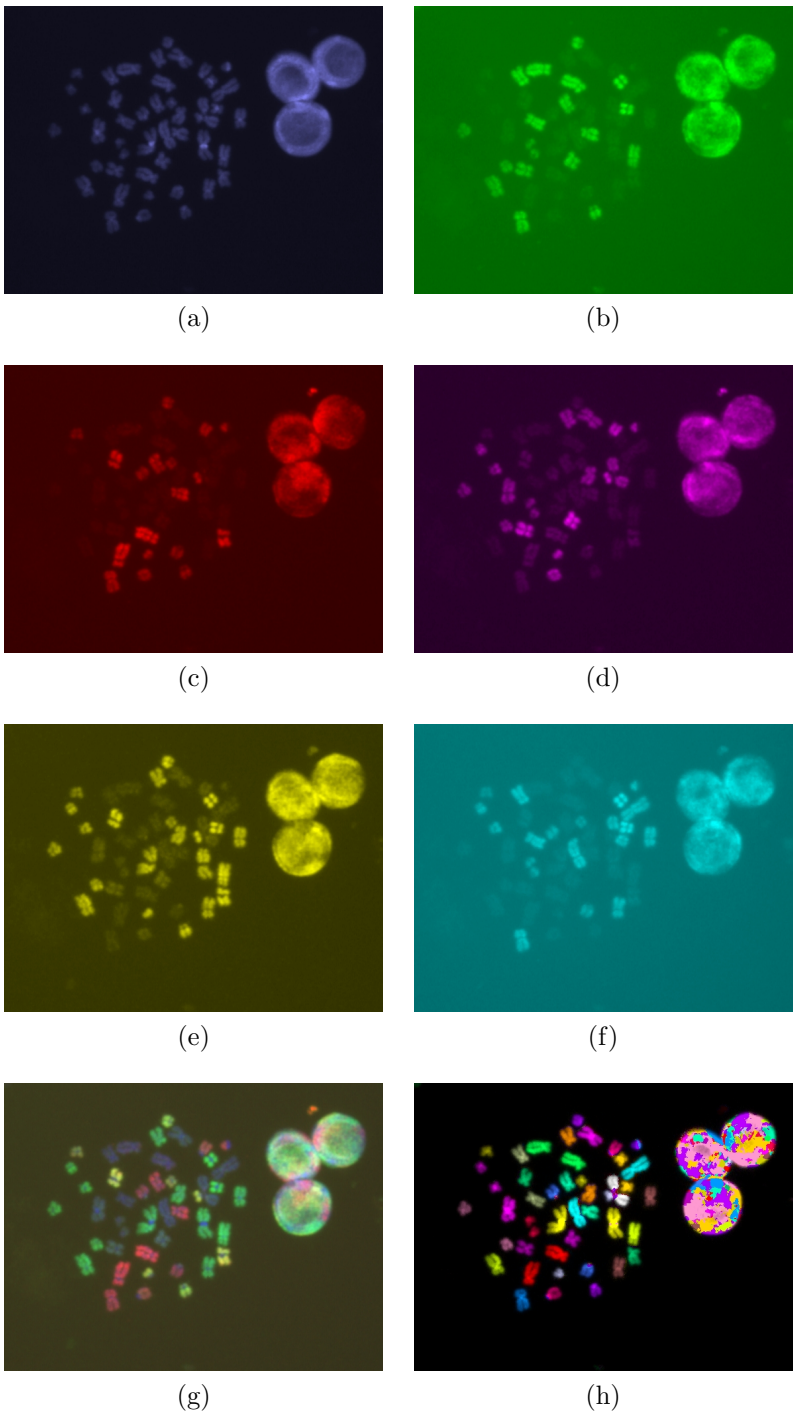

Figure 2.4.: Capture process of the mFISH images. This example shows one metaphase spread and three interphase nuclei. Panel (a) displays the DAPI color channel, Figures (b) to (f) show the FITC, SpO, TR, Cy5 and DEAC color channels. Panels (g) gives a three-color image composed of the DAPI, SpO and Cy5 images. The artificial color image is displayed in Panel (h).

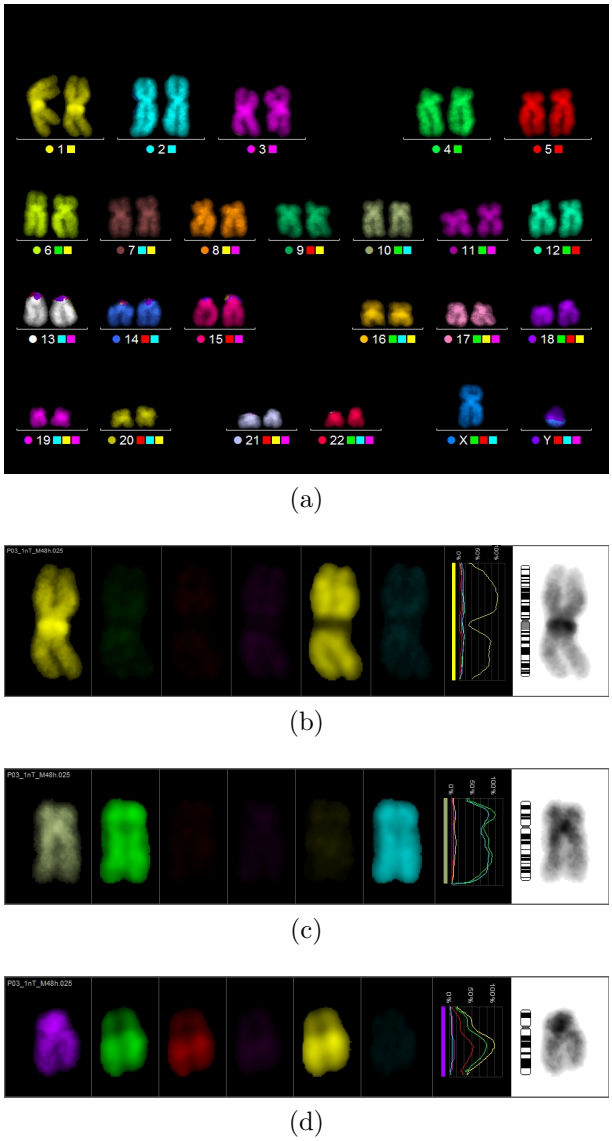

(a)

(b)

(c)

(d)

Figure 2.5.: Analysis of a mFISH stained metaphase. Panel (a) shows a normal human male karyotype; all chromosomes are displayed in artificial colors. Colored dots and squares in the karyogramm show the artificial color and the specific fluorochromes for each pair of homologue chromosomes. To check for aberrations, each chromosome is investigated using the single color gallery display, which is shown in Panels (b) to (d) for chromosome 1, 10 and 18. The single color gallery shows (from left to right) the chromosome in artificial colors, the five specific fluorochrome images, an intensity profile for the five specific fluorochromes and an inverted DAPI image.

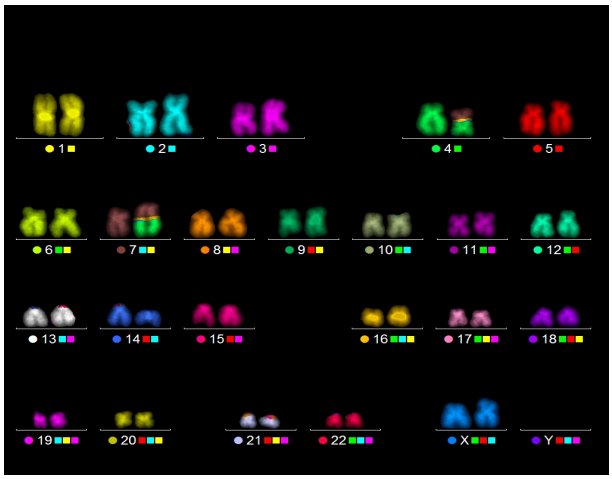

(a)

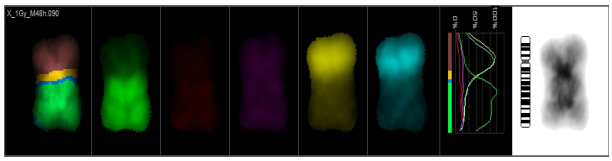

(b)

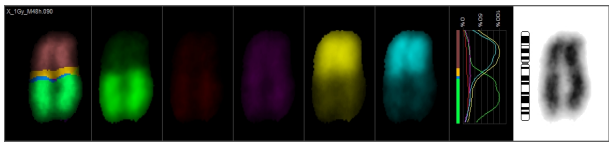

(c)

Figure 2.6.: mFISH stained female human metaphase with an aberration. Panel (a) shows the karyotype which displays a dicentric chromosome with an acentric fragment, panels (b) and (c) show the single color galleries for the two aberrant chromosomes. The changes of fluorochrome signals in the individual color channels and the intensity profile for these colors clearly indicate that there is a reciprocal exchange between chromosomes 4 and 7. Analysis of the inverted DAPI images reveals that it is a dicentric chromosome and an acentric fragment.

the dicentric chromosome and acentric chromosome involve chromosomes 4 and 7.

Intrachanges within one chromosome and exchanges between homologue chromosomes are only detectable on the basis of a changed length or shape of the chromosomes, but not on the basis of the characteristic color profile, as homologue chromosomes are painted with the same color pattern. In the case that an intrachange or exchange between homologue chromosomes was detected it was recorded.

2.6.3. mPAINT nomenclature

Aberrations observed using mFISH were recorded using the mPAINT descriptors [Cornforth, 2001; Loucas and Cornforth, 2001], which are an enhancement of the PAINT system (Protocol for Aberration Identification and Nomenclature Terminology) [Tucker et al., 1995] that is used for 1–3-color FISH. The mPAINT system describes the observed chromosomal aberrations by naming the chromosomes involved and indicating the position of the centromeres by an apostrophe following the chromosome number. Connections between chromosome parts are described by linking the chromosome numbers with a "-"sign, different aberrations are separated using a semicolon. Truncated chromosome are indicating by a "T", ring chromosomes by a "R". The aberration displayed in Figure 2.6 is written as (4'-7')(7-4) in mPAINT descriptors. Figure 2.7 shows examples of artificial color images of aberrations observed in this study. Figures 2.7 (a) - (g) show a truncated chromosome with linear acentric fragment, a dicentric chromosome with acentric fragment, a reciprocal translocation, a centric ring with acentric fragment, two complex exchanges that resulted from three or four breaks in three chromosomes and one insertion. The mPAINT descriptors for these aberrations are (T2')(2); (7'-9')(9-7); (4'-9)(9'-4); (R6')(6); (3-1')(1-X')(X-3'); (5-2'-4)(2)(5'-4'); and (5'-9-5)(T5').

2.6.4. Analysis of chromosomal aberrations

As mFISH allows a full analysis of chromosomal interchanges, many different aberrations can be distinguished and these aberrations can be grouped using different criteria. In this work, aberrations were grouped according to their complexity (excess acentric fragments, simple exchanges and complex exchanges), their transmissibility (transmissible or non-transmissible) and their completeness (complete, incomplete, one-way exchanges). In addition, the fraction of aberrant cells and the distribution of aberrations and breaks in the cells were determined.

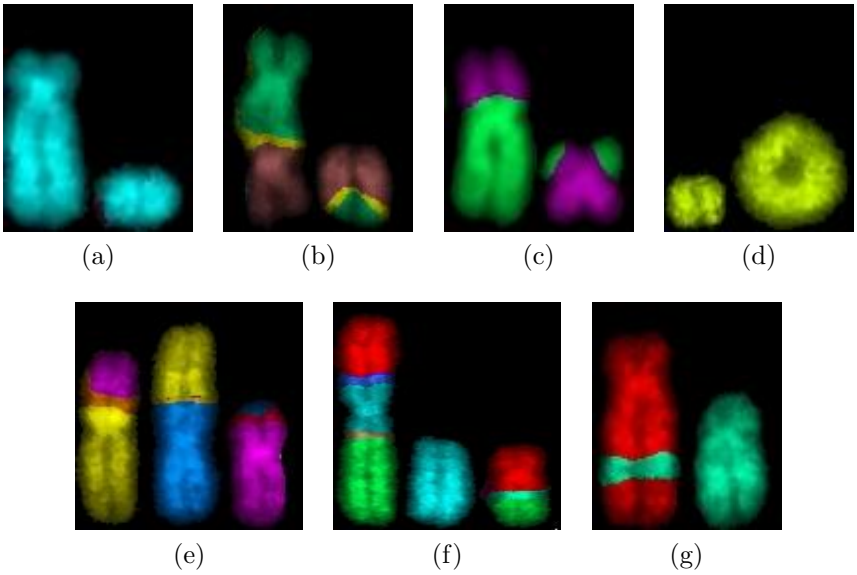

Figure 2.7.: Examples of chromosomal aberrations observed using mFISH analysis. The artificial color images of the aberrant chromosomes are shown. (a) truncated chromosome with acentric fragment, mPAINT (T2')(2); (b) dicentric chromosome with acentric fragment, mPAINT (7'-9')(9-7); (c) reciprocal translocation, mPAINT (4'-9)(9'-4); (d) centric ring with acentric fragment, mPAINT (R6')(6); (e) complex exchanges that resulted from three in three chromosomes, mPAINT (3-1')(1-X')(X-3'); (f) complex exchanges that resulted from four breaks in three chromosomes, mPAINT (5-2'-4)(2)(5'-4'); (g) insertion, i.e. complex aberration resulting from three breaks in two chromosomes, mPAINT (5'-9-5)(T5').

Excess acentric fragments

Excess acentric fragments include terminal deletions and interstitial deletions, as it is not possible to distinguish reliably between linear and circular fragments with mFISH staining. An example of a terminal deletion is shown in Figure 2.7 (a). Depending on the condensation of the chromosomes and the length of the fragment sometimes the difference in chromosome length is not visible and only the excess fragment is observed. It is also possible that a truncated chromosome is observed without an acentric fragment accompanying it, because small fragments can be lost during image processing due to their weak DAPI staining signal. The group of excess acentric fragments therefore includes three types of aberrations: truncated chromosomes with acentric fragments, lone truncated chromosomes and lone acentric fragments.

Simple exchanges

Simple exchanges are aberrations resulting from two double-strand breaks. The most frequent simple exchanges are reciprocal translocations and dicentrics with accompanying acentric fragments. Both aberration types are the result of two double-strand breaks in two chromosomes. Examples of a dicentric with acentric fragment and a reciprocal translocation are given in Figure 2.7 (b) and (c). Centric rings are less frequent; they result from two breaks in both arms of one chromosome. An example of a centric ring with accompanying linear acentric fragment is shown in Figure 2.7 (d). Pericentric inversions, i.e. breaks in both arms of one chromosome and inversion of the centromeric part, are rarely observed with mFISH, as they are detectable only if they result in a visible change of the centromere position in the chromosome, e.g. if chromosome 1, which is normally metacentric, displays a centromere close to the telomere region.

Complex exchanges

Complex aberrations are defined as aberrations resulting from at least three breaks in at least two chromosomes [Savage and Simpson, 1994]. They can be characterized by the use of the CAB (chromosomes/arms/breaks) system, which was introduced by Savage and Simpson [1994]. The CAB system gives the number of chromosomes involved in the aberration, the number of chromosome arms in which a break occurred and the total number of breaks that were necessary to produce the observed aberration. Examples of complex aberrations are given in Figure 2.7 (e) to (g). Figure 2.7 (e) shows an aberration with a CAB of (3/3/3), Figure 2.7 (f) shows an exchange with a CAB of (3/4/4). Figure 2.7 (g) shows an insertion, which is defined as a complex aberration with a CAB of (2/2/3).

Complete, incomplete and one-way exchanges

The system to classify aberrations in three groups according to their completeness was introduced by Cornforth [2001]. Complete exchanges are defined as exchanges which have all parts of the chromosomes visible and all "open DNA ends" induced by the initial breaks repaired. One-way exchanges are characterized by a missing part, e.g. there is a dicentric chromosome but the accompanying fragment is only displaying the color of one of both involved chromosomes. The missing part is assumed to be present but to small to be seen with the method applied. Incomplete exchanges are characterized by the presence of "open ends" i.e. there are unrejoined parts in the aberration. An example is a dicentric chromosome accompanied by two separate acentric fragments displaying only one of the two chromosome colors each.

Transmissible aberrations

Aberrations were subdivided according to their transmissibility to daughter cells. Specifically, reciprocal translocations were classified as transmissible and dicentrics, rings and acentric fragments as non-transmissible. Complex aberrations were classified as non-transmissible if they carried either a polycentric or an acentric part or a ring, or transmissible if neither of those.

Distribution of aberrations and breaks

The number of aberrations per cell was recorded for each analyzed metaphase. The resulting distribution of aberrations in the cell population was determined and compared to a Poisson and Neyman type A distribution.

After exposure to sparsely ionizing radiation like X-rays, where the dose-distribution is homogeneous on a microscopic scale, the distribution of aberrations in the cells is described by a Poisson distribution

$$P(k) = \frac{a^k e^{-a}}{k!} \tag{2.1}$$

with the expectation value a being the average number of aberrations per cell in the population. In contrast to X-rays, the microscopic dose distribution of densely ionizing radiation is inhomogeneous, with high local doses along the particle track (see Figure 1.3). To describe the distribution of aberrations in the cells induced by high-LET radiation, two independent variables are used, the number of particle tracks per cell and the number of aberrations induced by one particle traversal, both parameters are assumed to follow Poisson statistics [Virsik and Harder, 1981; Gudowska-Nowak et al., 2007]. With the mean number of particle traversals per cell nucleus λ, the distribution of particle tracks per cell nucleus is given by

$$P_\lambda(n) = \frac{\lambda^n e^{-\lambda}}{n!} \tag{2.2}$$

. The number of aberrations induced by n particle traversals is then described by

$$P_{n\mu}(m) = \frac{(n\mu)^m e^{-n\mu}}{m!} \tag{2.3}$$

with μ describing the mean number of aberrations induced by one particle traversal. The distribution of aberrations in the cells induced by densely ionizing radiation can then be described by a compound Poisson distribution

$$P(k) = \sum_{n=0}^{\infty} P_{n\mu}(m) P_\lambda(n) = \sum_{n=0}^{\infty} \frac{(n\mu)^m e^{-n\mu}}{m!} \frac{\lambda^n e^{-\lambda}}{n!} = \frac{\mu^k e^{-\lambda}}{k!} \sum_{n=0}^{\infty} \frac{n^k}{n!} (e^{-\mu}\lambda)^n \tag{2.4}$$

which is known as a Neyman type A distribution [Neyman, 1939]. Both distribution types, the Poisson and the Neyman type A distribution were used

in work presented here to describe the observed distribution of aberrations in the cells.

In addition, the total number of breaks per cell was calculated by summing up the number of breaks that lead to all visible aberrations in each cell. As the analysis was performed on metaphase cells 48 h after in vitro cultivation, the term "breaks per cell" does not refer to initially induced breaks, but to the breaks observed as aberrations after 48 h incubation, i.e. the breaks that were misrepaired leading to chromosomal exchanges and the unrepaired breaks that lead to terminal deletions.

2.7. Individual chromosomes

2.7.1. Involvement of individual chromosomes in aberrations

The involvement of individual chromosomes in aberrations was investigated. For this the number of breaks observed in each pair of homologue chromosomes was recorded and then plotted versus chromosome number and gene density. The number of genes on the individual chromosome and the length of the chromosome were taken from the homepage of the Ensembl project[1] and are given in Table A.1. The distribution of breakpoints in individual chromosomes was compared to two models, the length model, that assumes that the breakpoints observed on the basis of chromosomal aberrations are distributed according to the chromosome length, i.e. the DNA content f, and the surface model, which assumes that the breakpoints observed in chromosomal aberrations are distributed according to the surface of a chromosome territory in the interphase cell, i.e. according to $f^{2/3}$ [Cremer et al., 1996].

2.7.2. Exchanges between chromosomes - statistics for chromosome interphase positioning SCHIP

Chromosomes are believed to be located in distinct areas within the interphase cell nucleus, as described in Section 1.3.7. Chromosomal interchanges due to misrepair during the double-strand break repair process should then be more frequent between chromosomes located close to each other. Reversely, the observation of excess exchange rates for certain chromosome pairs can be regarded as a hint that theses chromosomes are located close to each other in the interphase nucleus.

For the analysis of exchange rates between chromosomes, a table was created with 22 rows and 22 columns, one for each pair of homologue chromosomes. All mFISH analyzed metaphases were analyzed regarding the observed

[1] http://www.ensembl.org/Homo_sapiens/Location/Genome

color changes, i.e. the interchanges between chromosomes. Each metaphase displaying at least one color change between chromosomes i and j increased in the table the value of the cell (i, j) by 1. The resulting table shows a triangular matrix with entries $f(i, j)$ that give the number of cells in which an interchange between chromosomes i and j was observed.

If a random participation of the chromosomes is assumed, the pairwise exchange yields can be written as products of single chromosome participation factors $f(i, j) = g(i)g(j)$. Deviations from this random model are a hint for the presence of chromosomal territories in the interphase nucleus. For the analysis of the table the software SCHIP (statistics for chromosome interphase positioning based on interchange data) was used, which is available on the Internet[2] and is described in publications by Cornforth et al. [2002]; Arsuaga et al. [2004]; Vives et al. [2005].

The table with the $f(i, j)$ values was uploaded to the SCHIP homepage. Candidate clusters that were to be tested in the data set were chosen from a set of reported clusters, or own candidate clusters were used. The first part of the output of the software is a table that shows the input data (pairwise chromosome yields) denoted by $f(i, j)$ in the upper left part of the table, the normalized single chromosome participation factors $g(i)$ along the diagonal of the table and the deviations from the expected values assuming a random model $\Delta(i, j)$ in the lower right part. The second part of the output is a list of p-values for the tested candidate clusters. For the comparison with the data obtained during the work presented here, tables with exchange yields provided on the SCHIP homepage were used, mainly the data set that was published by Arsuaga et al. [2004].

A set of chromosomes which are known to be located in close proximity to each other in the cell nucleus are the acrocentric chromosomes (i.e. chromosomes number 13, 14, 15, 21, and 22). Those chromosomes encode ribosomal genes on their short p-arms and are known to be located at the nucleoli in the interphase nucleus [Krystosek, 1998; Sullivan et al., 2001; Parada and Misteli, 2002; Kalmarova et al., 2007]. This chromosome cluster was used to test the method applied here using the SCHIP software to search for clusters.

2.8. Error propagation and statistical tests

2.8.1. Errors and error propagation

For stochastic events like aberrations induced by radiation the uncertainty of the counted number is estimated assuming Poisson statistics

$$\Delta x = \sqrt{\frac{x}{N}} \tag{2.5}$$

[2] http://cramer.stat.ub.es/schip/

where x is the counted number of events, e.g. simple or complex exchanges, and N is the total number of analyzed cells.

For the fraction of aberrant cells, the error bars were calculated assuming a binomial distribution

$$\Delta\left(\frac{a}{n}\right) = \sqrt{\frac{\frac{a}{n}\cdot\left(1-\frac{a}{n}\right)}{n}} \tag{2.6}$$

with a the number of aberrant cells and n the number of analyzed cells.

The errors of fractions such as the RBE values were calculated using error propagation

$$\frac{\Delta RBE}{RBE} = \sqrt{\left(\frac{\Delta D_{X-ray}}{D_{X-ray}}\right)^2 + \left(\frac{\Delta D_{C-ion}}{D_{C-ion}}\right)^2} \tag{2.7}$$

2.8.2. Chi-square test

The χ^2-test was applied to compare the observed distribution of breakpoints in the individual chromosomes to the expected distributions according to the chromosome length and chromosome surface model.

$$\chi^2 = \sum \frac{(O-E)^2}{E} \tag{2.8}$$

where E is the expected value and O the observed value for each chromosome pair. To test for significance, a χ^2 distribution table was used [Bailey, 1995]. A p-value of 0.05 was used for the significance tests based on χ^2.

2.8.3. Two-sample t-test

The two-sample t-test was used to test the patient group data for significant differences. For two sample sets 1 and 2 the two-sample t is calculated as

$$t = \frac{\overline{x}_1 - \overline{x}_2}{s\cdot\sqrt{\frac{1}{n_1}+\frac{1}{n_2}}} \tag{2.9}$$

where $\overline{x}_1$ and $\overline{x}_2$ are the mean values of the sample sets 1 and 2, n_1 and n_2 the sample sizes of both groups and s is an estimate of the standard deviation based on both samples. s is calculated as

$$s = \sqrt{\frac{\sum {x_1}^2 - \frac{(\sum x_1)^2}{n_1} + \sum {x_2}^2 - \frac{(\sum x_2)^2}{n_2}}{n_1+n_2-2}} \tag{2.10}$$

. The t-value is then compared to a Student's t-distribution table, e.g. Bailey [1995]. A p-value of 0.05 was used for the significance tests.

For comparison of different patient groups two-tailed tests were applied. When comparing the aberration yield one year after therapy with the yield

at the end of therapy a one-tailed test was applied, as it can be assumed that the aberration yield decreases or stays unchanged in the year after therapy but does not increase any further.

2.8.4. Fisher's exact test

Fisher's exact test was used on the number of aberrant and non-aberrant cells at the end of therapy and one year after therapy in each individual patient from whom both samples were obtained. To calculate the p-value, a 2x2-table was created:

	number of aberrant cells	number of non-aberrant cells
end of therapy	a	b
1 year after therapy	c	d

The p-value is then calculated via

$$p = \frac{(a+b)! \cdot (c+d)! \cdot (a+c)! \cdot (b+d)!}{n! \cdot a! \cdot b! \cdot c! \cdot d!} \tag{2.11}$$

with n the sum of all entries in the table. As mentioned above, for the comparison of aberration data obtained at the end of therapy with data obtained one year after therapy a one-sided test was used.

3. Results

3.1. In vitro experiments

In vitro experiments were carried out to investigate the effects of X-rays and C-ions of different energies on the aberration yield and aberration pattern induced in human peripheral blood lymphocytes. In addition, the resulting dose-effect curves were used for comparison with the data obtained in vivo in the peripheral blood lymphocytes of prostate-cancer patients irradiated with C-ion boost plus IMRT or only IMRT, which are described in Section 3.2.

3.1.1. Fraction of aberrant cells and aberrations per cell

The fraction of cells carrying at least one chromosomal aberration (excess acentric fragment, simple or complex exchange) was investigated on mFISH stained slides. In parallel to the mFISH analysis a FPG staining was performed to determine the fraction of M1 cells, and if it was found that less than 90% of the mitotic cells were in M1 a modified FPG protocol was applied to the mFISH stained sample to exclude cells in second or third metaphase from the analysis (see Section 2.5.2). The lymphocytes were irradiated in vitro with different doses of X-rays and accelerated C-ions. The percentage of aberrant cells is displayed in Figure 3.1. The fraction of aberrant cells increases with dose and approaches 100% for high doses. The increase with dose is steeper for low-energetic C-ions (extended Bragg peak and 100 MeV/u) than for high-energetic C-ions (270 MeV/u) and X-rays.

The mean number of aberrations per cell was determined for each radiation quality and dose. The resulting dose-effect curves are given in Figure 3.2 for irradiation with X-rays, 270 MeV/u, 100 MeV/u and extended Bragg peak C-ions. All types of chromosomal aberrations observed using mFISH analysis were included. The yield of aberrations per cell increases with dose, the slope is steeper for densely ionizing radiation (C-ions with an energy of 100 MeV/u and extended Bragg peak C-ions) compared to sparsely ionizing radiation (C-ions with an energy of 270 MeV/u and X-rays). The increase follows a linear-quadratic pattern in the case of exposure to X-rays and 270 MeV/u C-ions and shows a linear behavior in the case of exposure to C-ions with an energy of 100 MeV/u and extended Bragg peak C-ions.

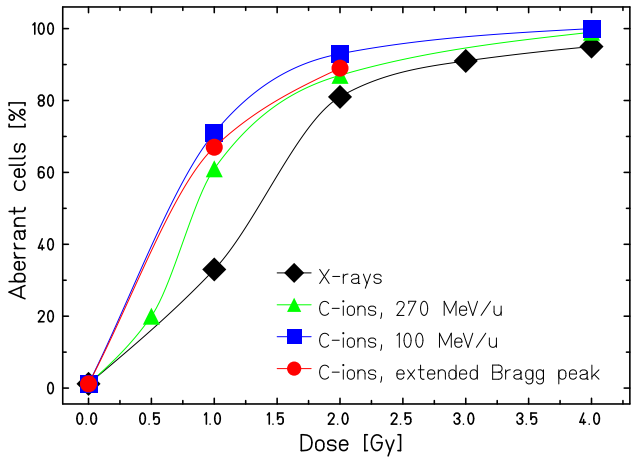

Figure 3.1.: Percentage of aberrant peripheral blood lymphocyte metaphases after exposure to different doses of X-rays and C-ions with different energies. Aberration analysis was performed on mFISH stained M1 metaphases after 48 h incubation. Lines are guides for the eye. Error bars are too small to be visible.

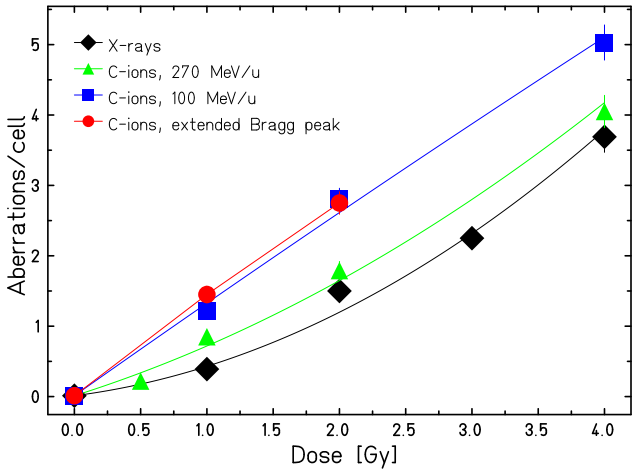

Figure 3.2.: Dose-effect curves for the mean number of aberrations per cell induced by doses of 0–4 Gy X-rays and C-ions with three different energies. The dose-effect curves of X-rays and 270 MeV/u C-ions were fitted using a linear-quadratic function, the dose-effect curves of 100 MeV/u and extended Bragg peak C-ions were fitted with a linear function. Erro

3.1.2. Simple and complex exchanges

To investigate differences in the aberration spectrum, the yields of simple exchanges, i.e. exchanges resulting from two chromosome breaks, and complex exchanges, i.e. exchanges involving three or more breaks in at least two chromosomes [Savage and Simpson, 1994], were analyzed separately. The resulting dose-effect curves for the induction of simple and complex chromosomal exchanges are displayed in Figures 3.3 (a) and (b). The number of exchanges per cell increases with increasing dose. The induction of simple exchanges follows a linear pattern in the investigated range of doses and LET values. The induction of complex exchanges follows a linear-quadratic pattern for the irradiation with X-rays and C-ions with energies of 270 MeV/u and 100 MeV/u. The induction of complex exchanges by extended Bragg peak C-ions was fitted by a linear function in the investigated dose range, however as only two doses (1 and 2 Gy) were used for this radiation quality extrapolation to higher doses would be associated with a high degree of uncertainty.

3.1.3. Relative biological effectiveness

From the dose-effect curves the RBE was determined for the induction of total aberrations, simple and complex exchanges as described in Section 1.3.5. Table 3.1 lists the RBE values for the induction of 0.5, 1 and 2 aberrations per cell (taking into account all aberrations detected with mFISH), 0.5 and 1 simple exchanges per cell and 0.5 and 1 complex exchanges per cell for the three energies of the C-ion beams used in the experiments. When the dose-effect curves are not purely linear, the RBE value depends on the level of damage, e.g. the RBE for the induction of 0.5 aberrations per cell by extended Bragg peak C-ions is 3.17 ± 0.41 while it is 1.92 ± 0.19 for the induction of two aberrations per cell. Table 3.1 shows, that only moderately elevated RBE values are found for C-ions with an energy of 270 MeV/u, while C-ions with an energy of 100 MeV/u and extended Bragg peak C-ions show RBE values of about three. In addition, the RBE_α values were determined from the initial slopes of the dose-response curves. The RBE_α values for the induction of chromosomal aberrations were calculated from Figure 3.2.

3.1.4. C-ratio

The ratio of complex to simple exchanges, the so-called C-ratio is discussed as a biomarker for densely ionizing radiation (see Section 1.3.6). The C-ratio is derived from the dose-effect curves for the induction of simple and complex exchanges. For the four investigated radiation types, Figure 3.4 shows that the C-ratio increases for a given dose with increasing LET of the radiation, confirming that a high C-ratio can indeed be regarded as a biomarker for an exposure to densely ionizing radiation. However, comparison of different

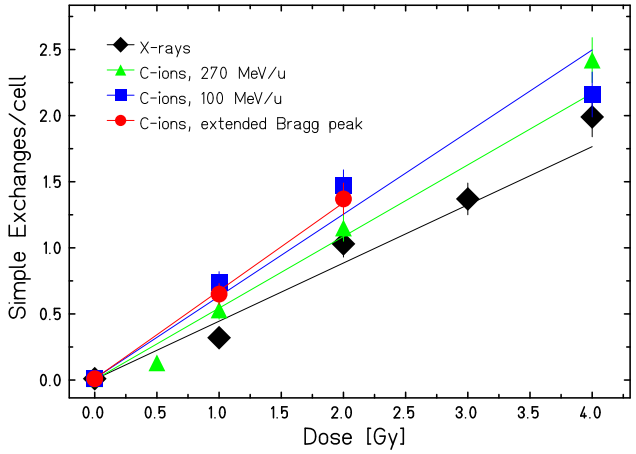

(a)

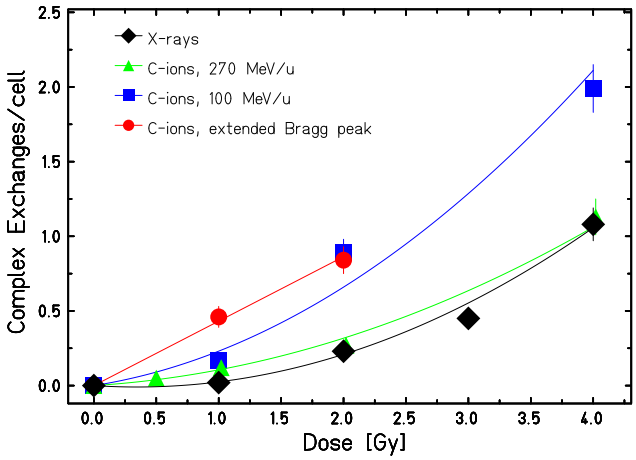

(b)

Figure 3.3.: Yield of chromosomal exchanges induced by different doses of X-rays and C-ions with energies of 270 MeV/u and 100 MeV/u and extended Bragg peak C-ions. (a) Simple exchanges, i.e. exchanges resulting from two chromosome breaks. Data were fitted using linear functions. (b) Complex exchanges, which are defined as aberrations involving three or more breaks in at least two chromosomes. Lines were fitted using linear-quadratic functions for X-rays and C-ions with energies of 270 MeV/u and 100 MeV/u or a linear function for the extended Bragg peak C-ions. (Figures are taken from Hartel et al. [2010].)

	C-ions 270 MeV/u	C-ions 100 MeV/u	C-ions ext. Bragg peak
0.5 aberrations/cell	1.54 ± 0.25	2.92 ± 0.38	3.17 ± 0.41
1 aberration/cell	1.34 ± 0.53	2.31 ± 0.24	2.51 ± 0.28
2 aberrations/cell	1.18 ± 0.17	1.79 ± 0.17	1.92 ± 0.19
0.5 simple exch./cell	1.22 ± 0.11	1.42 ± 0.13	1.51 ± 0.15
1 simple exch./cell	1.23 ± 0.10	1.42 ± 0.11	1.52 ± 0.14
0.5 complex exch./cell	1.08 ± 0.49	2.02 ± 1.32	2.47 ± 1.41
1 complex exch./cell	1.05 ± 0.38	1.66 ± 0.89	1.72 ± 0.74
initial slope	2.5 ± 0.6	5.5 ± 1.2	5.8 ± 1.2

Table 3.1.: RBE values for the induction of aberrations, simple and complex exchanges in the in vitro irradiated peripheral blood lymphocytes of a healthy donor. Aberrations were scored on mFISH stained metaphase spreads. RBE values were calculated from the data shown in the Figures 3.2, 3.3 (a) and 3.3 (b). The RBE_α values were determined from the initial slopes of the dose-responsponse curves for the induction of aberrations (Figure 3.2). The errors of the RBE values were calculated from the errors of the fit parameters of the dose effect curves. exch. = exchanges.

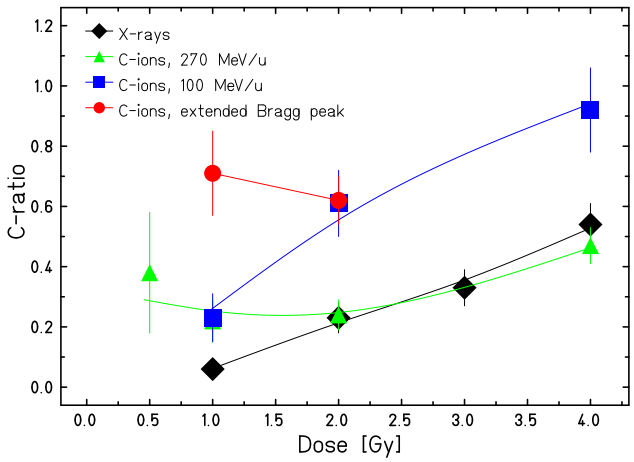

Figure 3.4.: Ratio of complex to simple exchanges, C-ratio, as a function of dose for the irradiation of lymphocytes with C-ions of different energies or X-rays. The C-ratio is derived from Figure 3.3 (a) and (b).

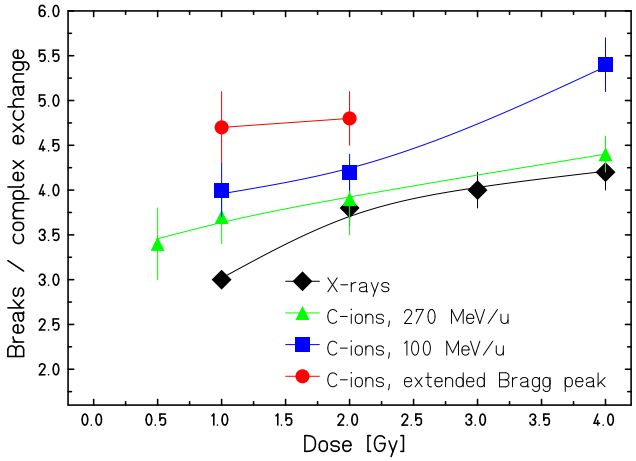

Figure 3.5.: Mean number of breaks per complex aberration induced by different doses of X-rays or C-ions of different energies in isolated peripheral blood lymphocytes irradiated in vitro.

doses of one radiation quality shows an increase of the C-ratio with the dose. This makes it difficult to conclude whether an observed elevated C-ratio was induced by densely ionizing radiation, or by a high dose of sparsely ionizing radiation. For extended Bragg peak C-ion irradiation, the C-ratios for doses of 1 Gy and 2 Gy are similar. However, to draw a definitive conclusion whether the C-ratio for extended Bragg peak C-ions is dose-dependent or not, broader dose ranges are necessary.

3.1.5. Complexity of complex exchanges

The mFISH method allows a detailed analysis of the complex aberrations regarding the involved chromosomes and the number of breaks that were necessary to produce the observed aberrations. Thus, not only the yield of complex exchanges was investigated, which is shown in Figure 3.3 (b), but also the complexity of each individual complex aberration. To show the effect of the radiation quality and dose on the complexity of the induced complex exchanges, the mean number of breaks per complex aberration was calculated for each dose and radiation quality and is shown in Figure 3.5. The mean number of breaks per complex aberration increases with the LET in the investigated LET range, but as the C-ratio, the complexity of complex aberrations is also dose-dependent and increases with higher doses.

3.1.6. Transmissible and non-transmissible exchanges

To investigate which fraction of induced aberrations can be passed to daughter cells without causing problems during cell division, the aberrations were

divided into transmissible and non-transmissible ones and the ratio of transmissible to non-transmissible aberrations was calculated (see Table 3.2).

The ratio of (transmissible) translocations to (non-transmissible) dicentrics with acentric fragments is close to one. Summing up translocations and dicentrics for all radiation qualities and doses yields 735 translocations and 730 dicentrics indicating that translocations and dicentrics are induced with the same probability.

Complex aberrations show a different pattern regarding their transmissibility. The induction of non-transmissible complex aberrations is much more frequent than the induction of transmissible ones. In addition, the fraction of transmissible complex exchanges seems to decrease with increasing dose, although large uncertainties at low doses hamper a statistical analysis.

3.1.7. Incomplete aberrations

The exchanges observed after in vitro exposure were analyzed regarding their completeness as defined in a publication by Cornforth [2001] and described in Section 2.6.4, i.e. the simple and complex exchanges were divided into the groups of complete exchanges, incomplete exchanges and one-way exchanges. Table 3.3 shows the numbers of observed exchanges and the fraction on incomplete simple and incomplete complex exchanges. To achieve smaller error bars, the fraction of incomplete exchanges was also calculated for both simple and complex exchanges together. The fraction of incomplete exchanges increases with dose. In addition, the fraction of incomplete exchanges increases with increasing LET.

3.1.8. Distribution of aberrations and breaks in the cells

The distribution of aberrations in the the cells was analyzed. As shown in Figure 3.6, the distributions of aberrations in the cells after irradiation with different doses of X-rays are in good agreement with Poisson distributions (Eq. 2.1), which are represented by the solid lines in the figure. The resulting fit parameters a, the mean value of the Poisson distribution, are 0.83 ± 0.04, 1.57 ± 0.13, 2.20 ± 0.14 and 3.84 ± 0.22 for doses of 1, 2, 3 and 4 Gy. Thus the mean value of induced aberrations per cell increases with dose. The maximum number of aberrations in one cell increased from 3 aberrations per cell at a dose of 1 Gy to 10 aberrations per cell at a dose of 4 Gy.

Radiation quality	Dose [Gy]	n	ace	t	dic	r	tr. comp.	ntr. comp.	ratio t/dic	ratio tr./ntr comp.	ratio tr./ntr.
X-rays	1	207	10	24	39	4	1	3	0.61 ± 0.15	0.33 ±0.38	0.45 ± 0.11
X-rays	2	101	25	49	49	5	0	24	1 ± 0.2	0	0.48 ± 0.08
X-rays	3	102	43	66	66	7	9	37	1 ± 0.17	0.24 ± 0.09	0.49 ± 0.07
X-rays	4	85	52	78	78	12	8	84	1 ± 0.16	0.095 ± 0.035	0.38 ± 0.05
C 270 MeV/u	0.5	101	4	6	7	0	2	3	0.86 ± 0.48	0.66 ± 0.61	0.57 ± 0.25
C 270 MeV/u	1	104	21	21	27	7	5	7	0.78 ± 0.22	0.71 ± 0.42	0.42 ± 0.10
C 270 MeV/u	2	106	39	55	53	10	5	24	1.03 ± 0.2	0.21 ± 0.1	0.48 ± 0.08
C 270 MeV/u	4	79	42	98	77	14	14	75	1.27 ± 0.19	0.19 ± 0.05	0.54 ± 0.07
C 100 MeV/u	1	107	35	41	38	0	4	14	1.07 ± 0.24	0.29 ± 0.16	0.52 ± 0.1
C 100 MeV/u	2	103	45	69	71	7	14	78	0.97 ± 0.16	0.18 ± 0.05	0.41 ± 0.05
C 100 MeV/u	4	79	69	89	74	8	18	139	1.20 ± 0.19	0.13 ± 0.03	0.37 ± 0.04
C ext. Bragg peak	1	102	35	24	36	7	7	40	0.66 ± 0.17	0.18 ± 0.07	0.26 ± 0.05
C ext. Bragg peak	2	103	55	66	64	9	8	79	1.03 ± 0.18	0.10 ± 0.04	0.36 ± 0.05

Table 3.2.: Aberrations found in in vitro irradiated peripheral blood lymphocytes after 48 h in vitro growth. From the observed aberrations the ratio of transmissible to non-transmissible exchanges was calculated. n = number of analyzed cells, ace = excess acentric fragments, t = translocations, dic = dicentric chromosomes, r = centric rings with acentric fragments, tr. comp. = transmissible complex exchange, ntr. comp. = non-tramsmissible complex exchange, tr. = transmissible exchanges (i.e. t + tr. comp.), ntr. = non-transmissible aberrations (i.e. ace + dic + r + n-tr. comp.).

	Dose	n	Simple exchanges			Complex exchanges			Fraction of incomplete		
	[Gy]		comp.	inc.	o-w.	comp.	inc.	o-w.	simple	complex	all
X-rays	1	207	53	1	13	4	0	0	0.015 ± 0.015	0	0.014 ± 0.014
X-rays	2	101	81	2	21	17	3	4	0.019 ± 0.014	0.125 ± 0.077	0.039 ± 0.018
X-rays	3	102	102	5	33	29	1	16	0.036 ± 0.016	0.022 ± 0.022	0.032 ± 0.013
X-rays	4	85	116	10	43	50	12	28	0.059 ± 0.019	0.133 ± 0.041	0.085 ± 0.019
C 270 MeV/u	0.5	101	11	0	2	1	0	4	0	0	0
C 270 MeV/u	1	104	48	0	7	8	0	4	0	0	0
C 270 MeV/u	2	106	109	1	12	17	3	9	0.008 ± 0.008	0.103 ± 0.063	0.026 ± 0.013
C 270 MeV/u	4	79	151	6	34	58	9	21	0.031 ± 0.013	0.102 ± 0.036	0.054 ± 0.014
C 100 MeV/u	1	107	66	2	11	14	1	3	0.025 ± 0.018	0.056 ± 0.056	0.031 ± 0.018
C 100 MeV/u	2	103	117	4	29	47	15	30	0.027 ± 0.014	0.163 ± 0.045	0.079 ± 0.019
C 100 MeV/u	4	79	142	9	21	86	29	41	0.052 ± 0.018	0.186 ± 0.038	0.116 ± 0.020
C ext. Bragg	1	102	52	2	12	32	8	7	0.030 ± 0.022	0.170 ± 0.065	0.088 ± 0.029
C ext. Bragg	2	103	96	16	29	56	9	22	0.113 ± 0.030	0.103 ± 0.036	0.110 ± 0.023

Table 3.3.: Chromosomal exchanges observed in peripheral blood lymphocytes after exposure to X-rays and C-ions of different LET, categorized according to their completeness. Ext. Bragg = extended Bragg peak, n = number of analyzed cells, comp. = complete exchanges, inc. = incomplete exchanges, o-w. = one-way exchanges according to the definitions in Loucas and Cornforth [2001].

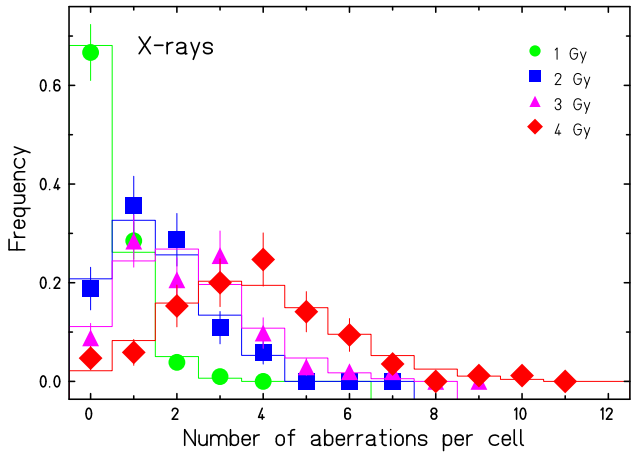

Figure 3.6.: Distribution of aberrations in the cells induced by different doses of X-rays. The solid lines represent a Poisson distribution fitted to the experimental data.

To compare the effects of different radiation qualities, the distributions of aberrations induced by 1 Gy and 2 Gy of X-rays and C-ions of different energies are shown in Figure 3.7 (a) and (b). Poisson distributions were fitted to the X-ray, 270 MeV/u and 100 MeV/u C-ion data, and are shown by the solid lines in the figures. The resulting fit parameters a are given in Table 3.4. For the extended Bragg peak C-ion data, it was found that a Neyman type A distribution (Eq. 2.4) is in better agreement with the measured data than a Poisson distribution. This can be expected, as described in Section 2.6.4, by the inhomogeneous microscopic dose distribution of the densely ionizing extended Bragg peak C-ions. The fit parameters λ, the mean number of particle traversals per cell nucleus, and μ, the mean number of aberrations induced by one particle traversal, are given in Table 3.5. The mean number of aberrations per cell can then be calculated as the product of λ and μ and is given in Table 3.5.

As mFISH allows a good analysis of the breaks that lead to the observed aberrations, it is possible to determine the minimum number of breaks necessary to produce the observed aberration(s) in each analyzed metaphase. The resulting distribution of breaks involved in aberrations is given in Figure 3.8 for irradiation with different doses of X-rays and in Figure 3.9 (a) and (b) for irradiation with X-rays, 270 MeV/u, 100 MeV/u and extended Bragg peak C-ions with doses of 1 Gy and 2 Gy. As the analysis was performed in metaphase cells 48 h after irradiation, the term "breaks per cell" refers to the breaks that lead to the observed aberrations, not to the number of initially induced breaks. The distributions show a up and down pattern with high incidences of cells with 0, 2 and 4 breaks involved in aberrations and low frequencies of cells with 1 and 3 breaks involved in aberrations. This is a result of the different frequencies of the aberration types. Simple exchanges (i.e.

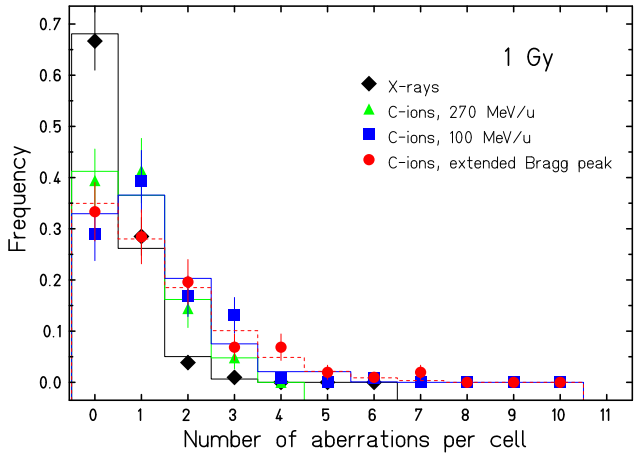

(a)

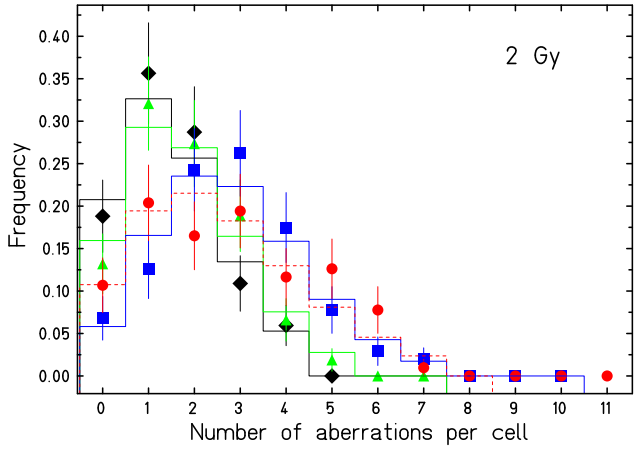

(b)

Figure 3.7.: Distribution of aberrations in the cells induced by (a) 1 Gy and (b) 2 Gy of X-rays, 270 MeV/u C-ions, 100 MeV/u C-ions and extended Bragg peak C-ions. Solid lines were fitted using a Poisson distribution; dashed lines represent a Neyman type A distribution fitted to the data.

Radiation quality	1 Gy	2 Gy
X-rays	0.38 ± 0.04	1.57 ± 0.13
C-ions 270 MeV/u	0.88 ± 0.10	1.84 ± 0.13
C-ions 100 MeV/u	1.11 ± 0.10	2.84 ± 0.17

Table 3.4.: Fit parameters a obtained from the Poisson distribution fitted to the distribution of aberrations in the peripheral blood lymphocytes exposed to doses of 1 and 2 Gy X-rays, 270 MeV/u C-ions and 100 MeV/u C-ions in Figure 3.7.

	1 Gy	2 Gy
λ	2.6 ± 1.0	6.7 ± 3.4
μ	0.52 ± 0.22	0.41 ± 0.22
$\lambda\mu$	1.35 ± 0.77	2.7 ± 1.9

Table 3.5.: Fit parameters λ and μ obtained from the Neyman type A distribution fitted to the distribution of aberrations induced by extended Bragg peak C-ions. The distribution of aberrations and the Neyman type A fit are shown in Figure 3.7.

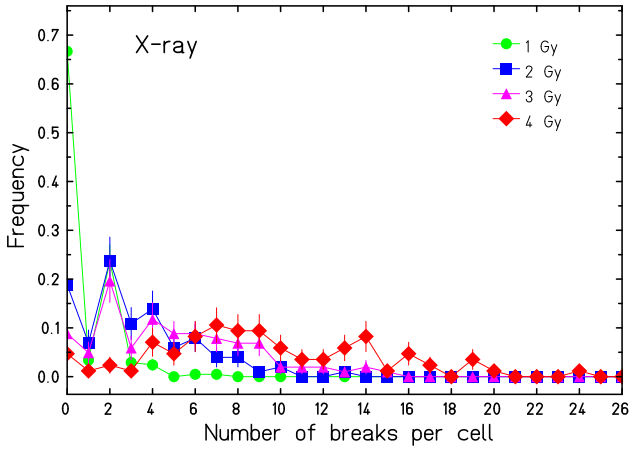

Figure 3.8.: Distribution of breaks involved in aberrations in the cells irradiated with different doses of X-rays.

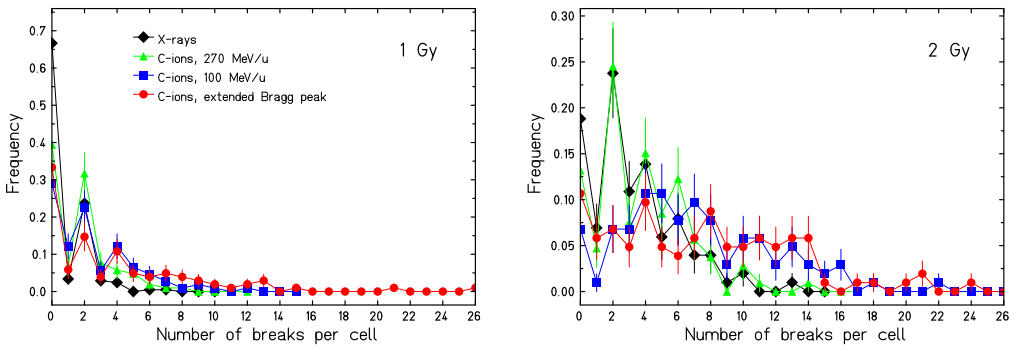

(a) (b)

Figure 3.9.: Distribution of breaks involved in aberrations in the cells induced by (a) 1 Gy and (b) 2 Gy of X-rays, 270 MeV/u C-ions, 100 MeV/u C-ions and extended Bragg peak C-ions.

reciprocal translocations, dicentrics and centric rings) are the most frequent chromosomal aberrations found after exposure to ionizing radiation, unless very high doses or very high LET radiations are applied (see Table 3.2). Cells carrying one simple exchange are therefore frequent and this explains the peak at 2 breaks per cell. Two simple exchanges in one cell are the main contribution to the peak at 4 breaks per cell, only for high doses complex aberrations with 4 breaks contribute to this peak to a large extend. Aberrations with one break, i.e. excess acentric fragments, are less frequent (again, see Table 3.2). This results in the low frequency of cells with one break. Three breaks involved in aberrations in one cell are visible either as the result of one complex aberration or as a simple exchange plus an excess acentric fragment. Excess acentric fragments are rare, and complex aberrations are frequent after exposure to high doses only leading to a reduced frequency of cells containing three breaks involved in aberrations.

3.1.9. Time-dependence of aberration yield

High-LET radiation induces, in contrast to low-LET radiation, a pronounced cell cycle delay of heavily damaged cells [George et al., 2001; Ritter et al., 2002a,b; Gudowska-Nowak et al., 2005; Lee et al., 2005]. To see whether this occurs in the LET range applied in this study, cells were harvested at 72 h in addition to the standard harvesting time and analyzed using mFISH for selected radiation qualities and doses. Table 3.6 compares the aberrations observed in M1 cells after exposure to 2 Gy 270 MeV/u and extended Bragg peak C-ions after 48 h and 72 h incubation. After exposure to 270 MeV/u C-ions the fraction of aberrant cells, the mean number of aberrations per cell and the incidences of simple and complex exchanges are in excellent agreement in M1 cells incubated for 48 h and 72 h, indicating that there is no cell cycle delay of heavily damaged cells. In contrast, in the cells exposed to extended Bragg peak C-ions an increase in aberration frequency from 48 h to 72 h incubation time is observed. This increase is highest for complex aberrations, where the number of complex aberrations per cell increases by about 50%.

	270 MeV/u C-ions		Ext. Bragg peak C-ions	
	M48 h	M72 h	M48 h	M72 h
aberrant cells (%)	87 ± 3.3	90 ± 2.9	89 ± 3	99 ± 1
aberrations/cell	1.79 ± 0.13	1.76 ± 0.13	2.75 ± 0.16	3.30 ± 0.18
simple exch./cell	1.15 ± 0.10	1.15 ± 0.11	1.37 ± 0.12	1.48 ± 0.12
complex exch./cell	0.27 ± 0.05	0.33 ± 0.06	0.84 ± 0.09	1.31 ± 0.11

Table 3.6.: Time-dependence of aberrations induced in peripheral blood lymphocytes by 2 Gy C-ions with an energy of 270 MeV/u and extended Bragg peak C-ions. Aberration analysis was performed in M1 cells after 48 h and 72 h of incubation. exch. = exchanges.

3.2. Aberrations in prostate-cancer patients

To monitor the cytogenetic effect of radiotherapy, blood samples from patients with prostate cancer were obtained before, during and at the end of radiotherapy as well as one year after treatment. Special interest was the comparison of patients treated with a C-ion boost followed by IMRT with patients receiving only IMRT. These two patient groups had similar tumor stages and target volumes. A third group of patients was included in the study to investigate the influence of the target volume on the aberration yield, to these patients a larger PTV that included the pelvic lymph nodes was applied. Details about the three patient groups have been given in Section 2.1.1.

3.2.1. In vitro irradiation of blood samples received before therapy

A blood sample of about 8 ml was obtained from each patient before the beginning of radiotherapy. The isolated lymphocytes were divided into two samples, one served as unirradiated control to detect possible chromosomal aberrations present before the beginning of therapy, the other was irradiated in vitro with X-rays with a dose of 3 Gy to test for individual radiosensitivity (see Section 2.3.1). Blood samples of healthy volunteers were used for comparison. Samples from all patients and healthy volunteers were analyzed using FPG staining. The scoring of dicentrics was used as described in Section 2.6.1. Samples from selected patients and from one healthy volunteer were additionally analyzed using mFISH.

The aberration yield observed in the unirradiated blood samples was low. Analysis of FPG-stained slides yielded 9 dicentrics in 4250 analyzed cells (=0.002 per cell) in the samples from patients and 0 dicentrics in 2300 analyzed cells in the samples from healthy volunteers. Results of the mFISH analysis are given in Table 3.7.

A sample of isolated peripheral blood lymphocytes from each patient was exposed to 3 Gy X-rays. The yield of dicentrics (based on FPG analysis) is given in Figure 3.10 for each individual patient and for the healthy volunteers. Each symbol in Figure 3.10 represents a different patient or healthy volunteer. The mean values are very similar for the patient group and the healthy volunteer group, 3 Gy of X-rays induced on average 1.00 ± 0.11 and 0.99 ± 0.05 dicentric chromosomes per cell in the patients and healthy volunteers, respectively. Remarkably, there is no outstanding radiosensitive patient observed.

To investigate the variation of induced damage within a single individual, two or more samples were obtained from some healthy volunteers at different times. Samples from the same donor are displayed in Figure 3.10 by the same symbol (e.g. upright triangle symbols and square symbols). From this it can

	Patients	Health volunteer
scored cells	773	595
translocations	10 (1.29 ± 0.41)	1 (0.168 ± 0.168)
dicentrics	1 (0.129 ± 0.129)	1 (0.168 ± 0.168)
complex exchanges	1 (0.129 ± 0.129)	2 (0.336 ± 0.237)
all transmissible exchanges	10 (1.29 ± 0.41)	2 (0.336 ± 0.237)
all acentric fragments[a)]	10 (1.29 ± 0.41)	10 (1.68 ± 0.531)

Table 3.7.: Aberrations found in mFISH stained metaphase spreads from selected patients (n=6) before therapy and in a sample from one healthy volunteer. Values in parentheses give the frequency of aberration per 100 cells. [a)]All acentric fragments include fragments associated with dicentric chromosomes, this modified scoring criterion is used to allow comparison with literature data [Ramsey et al., 1995].

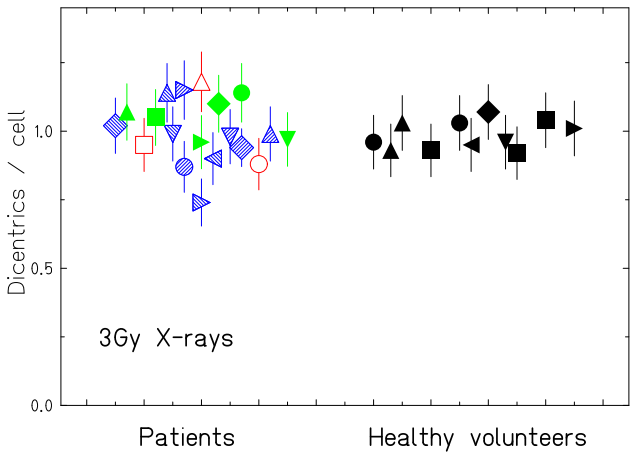

Figure 3.10.: Dicentrics observed in peripheral blood lymphocytes taken from prostate-cancer patients before the beginning of therapy or from healthy volunteers and exposed in vitro to 3 Gy X-rays. Patient symbols are the same ones used in Figure 3.12, i.e. the three patient groups are represented by solid (IMRT), patterned (C-ion boost plus IMRT) and open (IMRT*) symbols. Identical symbols in the healthy volunteer data represent blood samples obtained at different times from the same donor.

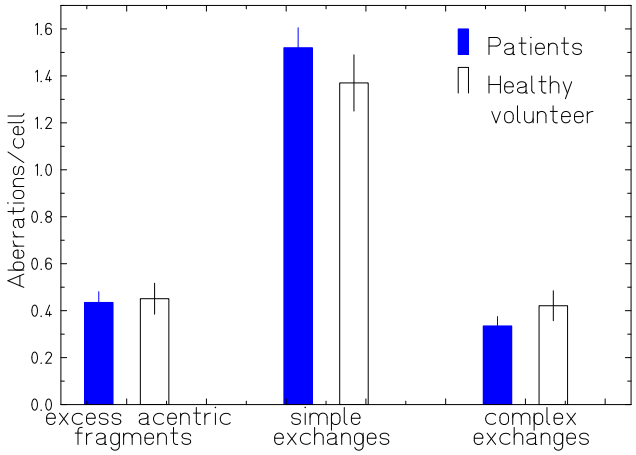

Figure 3.11.: Chromosomal aberrations observed in peripheral blood lymphocytes from two patients and one healthy volunteer after in vitro exposure to 3 Gy X-rays using mFISH staining.

be seen that the variation within one donor is about as large as the variation in the group of healthy donors.

The results of the mFISH stained samples are shown in Figure 3.11. The frequencies of non-exchange aberration, simple and complex exchanges are very similar in the analyzed patients' and healthy volunteer's samples, indicating that there is no difference between patients and healthy individuals regarding their response to ionizing radiation.

To compare the two staining methods FPG and mFISH, the yield of all dicentric chromosomes observed with mFISH was determined (all dicentrics were scored for this analysis, including dicentrics which are part of a complex exchange). FPG analysis yielded 1.00 ± 0.11 and 0.99 ± 0.05 dicentric chromosomes per cell in the patients and healthy volunteers groups after exposure to 3 Gy X-rays, mFISH analysis yielded 0.85 ± 0.06 and 0.90 ± 0.09 dicentrics per cell in the healthy donors and patients, respectively, showing a good agreement between the two staining methods regarding the recognition of dicentric chromosomes.

3.2.2. Aberration yield during therapy course

To investigate the effect of the radiotherapy on the aberration yield blood samples were obtained during therapy course. The results from aberration analysis on mFISH stained slides are shown in Figure 3.12, where the yield of chromosomal exchanges is plotted versus the dose applied to the target volume. Each symbol in Figure 3.12 represents a different patient. Solid symbols (green) represent patients treated with IMRT only (IMRT), patterned symbols (blue) represent patients treated with C-ion boost followed by IMRT

(C-ion boost + IMRT). Patients treated with IMRT with a larger target volume including the pelvic lymph nodes (IMRT*) are represented by open symbols (red). The yield of exchanges observed in the peripheral blood lymphocytes of prostate-cancer patients increases during the radiation therapy course. The increase is most pronounced in the IMRT* patients.

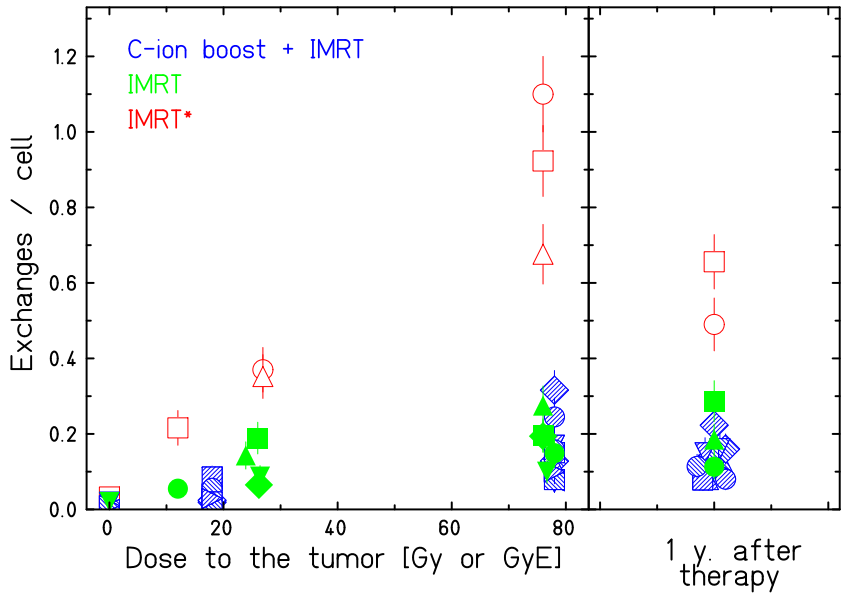

Figure 3.12.: Exchange-type aberrations (i.e. simple and complex exchanges) as a function of dose to the tumor (measured in Gy for IMRT treatment and in GyE for the C-ion boost). Each symbol in the figure represents an individual patient. (This figure is taken from Hartel et al. [2010].)

To study in more detail the differences between the three patient groups the aberrations were classified into excess acentric fragments, simple exchanges and complex exchanges and the data were pooled for each group. Figure 3.13 shows the aberrations for each patient group. Figure 3.13 reveals that predominantly simple exchanges are induced by the therapy in all three patient groups. During therapy one sample was taken at the end of the C-ion boost irradiation (which is after 6 daily fractions of 3 GyE) for the C-ion boost + IMRT patient group and after irradiation with similar tumor doses for the other two patient groups. A statistically significant increase is observed for all three patient groups from the aberration yield measured before therapy to the yield after the C-ion boost or similar doses of IMRT ($p=0.023$, $p=0.012$ and $p=0.013$ for the C-ion boost + IMRT, IMRT and IMRT* patient groups, respectively, statistical significance was determined using t-test). At the end of the therapy, the aberration yield was significantly higher in all three patient groups than during the therapy ($p=0.0002$, $p=0.0037$ and $p=0.0078$ for the C-ion boost + IMRT, IMRT and IMRT* patient groups, respectively).

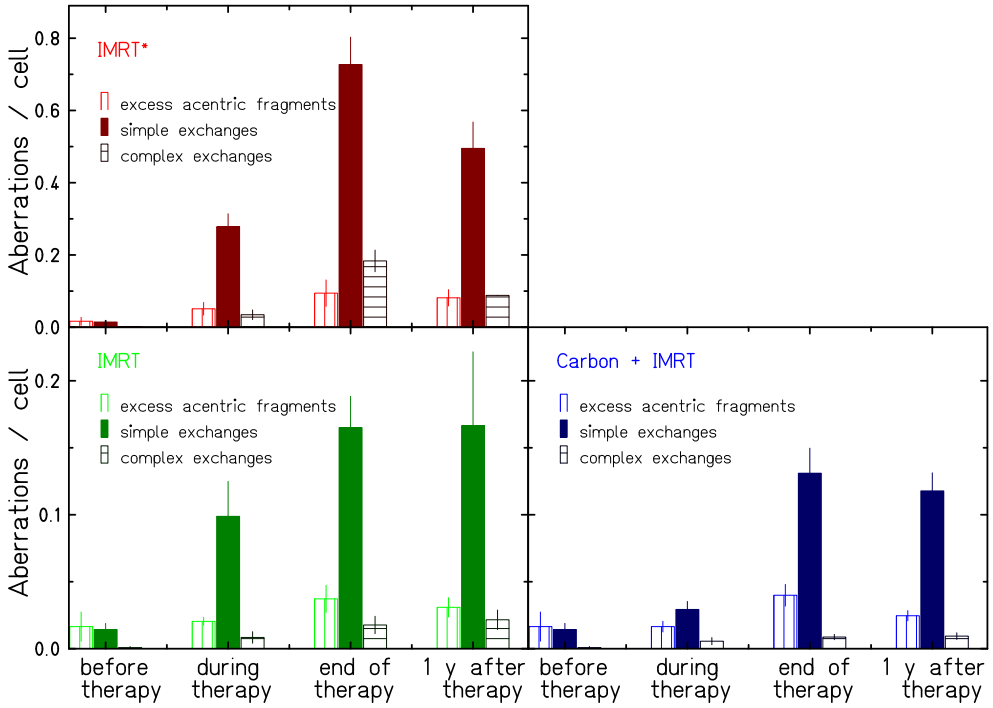

Figure 3.13.: Aberration spectrum observed in the three patient groups using with mFISH technique. Note the different y-axis scale in the upper and lower panel. Error bars represent standard errors of the mean.

During therapy, the two patients groups with the small PTV, C-ion boost + IMRT patients and IMRT patients, differ significantly with the aberration yield being lower in the patients receiving C-ion boost (p=0.036). This is a most important result regarding the future of C-ion therapy, as it proofs that C-ion radiotherapy induces less aberrations in the peripheral blood lymphocytes, which represent the surrounding normal tissue than IMRT. The aberration yield in the patient group with the large PTV (IMRT*) is significantly higher than the aberration yield in the patients receiving C-ion boost + IMRT and in the IMRT patients with the smaller PTV (p=0.030 and p=0.031).

At the end of the therapy, the difference between the two groups with the small PTV, which was present during the therapy, is no longer observable (p=0.38). The aberration yield in the IMRT* patients is significantly higher compared to the C-ion boost + IMRT and IMRT patient groups (p=0.032 and p=0.036).

At the end of the C-ion boost, the ratio of complex to simple exchanges, C-ratio, is higher in the C-ion boost + IMRT patients compared to the IMRT patients (8/39 versus 7/61). However, this difference is statistically not significant (p=0.22 using a one-sided Fisher's exact test).

3.2.3. Aberration yield one year after therapy

To study the persistence of aberrations in peripheral blood lymphocytes after radiotherapy, a blood sample was obtained one year after therapy. The yield of exchanges found by mFISH analysis in each patient is displayed in Figure 3.12.

The persistence of aberrations in the year after therapy was tested for each patient individually using Fisher's exact test on the number of aberrant cells. Samples from 16 patients were available one year after therapy and from these patients, only two showed a statistically significant decrease in the fraction of aberrant cells in the first year after therapy (one patient from the IMRT* group and one from the C-ion boost + IMRT group).

Figure 3.13 shows that the aberration pattern, i.e. the frequencies of excess acentric fragments, simple and complex exchanges are also similar at the end of therapy and one year after. Statistical analysis using t-test showed that in the year after the therapy, no significant decrease was observed in any of the three patient groups ($p=0.17$, $p=0.48$ and $p=0.096$ for the C-ion boost + IMRT, IMRT and IMRT* patients, respectively).

3.2.4. Time-dependence of aberration yield

The aberration yield found in first metaphase cells exposed to densely ionizing radiation depends on harvesting time, as described in Section 3.1.9. To investigate whether the C-ion boost induces a delay of heavily damaged cells, cells were harvested at 72 h in addition to the standard harvesting time at 48 h and the yield of dicentric chromosomes was scored on FPG stained slides in M1 cells. The resulting Figure 3.14 shows no time-dependent increase in the aberration yield for any of the three patient groups.

3.2.5. Transmissibility of aberrations

The aberrations observed in the patients' samples during and after therapy were classified according to their transmissibility. The frequencies of transmissible and non-transmissible simple and complex exchanges observed in the patients are given in Table 3.8. The resulting ratio of translocations to dicentrics is close to one during and at the end of therapy, but one year after therapy more translocations than dicentrics are observed. Transmissible complex aberrations are clearly less frequent than non-transmissible complex aberrations. However, the low numbers of complex aberrations result in larger uncertainties regarding the ratio of transmissible to non-transmissible complex exchanges.

Patient group	Sample nr	n	ace	t	dic	r	tr. comp.	ntr. comp.	ratio t/dic	ratio tr./ntr comp.	ratio tr./ntr.
C+IMRT	2	1377	22	29	10	0	3	5	2.9± 1.1	0.6 ±0.44	0.86 ± 0.21
IMRT	2	666	14	35	23	0	2	5	1.52 ± 0.41	0.4 ±0.33	0.88 ± 0.20
IMRT*	2	315	16	42	42	2	3	8	1 ± 0.22	0.38 ± 0.25	0.66 ± 0.13
all	2	2358	52	106	75	2	8	18	1.41 ± 0.21	0.44 ± 0.19	0.78 ± 0.10
C+IMRT	3	1347	54	87	87	5	4	8	1.00 ± 0.15	0.50 ± 0.31	0.59 ± 0.08
IMRT	3	517	19	39	43	1	1	8	0.91 ± 0.20	0.13 ± 0.13	0.56 ± 0.11
IMRT*	3	314	30	115	104	8	4	54	1.11 ± 0.15	0.07 ± 0.04	0.61 ± 0.07
all	3	2178	103	241	234	14	9	70	1.03 ± 0.09	0.13 ± 0.05	0.59 ± 0.05
C+IMRT	4	1164	29	92	42	2	3	8	2.19 ± 0.41	0.38 ± 0.25	1.17 ± 0.18
IMRT	4	323	10	27	23	3	3	4	1.17 ± 0.33	0.75 ± 0.57	0.75 ± 0.18
IMRT*	4	227	19	68	43	2	4	16	1.58 ± 0.31	0.25 ± 0.14	0.9 ± 0.15
all	4	1714	50	187	108	7	10	28	1.73 ± 0.21	0.36 ± 0.13	0.98 ± 0.10

Table 3.8.: Aberrations found in peripheral blood lymphocytes obtained from prostate-cancer patients during and after therapy. The sample number indicates when the blood sample was taken: 2 = during therapy (at the end of the C-ion boost for C + IMRT patients), 3 = at the end of therapy, 4 = one year after therapy. From the observed aberrations the ratio of transmissible to non-transmissible exchanges was calculated. n = number of analyzed cells, ace = excess acentric fragments, t = translocations, dic = dicentric chromosomes, r = centric rings with acentric fragments, tr. comp. = transmissible complex exchange, ntr. comp. = non-tramsmissible complex exchange, tr. = transmissible exchanges (i.e. t + tr. comp.), ntr. = non-transmissible aberrations (i.e. ace + dic + r + ntr. comp.).

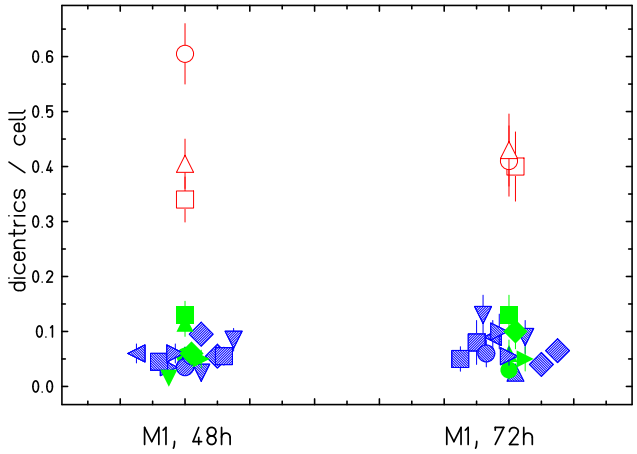

Figure 3.14.: Yield of dicentric chromosomes found in peripheral blood lymphocytes of prostate-cancer patients at the end of the radiotherapy course after 48 h and 72 h incubation. Dicentric scoring was performed in M1 cells on FPG-stained slides. The symbols correspond to the individual patients.

3.2.6. Equivalent whole-body dose

The equivalent whole-body dose can be estimated by comparing the yield of in vivo induced aberrations with the X-ray in vitro calibration curve which is shown in Figure 3.2 [Durante et al., 1999]. At the end of therapy, the mean values and standard errors of the induced exchanges for each patient group corresponded to a total body dose of 0.39 ± 0.05 Gy for the C-ion boost plus IMRT patients, 0.52 ± 0.10 Gy for the IMRT patients and 1.84 ± 0.25 Gy for the IMRT* patients.

3.2.7. Rogue cell observed using mFISH staining

Rogue cells are multiaberrant cells including several dicentric and polycentric chromosomes and numerous fragments. They are rarely observed in peripheral blood lymphocytes (e.g. Mustonen et al. [1998]; Neel [1998]; Lazutka [1996]). In one patient sample taken at the end of therapy, a metaphase was observed displaying multiple aberrations involving 31 breaks in 25 chromosomes. Other cells in this patient's sample showed on average 0.15 aberrations per cell and no other complex aberration was observed in 100 analyzed cells. Therefore this cell was believed to be a rogue cell and was excluded from the analysis. Figure 3.15 shows a DAPI and artificial color image of this cell together with a karyotype. Most rogue cells reported in the literature were found on the basis of solid staining, there is only one report about a rogue cell observed in an mFISH stained lymphocyte metaphase. In this report an image of the

multiaberrant cell is shown, but no attempt to analyze the exchanges was made [Wahab et al., 2008].

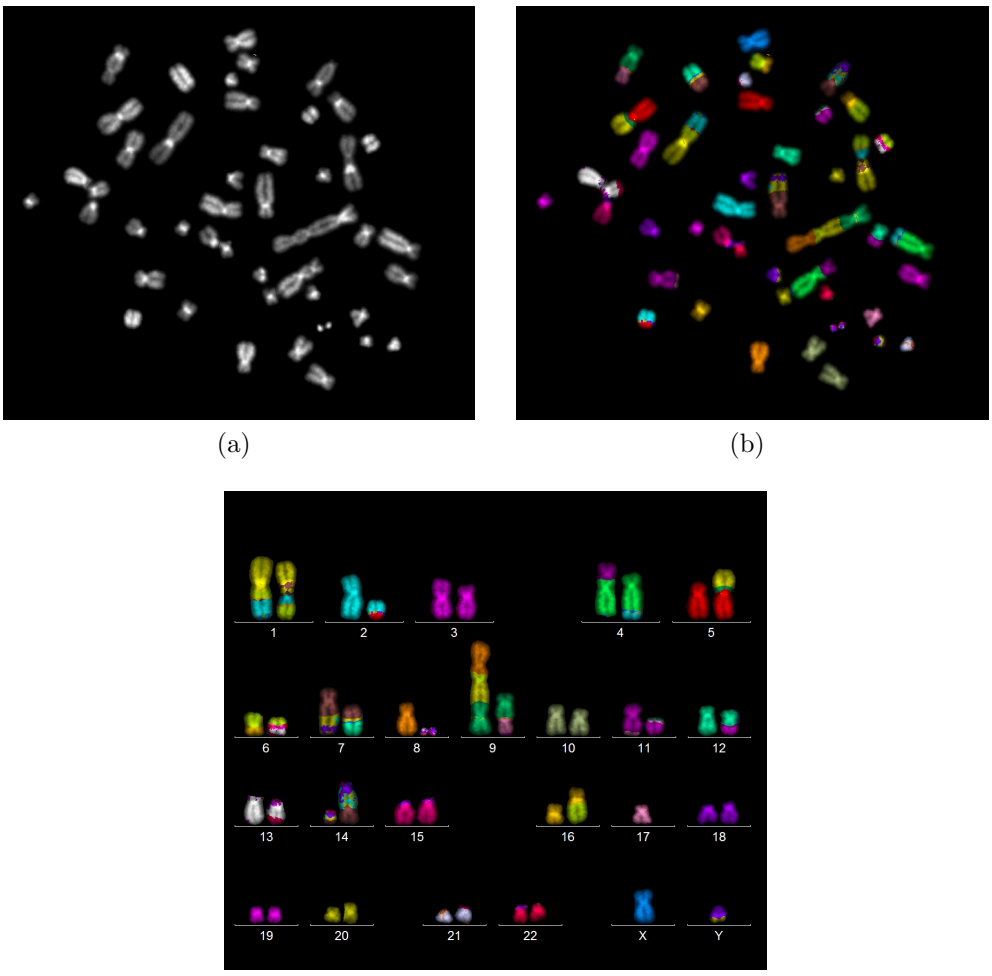

(a) (b)

(c)

Figure 3.15.: Rogue cell (multiaberrant cell) found in a patient's sample stained with mFISH. (a) DAPI image. (b) Artificial color image. (c) The analysis of the karyotype revealed that at least 31 breaks in 25 chromosomes were necessary to produce the observed aberrations (four aberrations, two reciprocal translocations (7'-14)(14'-7); (6'-16)(16'-6) and two complex exchanges with CAB (4/4/4) and (17/20/23)). All 46 centromeres were found.

3.3. Analysis of damage produced in individual chromosomes

3.3.1. Involvement of individual chromosomes in aberrations

To address the question whether chromosomal aberrations occur in all chromosomes with the same probability, the aberrations observed by mFISH were analyzed regarding the distribution of breakpoints in the individual chromosomes.

Breaks in individual chromosomes in vitro

The breaks in the individual chromosomes 1 to 22 and in the X chromosomes found after in vitro irradiation are shown in Table A.1. As the in vitro experiments were performed with blood samples from one healthy female donor no data for the Y-chromosome were obtained from these experiments. As mentioned earlier, the term "breaks" refers to breaks that lead to the observed chromosomal aberrations, not to the initially induced breaks.

The number of breaks in the individual chromosomes was plotted versus the chromosome number. The resulting Figure 3.16 shows a decrease of the number of breaks involved in aberrations with increasing chromosome number. The chromosomes are sorted according to their length with chromosome number one being the largest chromosome; the only exception is chromosome X which has about the same length as chromosomes number 7 and 8.

In Figure 3.16, the distribution of breaks in the individual chromosomes is compared to two models, the chromosome length model and the chromosome surface model, which are described in Section 2.7.1. Both models differ considerably from the observed results, a χ^2 test yielded values of 101 and 74 for the f- and $f^{2/3}$-model, respectively. $\chi^2_{0.01} = 40.3$ for a significance level of 1% and the number of degrees of freedom being 22.

Another possible correlation could be between the involvement in aberrations and the gene density on the chromosome. Therefore, the breaks in the individual chromosomes were plotted versus the gene density, which is given in Table A.1. However, the resulting Figure 3.17 shows no correlation between the gene density and the number of breaks involved in aberrations.

Breaks in individual chromosomes in vivo

The analysis of the distribution of breaks in individual chromosomes, which is described in the previous section for in vitro irradiated samples, was also performed for the samples obtained from the patients during and after the therapy. The resulting distribution is given in Table A.2 and is shown in Figure 3.18 together with the f- and $f^{2/3}$-models. A χ^2 test yielded $\chi^2 = 95$

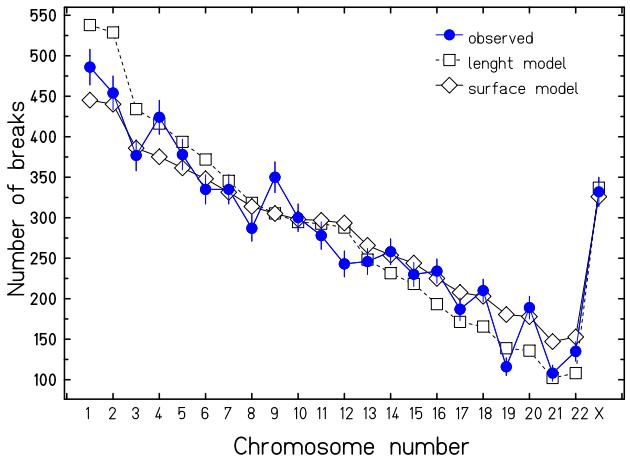

Figure 3.16.: Distribution of breaks in the individual chromosomes. Data were obtained from the analysis of mFISH stained metaphases after in vitro irradiation (results from all in vitro experiments were pooled).

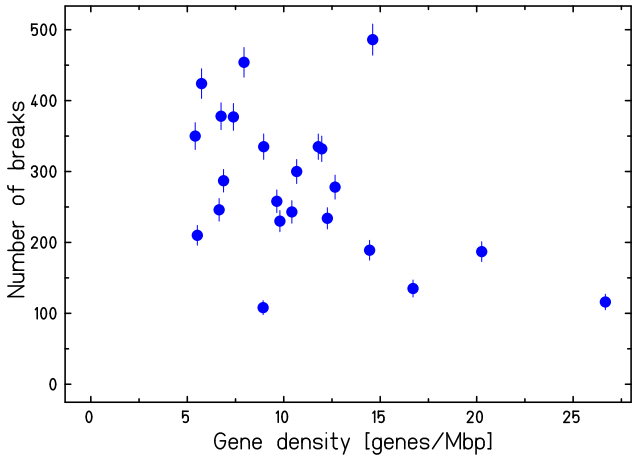

Figure 3.17.: Distribution of breaks in the individual chromosomes. Breaks are plotted versus gene density (genes per mega-basepair (Mbp) length). Data were obtained from the analysis of mFISH stained metaphases after in vitro irradiation.

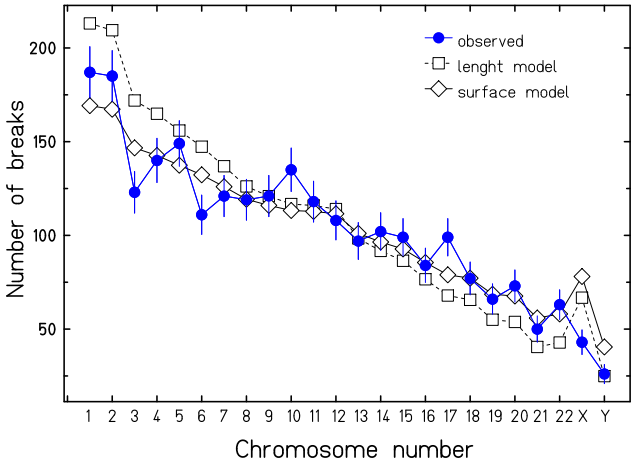

Figure 3.18.: Distribution of breaks in the individual chromosomes. Data were obtained from the analysis of mFISH stained metaphases after in vivo irradiation (i.e. lymphocytes obtained from prostate-cancer patients during, at the end and one year after radiotherapy).

and $\chi^2 = 41$ for the f- and $f^{2/3}$-model, respectively. $\chi^2_{0.01} = 41.6$ for a significance level of 1% and the number of degrees of freedom being 23 (one more as for the in vitro data, as in the in vivo data one X and Y chromosome was present, in contrast to the in vitro data where two X chromosomes were present).

3.3.2. Exchange frequencies between chromosome pairs: statistics for chromosome interphase positioning SCHIP

The exchange frequencies between pairs of chromosomes were analyzed by using the SCHIP software, which is described in Section 2.7.2. As it was found during this work that the number of entries in the table must be as high as possible for a successful search for chromosome clusters, data from all experiments were pooled for the analysis. A table with 5223 entries was achieved and was uploaded to the SCHIP homepage to search for clusters. The resulting Table A.3 shows the number of cells with exchanges between chromosomes i and j, the calculated normalized single chromosome participation factors $g(i)$ and the deviations from the expected values assuming a random model $\Delta(i,j)$.

The candidate clusters for lymphocytes provided at the SCHIP homepage (taken from literature) were tested for significance in the data set. These candidate clusters are (1;16;17;19;22) [Boyle et al., 2001], (6;7) [Pombo et al., 1998], (8;11) [Nagele et al., 1999], the Philadelphia Chromosome found in most chronic myeloid leukemia (9;22) [Mitelman et al., 2007], (13;21) [Alcobia

et al., 2000], (13;14;15;21;22) [Krystosek, 1998], (14;18) [Lukasova et al., 1999], (14;22) [Alcobia et al., 2000]; (15;17) [Neves et al., 1999] and (17;19;20) [Cremer et al., 2003]. The resulting p-values for the provided candidate clusters are shown in the upper part of Table 3.9. From the 10 provided clusters only 4 are significantly different from the random model and yielded p-values below 0.05. One of them was the cluster of acrocentric chromosomes ($p \leq 0.0001$, highly significant deviation from the random model), which are known to be located in close proximity to each other around the nucleoli, as described in Section 2.7.2. Thus, the SCHIP method applied to the present data set was able to confirm the clustering of the acrocentric chromosomes.

Next, own candidate clusters were searched on the basis of the $\Delta(i, j)$ values and tested for significance in the data set. Altogether, 30 cluster candidates were tested and all yielded p-values below 0.05, as can be seen from the lower part of Table 3.9. However, the choice of candidate clusters on the basis of the $\Delta(i, j)$ values of the data set in which they are tested later is biased, as false-positives (which are to be expected from the table size and the choice of p=0.05 as significance level) could be depicted. The candidate clusters chosen on the basis of the data reported here were therefore tested in the largest table provided at the homepage of SCHIP, i.e. a table published by Arsuaga et al. [2004] (3700 table entries). The numbers of lymphocytes with exchanges between all chromosome pairs, the single chromosome participation factors $g(i)$ and the $\Delta(i, j)$ values for this data set are given in Table A.4. The resulting p-values are shown in the right column of Table 3.9. From the 10 provided candidate clusters 2 reached p-values below 0.05, from the 30 candidate clusters chosen on the basis of the present data set, 24 yielded p-values below 0.05 in the data set published by Arsuaga et al. [2004]. This indicates that at least some of the candidate clusters chosen in the present data set are indeed chromosome clusters and not false-positive results.

The own candidate clusters were also tested for significance in other lymphocyte data sets provided at the SCHIP homepage. For the 30 candidate clusters tested, p-values below 0.05 were found for 10 candidate clusters in the data set provided by Cornforth et al. [2002] (1877 table entries), for 13 candidate clusters in the table provided by Loucas and Cornforth [2001] (786 table entries) and for 11 candidate clusters in the data set provided by Cornforth and Loucas (unpublished data, iron ion irradiation, 959 table entries) (these data are not shown). This indicates that large tables are essential for a successful search for candidate clusters.

Candidate cluster	present study	published data[(a)]
(1;16;17;19;22)	0.0281	0.0006
(13;14;15;21;22)	0.0000	0.0013
(17;19;20)	0.3915	0.4692
(13;21)	0.0001	0.5105
(14;22)	0.4524	0.2055
(6;7)	0.9315	0.8383
(9;22)	0.0744	0.6622
(15;17)	0.8001	0.5783
(14;18)	0.0002	0.4767
(8;11)	0.4057	0.085
(5;7;11;12;19)	0.0000	0.0003
(4;8;13;14;18)	0.0000	0.0000
(4;8;13;14)	0.0000	0.0004
(9;16;20)	0.0000	0.1333
(4;10;13;14)	0.0001	0.016
(8;13;14;18)	0.0000	0.0000
(3;6;10)	0.0003	0.0108
(3;6;10;12)	0.0003	0.0007
(2;12;17)	0.0003	0.0455
(9;16;18;20)	0.0000	0.0008
(16;20;22)	0.0000	0.001
(15;16;20;22)	0.0000	0.0005
(7;12;17;19)	0.0000	0.0196
(5;7;12;19)	0.0000	0.0142
(1;15;22)	0.0000	0.0033
(9;16;20;22)	0.0000	0.0274
(2;12;17;19)	0.0001	0.1015
(1;9;16)	0.0079	0.0652
(1;3;6;10)	0.0000	0.0511
(9;15;16;20)	0.0000	0.0150
(4;8;13;18)	0.0000	0.0013
(3;6;12;17)	0.0000	0.0285
(2;3;17)	0.0032	0.0408
(2;3;6;17)	0.0005	0.0385
(15;20;22)	0.0000	0.1704
(1;9;22)	0.0011	0.0140
(1;16;22)	0.0105	0.0004
(16;19;20;22)	0.0000	0.0000
(9;16;22)	0.0006	0.1842
(1;9;16;22)	0.0000	0.0032

Table 3.9.: P-values for candidate clusters tested in the table of pairwise chromosomal exchanges of the present work and in a published data set ([(a)] Arsuaga et al. [2004]). Upper part: candidate clusters suggested in the literature as provided at the SCHIP homepage. Lower part: own candidate clusters chosen on the basis of the $\Delta(i, j)$ values of Table A.3.

4. Discussion

4.1. Cytogenetic effects of sparsely and densely ionizing radiation - in vitro experiments

Knowledge of the cytogenetic effects of sparsely and densely ionizing radiation is of great importance. In cancer therapy, X-rays and particle beams are used to irradiate tumors. While X-rays are widely used in radiotherapy for many years, the application of charged particle beams is comparably new and applied only at a few facilities [Skarsgard, 1998; Schulz-Ertner, 2009]. Especially when young patients are treated there is concern about the risk of secondary malignancies or non-malignant diseases that arise from the damage induced in the normal tissue surrounding the tumor [Hall and Wuu, 2003; Dickerman, 2007]. Better knowledge about the cytogenetic effects of the different radiation qualities can help to predict the late effects of radiotherapy. As transmissible aberrations are the crucial aberration type regarding the risk of secondary cancers, the mFISH technique, which reveals all types of interchromosomal rearrangements including transmissible ones, was applied in the work presented here.

Another field where the knowledge about the cytogenetic effects of different radiation qualities is of interest is space travel. In manned space missions, the health risk associated with the exposure to galactic cosmic radiation is afflicted with large uncertainties, as little is known about the biological effects of these radiation qualities [Durante and Cucinotta, 2008]. A third field where cytogenetic effects of radiation exposure are investigated is biological dosimetry. In case an individual was exposed to ionizing radiation, retrospective dose estimation using biological dosimetry together with physical dose estimation is important for choosing an adequate treatment [International Atomic Energy Agency, 2001].

The main purpose of the study presented here was to gain information about the cytogenetic effects of the radiation qualities applied in radiotherapy and to compare the cytogenetic effects in vitro with those of different radiotherapy regimes in vivo. The radiation qualities used for this work were chosen accordingly, i.e. the C-ion energies cover the energy range which is typical for tumor therapy.

4.1.1. Analysis of dose-response curves for the induction of aberrations

One of the main purposes of the present work was to generate dose-effect curves that can be used for comparison with the in vivo results of prostate-cancer patients that underwent radiotherapy. As these patients were treated either with photon IMRT or a combination of IMRT and C-ion boost, the in vitro experiments focused on these radiation qualities as well. The mFISH method was used which allows full analysis of chromosomal interchanges.

Photon dose-effect curve

For photon irradiation, a detailed study by Loucas and Cornforth [2001] describes the dose dependence of aberrations induced by γ-rays in human peripheral blood lymphocytes using mFISH technique. Doses of 0, 1, 2, and 4 Gy were applied and cells were cultured for 48 h. mFISH analysis was performed, and aberrations were classified according to their complexity (terminal deletions, simple exchanges, complex exchanges), their completeness and transmissibility. The simple and complex exchanges observed in the present study and in the study by Loucas and Cornforth [2001] are compared in Figure 4.1.

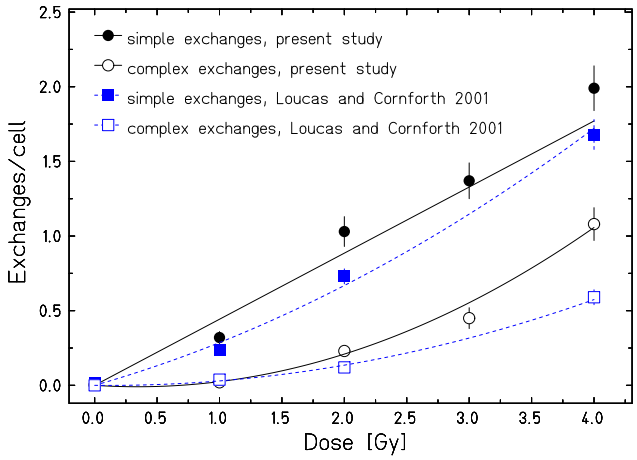

Figure 4.1.: Comparison of the number of simple and complex exchanges induced by X-ray and γ-ray exposure. X-ray data taken from Figure 3.3, γ-ray data taken from Table 2 in a publication by Loucas and Cornforth [2001]. In both studies, mFISH analysis was performed on peripheral blood lymphocytes after 48 h in vitro growth.

The mean number of exchanges per cell was higher in the study presented here compared to the data obtained by Loucas and Cornforth [2001]. However, taking into account that the results were obtained in different laboratories and that the used photon energies were different, the dose-effect curves in Figure 4.1 show a very good similarity between both data sets. From Figure 4.1,

an attempt was made to estimate the RBE of X-rays compared to γ-rays. A higher RBE for chromosomal aberrations induced in peripheral blood lymphocytes for X-rays compared to γ-rays was found by the scoring of dicentric chromosomes and acentric fragments on solid stained sides (reviewed by Hill [2004]). From Figure 4.1, which is based on mFISH analysis, the RBE_α (i.e. the comparison of the initial slopes of the fitted curves), which is used in the review by Hill [2004], was calculated to be 1.8 for the induction of simple exchanges, which is in good agreement with the RBE_α values of 1.5 and 2.8 reported in the review by Hill [2004]. The RBE_α for the induction of complex exchanges was not calculated as the initial slope of the fit-curve for the complex exchanges is around zero in both data sets as can be seen in Figure 4.1. The RBE of 250 kV X-rays compared to γ-rays was calculated to be 1.4 for the induction of 0.5 simple exchanges per cell, 1.2 for the induction of 1 simple exchange per cell and 1.3 for the induction of 0.5 complex aberrations per cell.

Dose-effect curves for charged particles

Determining the RBE of C-ions with different energy for the induction of different aberration types was one of the main purposes of this work. To calculate the RBE it was necessary to measure dose-effect curves. Other studies that addressed the cytogenetic effects of heavy ions by means of the mFISH method used only one or two doses, and therefore no dose-effect curves were achieved in these studies [Durante et al., 2002; Anderson et al., 2003; Wu et al., 2003; Pignalosa et al., 2008].

However, studies applying other staining techniques exist, that obtained dose-effect curves for the induction of aberrations by heavy ion irradiation. For example, Nasonova and Ritter [2004] reported about the exposure of human peripheral blood lymphocytes to X-rays and extended Bragg peak C-ions (LET 60–85 keV/µm). Analysis of metaphase cells and prematurely condensed chromosomes (PCC) in G2 cells was performed on FPG stained slides. Extended Bragg peak C-ions were more effective in inducing aberrations in metaphase cells, and the dose-effect curves for X-rays showed a linear-quadratic behavior while extended Bragg peak C-ion irradiation resulted in a linear dose-response curve, in agreement with the results obtained in the present study.

4.1.2. Relative biological effectiveness for cytogenetic damage

Since the first publication on RBE for the induction of cytogenetic damage in 1967 by Skarsgard [Skarsgard et al., 1967] the effectiveness of different radiation qualities in inducing chromosomal damage was investigated in many

studies (a recent review can be found in Ando and Kase [2009]). For lymphocytes, George et al. [2003a] reported a RBE_α value of 2.4 ± 0.2 for the induction of total exchanges by C-ions with an energy of 290 MeV/u; exchanges were detected using two-color FISH. In the present study, a RBE_α value of 2.5 ± 0.6 was derived from Figure 3.2 for the induction of aberrations by 270 MeV/u C-ions, which is in good agreement with the data reported by George et al. [2003a]. In a report by Monobe and Ando [2002], the initial slopes of the dose-effect curves for the induction of dicentric chromosomes in peripheral blood lymphocytes by 290 MeV/u C-ions passively decelerated to an average LET of 50 keV/µm and X-rays are reported. From this, a RBE_α of 3.3 ± 0.4 was calculated. This is lower than the RBE_α values obtained in the present study for the induction of aberrations in lymphocytes by C-ions with an energy of 100 MeV/u and extended Bragg peak C-ions, $RBE_\alpha = 5.5 \pm 1.2$ and $RBE_\alpha = 5.8 \pm 1.2$ respectively, derived from Figure 3.2. However, the use of passive energy reduction, in contrast to the active energy variation used in the study reported here, may be the reason for the lower RBE observed in the study by Monobe and Ando [2002], as passive energy degradation leads to range straggling and the production of light fragments including neutrons.

In the present study, mFISH analysis was used to generate the dose-effect curves of X-rays and C-ions with three different energies. This is the first set of dose-effect curves for chromosomal aberrations induced by heavy ions measured with mFISH. The mFISH analysis allowed calculating not only the RBE values for the total aberrations, but for different aberration categories like simple exchanges and complex exchanges separately. It was found that the RBE for complex exchanges is higher than for simple exchanges after irradiation with 100 MeV/u and extended Bragg peak C-ions (see Table 3.1). In the tumor therapy with C-ions, this high biological effectiveness ensures the inactivation of the tumor cells. Especially the high RBE for complex exchanges is important, as they are mostly non-transmissible leading to the death of the damaged cell (see Tables 3.2 and 3.8). On the other hand, the high RBE radiation must be restricted to the tumor tissue as precisely as possible to avoid severe side effects in the surrounding tissue. Therefore the raster scanning technique and the active energy variation are advantageous, as they ensure a good tumor conformation.

4.1.3. Complex aberrations - a biomarker for densely ionizing radiation

A biomarker for the exposure of cells to densely ionizing radiation has been suggested in several studies (e.g. Anderson et al. [2000]; Deng et al. [2000]; Brenner et al. [2001]; Anderson et al. [2003]). The most promising biomarker candidate is the *C*-ratio, the ratio of complex to simple exchanges. An elevated *C*-ratio is found after in vitro exposure to densely ionizing radiation

compared to photons in several studies applying different staining methods (e.g. Testard et al. [1997]; Wu et al. [2003]; George et al. [2003b]; Johannes et al. [2004]). This is confirmed by the present study, where an increasing C-ratio was observed with increasing LET (see Figure 3.4). However, Figure 3.4 also shows that the C-ratio is dose-dependent in the LET range investigated in this work, e.g a C-ratio of 0.5 is induced by about 4 Gy X-rays and 2 Gy 100 MeV/u C-ions. The highest C-ratio observed here is 0.92 ± 0.10 after 4 Gy 100 MeV/u C-ions; however, a similar C-ratio is found after a dose of 6 Gy X-rays [Lee et al., 2010]. Therefore it is necessary to compare not only the C-ratio, but also the aberration yield observed in a sample exposed to a unknown radiation quality with the known dose-effect curves, to determine whether an observed high C-ratio was induced by high-LET particles or by high doses of low-LET radiation. Consequently, application of the C-ratio in biological dosimetry to determine the radiation quality to which the victim was exposed will be very sophisticated, as the victim was probably not exposed to a monoenergetic homogeneous beam, but to a mixture of energies.

4.1.4. Completeness of exchanges - is there an influence of dose and LET?

Although it was not a main topic of this work to analyze the chromosomal aberrations regarding their completeness, it was carried out as this information is easily obtained in parallel to the normal mFISH analysis. Table 3.3 shows the chromosomal exchanges observed after in vitro irradiation classified according to their completeness, i.e. distinguishing complete, incomplete and one-way exchanges, following the definitions made by Loucas and Cornforth [2001]. As can be seen from Table 3.3, a dose-dependent increase in the fraction of incomplete simple exchanges was found in the experiments reported here. This is in contrast to the findings by Loucas and Cornforth [2001] where in lymphocytes irradiated with γ-rays a dose-independent fraction of incomplete simple exchanges (of 2.3–2.4%) was found. Regarding the complex aberrations, lower numbers hamper a definite conclusion wheter the fraction of incomplete complex exchanges increases with dose as well. To yield smaller error bars (higher number of exchanges) the simple and complex exchanges were summed and analyzed regarding the fraction of incomplete exchanges (right column in Table 3.3). An increase in the fraction of incomplete exchanges with increasing dose is observed then. In addition, an increase with LET is observed as well, e.g. for a dose of 1 Gy the fraction of incomplete exchanges increases from 0.014 ± 0.014 to 0.088 ± 0.029 and for a dose of 2 Gy from 0.039 ± 0.018 to 0.110 ± 0.023.

Regarding the one-way exchanges, Loucas and Cornforth [2001] found that the fraction of simple one-way exchanges is independent of dose, while the fraction of complex one-way exchanges increases with dose. In the present

study, the fraction of simple one-way exchanges varied from 10% to 25% with no dose-dependence or LET-dependence visible (calculated from the data displayed in Table 3.3), which is in good agreement with the fraction of 14% to 29% found by Loucas and Cornforth [2001]. For the fraction of complex one-way exchanges, values between 15% and 80% were found in the present work, but in contrast to the findings by Loucas and Cornforth [2001] no general dose-dependence was observed (an increase with dose is found for the X-ray and spread-out Bragg peak C-ion data, while a decrease with increasing dose is observed after 270 MeV/u C-ion exposure and no correlation is found for 100 MeV/u C-ions).

Other studies with high statistical power are necessary to confirm or disprove the findings about the dose- and LET-dependence of the fractions of incomplete and one-way simple and complex exchanges. However, as the dose-dependent increase in the fraction of incomplete exchanges was found in all four data sets of the present study, and the LET-dependent increase was found for both doses which were applied in all four data sets, a dose- and LET-dependent increase of the fraction of incomplete exchanges can be assumed from the present study.

4.1.5. Fate of aberrant cells

To understand the mechanisms involved in aberration formation it is most useful to investigate aberrations in cells soon after irradiation, i.e. in G2-PCC cells or in first cycle metaphase (M1) cells. The latter were used in the present study. However, for the late effects of tumor therapy the long-term survival of cells carrying an aberration is more relevant than the initial damage. The aberrations induced in the peripheral blood lymphocytes by in vitro irradiation with different radiation qualities were therefore analyzed regarding their transmissibility. With regard to simple exchanges, it can be seen from Table 3.2 that translocations (which are transmissible) and dicentric chromosomes with acentric fragments (which are non-transmissible) are induced with the same frequency, therefore about half of all simple exchanges are transmissible. (Centric ring chromosomes with acentric fragments are non-transmissible simple intrachanges, but they are rare compared to dicentrics and translocations, not affecting the ratio of transmissible to non-transmissible exchanges substantially.) This is in line with several studies and theoretical predictions (see e.g. Lucas et al. [1996]; Loucas and Cornforth [2001]). Therefore half of the cells carrying a simple exchange are assumed to die during the next few replication rounds. In a study by Pignalosa et al. [2008], the numbers of dicentrics and translocations found in lymphocytes incubated 144 h after irradiation with X-rays and iron ions were analyzed using arm-specific mFISH. Translocations were about twice as frequent as dicentrics, indicating that dicentrics indeed die out during a few replication rounds. In an experiment by Durante et al. [2006], RxFISH was used on lymphocytes incubated for

144 h after irradiation with gamma rays and iron ions and a higher yield of translocations compared to dicentrics was found as well.

In contrast to simple exchanges, most complex aberrations induced by ionizing radiation are non-transmissible (see Table 3.2). Thus, albeit complex aberrations seem to be the more severe damage to a cell compared to simple exchanges, the majority of cells carrying a complex exchange will die and will therefore not increase the risk of secondary malignancies induced by radiotherapy.

As can be seen from Figure 3.4, the fraction of complex aberrations induced in cells is high after exposure to high-LET radiation or exposure to high doses of low-LET radiation. Regarding the risk of late effects of radiotherapy this strongly underlines the advantage of C-ion radiotherapy, where a comparably small volume of normal tissue is exposed to radiation, and this radiation induces a higher fraction of complex exchanges compared to X-rays causing the damaged cells to die rather than to continue growing. Compared with C-ion radiotherapy, IMRT exposes a large volume of normal tissue to low or moderate doses. Such an exposure of large volumes to lower doses can increase the risk of secondary cancers [Hall and Wuu, 2003; Hall, 2006].

4.1.6. Distribution of aberrations in the cells

While the distribution of aberrations induced in first cycle metaphase cells by X-rays or other sparsely ionizing radiation follows a Poisson distribution, the experimental results after exposure to densely ionizing heavy ions are better described by a Neyman type A distribution [Virsik and Harder, 1981; Lee, 2006; Gudowska-Nowak et al., 2007] (see Figure 3.7). The Neyman type A distribution takes into account the microscopically inhomogeneous dose distribution of densely ionizing radiation. In the present study, it was found that the distributions of aberrations induced by X-rays, 270 MeV/u C-ions and 100 MeV/u C-ions are in good agreement with Poisson statistics, while the distribution found after extended Bragg peak C-ion exposure is better described by a Neyman type A distribution. Regarding the tumor therapy with heavy ions, this result is most favorable, as it confirms that only in the case of extended Bragg peak C-ions the inhomogeneous local dose distribution typical for densely ionizing particles is relevant for the cytogenetic effects, while 270 MeV/u C-ions and 100 MeV/u C-ions, which are found in the entrance channel of the beam, i.e. in normal tissue, show a more X-ray-like behavior.

The parameter λ of the Neyman type A distribution corresponds to the mean number of particle traversals per cell nucleus. It was found to be 2.6 ± 1.0 and 6.7 ± 3.4 for irradiation with 1 Gy and 2 Gy extended Bragg peak C-ions (see Table 3.5). The particle traversals per cell nucleus calculated from the particle fluence and a mean cell nucleus are of $25\,\mu m^2$ were 2.15 and 4.3 for 1 Gy and 2 Gy extended Bragg peak C-ions (see Table 2.5). Thus, the fit parameters of the Neyman type A distribution are in agreement with the

values calculated from the particle fluence. The parameter μ of the Neyman type A distribution describes the mean number of aberrations induced by one particle traversal. It was found to be 0.52 ± 0.22 and 0.41 ± 0.22 for 1 Gy and 2 Gy extended Bragg peak C-ions. Thus, as can be expected, the average number of aberrations induced by a single particle traversal does not depend on the applied dose.

4.1.7. Time-dependence of aberrations

The standard protocol for the preparation of M1 cells from human peripheral blood lymphocytes schedules one sampling time at 48 h after the onset of the culture. However, high-LET radiation produces a pronounced cell cycle delay [Scholz et al., 1994; George et al., 2001; Ritter et al., 2002b; Tenhumberg et al., 2007]. Thus, if only one sampling time is used this would result in an underestimation of the damage induced by high-LET radiations because of the delay of heavily damaged cells [Scholz et al., 1998]. In the present study, a second sampling time 72 h after onset of the culture was therefore used in addition to the standard sampling time at 48 h. No increase in aberration level with sampling time in M1 cells was found after cell exposure to 2 Gy 270 MeV/u C-ions. A moderate cell cycle delay of heavily damaged cells was found after exposure to 2 Gy extended Bragg peak C-ions, the aberration yield found in M1 cells collected at 72 h was 20% higher than in cells collected at 48 h (see Table 3.6). In contrast, for 9.5 MeV/u C-ions (LET=175 keV/µm) a pronounced delay of heavily damaged cells is reported by Lee et al. [2010] (in this publication, for 2 Gy of 9.5 MeV/u C-ions a 5-fold increase in aberration yield from 48 h to 72 h sampling time is reported for lymphocytes analyzed using mFISH). The findings are in line with previous publications [Anderson et al., 2000; George et al., 2001; Ritter et al., 2002a; Nasonova and Ritter, 2004] where no effect of the sampling time on the aberration yield for LET values below 30 keV/µm was found.

4.2. Background aberration level and test of individual radiosensitivity

In the present study, the aberration yield in peripheral blood lymphocytes from prostate-cancer patients during the course of radiotherapy with IMRT and C-ion boost was investigated to search for differences between the radiotherapy schemes. To ensure that the aberration level in the patients before the beginning of the therapy was similar to the one found in control populations, a blood sample from every patient was taken before the onset of radiotherapy and the cytogenetic damage in the lymphocytes was analyzed. In addition, a part from this sample was irradiated in vitro to search for extraordinarily radiosensitive patients.

4.2.1. Background aberration level

The cytogenetic damage in peripheral blood lymphocytes is a sensitive tool for detecting the exposure of individuals to mutagens and carcinogens, including radiation. To detect small increases in the aberration level, a precise knowledge about the aberration level in unexposed control groups is essential. Many studies have therefore focused on the measurement of aberration frequencies in control populations, using classical cytogenetic methods or fluorescence in situ hybridization (FISH). Studies investigating translocation frequencies are of special interest as translocations are believed to be transmissible through the cell cycle, and an exposure to a mutagen or carcinogen can be detected by an increased yield of translocations even decades after the exposure. The use of the dicentric chromosome frequency as a monitor of exposure is limited to the detection of recent or ongoing events since cells with dicentrics are unstable and will not be maintained in the peripheral blood lymphocytes [International Atomic Energy Agency, 2001].

An early study using FISH for the investigation of aberration levels in control populations is reported by Ramsey et al. [1995], this study also addressed the question of possible influence of age and lifestyle factors. Peripheral blood lymphocytes from 91 subjects ranging from newborn to adults up to 79 years old were investigated. The analysis revealed a clear age-dependent increase of transmissible aberrations, increasing 10-fold from the cord blood of newborn to the adults older than 50 years. The increase in dicentrics and acentric fragments was less pronounced. In the study reported here 1.3 stable aberrations per 100 cells were found in the mFISH analyzed patients' samples taken before therapy, and 0.3 stable aberrations in the unirradiated samples from one healthy volunteer (see Table 3.7). Both values are lower than in the study reported by Ramsey et al. [1995] where in adults 50 years and older 2.5 stable aberrations per 100 cells were found. Ramsey et al. [1995] found 0.126 dicentrics per 100 cells and 0.24 acentric fragments per 100 cells, while in the present study 0.13 dicentrics per 100 cells and 1.3 acentric fragments per 100 cells were found in patients' samples and 0.17 dicentrics per 100 cells and 0.67 acentric fragments per 100 cells in the samples from a healthy volunteer analyzed with mFISH. The FPG analysis revealed on average 0.2 dicentrics per 100 cells in the patients' samples. Thus, while the dicentric yields are in good agreement, more acentric fragments were observed in the present study compared to Ramsey et al. [1995]. In addition to the age-dependence discussed here, the study by Ramsey et al. [1995] found other factors significantly associated with the frequency of stable aberrations, these are smoking, consumption of diet drinks/diet sweeteners, exposure to asbestos or coal products and having a previous major illness.

Other studies addressed the background level and age-dependence of aberrations as well [Sorokine-Durm et al., 2000; Tawn and Whitehouse, 2001; Vorobtsova et al., 2001; Whitehouse et al., 2005]. The aberration levels re-

ported there are generally in agreement with the aberration levels found in the patients' samples before the beginning of therapy and the sample of a healthy volunteer reported here.

A study reported by M'kacher et al. [2003] addressed the question whether there is a difference in the background aberration level in lymphocytes from cancer patients and healthy volunteers. For this, they investigated the chromosomal aberrations in Hodgkin's lymphoma patients and two groups of control individuals, healthy donors and cancer patients (thyroid, urologic, head and neck) before treatment. This study did not find a significant difference in the level of aberrations between the cancer patients group and the healthy volunteers group, which is in agreement with the results reported here (see Section 3.2.1).

4.2.2. In vitro test to determine individual radiosensitivity

In the present work, blood samples obtained from the patients before therapy were irradiated in vitro with 3 Gy X-rays to examine the individual radiosensitivity. The main goal was to find possible outliers. Some genetic defects are correlated with an extremely high radiosensitivity (e.g. patients with ataxia-telangiectasia [Gatti, 2001], Nijmegen breakage syndrome or Fanconi anemia [Obe and Vijayalaxmi, 2007]). Irradiating a patient with such a gene defect would result in severe side effects for the patient and would lead to unexpected results in the in parallel performed study investigating the cytogenetic damage induced by radiotherapy in peripheral blood lymphocytes. Such outliers were not observed in the patient group investigated in this study, as can be seen in Figure 3.10. It is also visible from Figure 3.10 that the aberration frequencies induced in the patients and in healthy volunteers are similar, indicating that the patients have no elevated radiosensitivity. Furthermore, Figure 3.10 shows a considerable variation within samples taken from the same healthy donor at different times.

In addition to the identification of outliers with an extremely high radiosensitivity, in vitro tests may predict the risk of acute reactions after radiotherapy. A publication by Borgmann et al. [2008] proposes the in vitro exposure of peripheral blood lymphocytes to a dose of 6 Gy X-rays and the scoring of excess acentric fragments. In this report the mean value (MV) and standard deviation (SD) of the excess fragments per cell were determined. The patients with less excess fragments per cell than MV–SD were categorized as radioresistant, patients that had between MV–SD and MV+SD excess fragments per cell were categorized as normal and patients with an higher yield than MV+SD were categorized as radiosensitive. With this categorization, a correlation between in vitro radiosensitivity and fraction of patients with severe side effects was observed. The knowledge of the radiosensitivity of each individual patient is of course highly useful, as treatment schemes could be adapted to reduce severe side effects in the group of sensitive patients by re-

ducing the total dose and to enhance the tumor control rate by giving higher doses to radioresistant patients. Although this seems highly desirable, such an attempt was outside the aims of the study reported here. However, the inter-individual variation found in the present study can be compared to the variation reported by Borgmann et al. [2008], although the absolute values are not comparable because different scoring criteria were used and different X-ray doses were applied. In the present study, 1.00 ± 0.11 ($MV \pm SD$) dicentrics per cell were observed after 3 Gy of X-rays, in the study reported by Borgmann et al. [2008], 3.29 ± 0.55 and 3.59 ± 0.57 ($MV \pm SD$) excess acentric fragments per cell were observed. Thus, the variation found in the present study is smaller than in the study published by Borgmann et al. [2008].

4.3. Chromosomal aberrations induced by radiotherapy

Radiotherapy for tumor treatment, alone or in combination with surgery or chemotherapy, improves steadily resulting in an increasing probability of cancer cure and patient survival. A long-term survival of patients brings attention to the risk of radiation-induced secondary cancer and of late tissue injury [Allan and Travis, 2005; Suit et al., 2007]. Radiotherapy must therefore be optimized to minimize the risk of secondary diseases, while providing good tumor control. Chromosomal aberrations in peripheral blood lymphocytes are a useful tool to monitor the cytogenetic damage induced by radiation and to estimate the risk of late effects.

4.3.1. Influence of radiation quality and target volume on aberration yield

In this study, chromosomal aberrations found in lymphocytes taken from three sets of patients are compared. Two patient groups were treated with the same radiation quality, i.e. IMRT, and different target volumes, comparison of these groups therefore provides information about the influence of different target volumes. A third group of patients had a target volume similar to one of the former groups, but was treated with a C-ion boost followed by IMRT. Comparison of these two groups therefore yields information about the effect of radiation quality.

Effect of target volume on aberration yield

In the data reported here, a pronounced influence of the target volume on the aberration yield is visible (see Figure 3.12). A dependence of the aberration yield on the target volume was previously observed by the use of PCC-FISH for different tumor types and radiation qualities. Durante et al. [1999] and

Yamada et al. [2000] investigated chromosomal damage in peripheral blood lymphocytes of patients with esophageal carcinoma treated with X-rays using two-color FISH. For 15 patients the fraction of aberrant peripheral blood lymphocytes after 45 Gy X-rays to the target volume along the esophagus was investigated and a linear increase of the fraction of aberrant cells with increasing target volume was observed. In esophageal cancer, increasing the field size proportionally increases the number of lymph nodes irradiated along the lymph canal. As lymphocytes reside most of the time in the lymph nodes, it is especially the number of lymph nodes in the field that determines the fraction of irradiated lymphocytes. In a study published by Lee et al. [2004] it was found that the fraction of aberrant cells in 22 lung cancer patients at the end of C-ion treatment increases linearly with the target volume. In a study with prostate cancer or endometrial cancer patients treated with radiotherapy a correlation of dicentric yield with planning target volume and mean bone marrow dose was found [Gershkevitsh et al., 2002]. D'Alesio et al. [2003] reported in breast cancer patients that the aberration yield is not only dependent on the target volume, but also on the number of lymph nodes irradiated. This is in line with the study mentioned above [Yamada et al., 2000] where it is concluded that especially the number of lymph nodes in the field determines the fraction of aberrant cells. In the study reported here the patients with the larger target volume showed a higher aberration yield, the planning target volume for these patients included the pelvic lymph nodes. Thus the findings of the previous studies are confirmed with the mFISH method. However, whether the irradiated volume or the number of irradiated lymph nodes is the major factor determining the aberration yield, or whether both factors are equally important can presently not be determined.

Effect of radiation quality on aberration yield

One of the main goals of this study was to achieve information about the different aberration yields and aberration patterns induced by C-ion boost irradiation compared to IMRT. The present study revealed that at the end of the C-ion boost irradiation the aberration yield was significantly lower in the patients treated with the C-ion boost compared to patients irradiated with IMRT with a comparable target volume (see Figure 3.13). This result is highly relevant with respect to the increasing use of C-ion therapy worldwide. As can be seen from the treatment plans shown in Figure 1.9, the volume of irradiated normal tissue is smaller in case of C-ion boost irradiation (2 opposite irradiation fields, compared to 7 fields in case of IMRT) and this is reflected by a lower aberration yield at the end of the C-ion boost. Such an effect of C-ion irradiation compared to photon therapy was reported previously by Durante et al. [2000] in patients treated for uterus or esophageal cancer by the use of two-color FISH. The lower cytogenetic toxicity of C-ion therapy compared to a biologically equivalent tumor dose applied with IMRT

is now confirmed with the full-genome paining mFISH. The whole-genome analysis is of great importance as it ensures, in contrast to 1–3-color FISH, that all types of chromosomal interchanges, including complex exchanges, are detected. Concerns that C-ion radiotherapy may induce aberrations which were underestimated with previous staining methods, e.g. a high fraction of complex exchanges, can therefore now be dispelled.

As cytogenetic damage represents an indicator for the risk of late effects, it can be expected from these findings that C-ion therapy induces less late effects compared to IMRT. As mentioned earlier, late effects, which occur several years after the therapy are increasingly important with the improvements in cancer therapy leading to increased tumor control rates and longer patient survival. Therefore, especially for young patients, C-ion tumor therapy can be a good choice, as it provides good tumor control rates [Schulz-Ertner et al., 2007a,b; Tsujii et al., 2008; Combs et al., 2009; Schulz-Ertner, 2009] and in addition, as it is shown in the present study and in the study by Durante et al. [2000], a lower risk of late effects, compared to IMRT, can be assumed.

4.3.2. Is there a fingerprint of C-ions in vivo?

The ratio of complex to simple exchanges (C-ratio) has been proposed as a biomarker for densely ionizing radiation (see Section 1.3.6). The in vitro experiments show an increased C-ratio after extended Bragg peak C-ion irradiation, i.e. high-LET irradiation (see Section 3.1.4), in agreement with previous in vitro studies [Durante et al., 2002; Wu et al., 2003; George et al., 2003b; Johannes et al., 2004]. The C-ratio therefore seems to be a good cytogenetic marker for in vitro exposure to densely ionizing radiation (see Figure 3.4). However, in contrast to the in vitro results, no significant increase in the C-ratio was observed in patients treated with C-ion boost, compared to the IMRT patients in the present study (see Section 3.2.2). This is in line with other studies, where no increase in the C-ratio was detected in vivo for C-ion radiotherapy patients [Durante et al., 2004], mice exposed to Fe-ions [Rithidech et al., 2007] or astronauts returning from long-term space flights [George et al., 2003b]. A possible explanation for the different findings in vitro and in vivo is the mixture of energies and corresponding LET values to which a human or animal is exposed, as the particles change their energy while traversing the body, in contrast to the more homogeneous beam energies applied in in vitro experiments. In the case of prostate cancer radiotherapy with C-ions, the ions enter the body with an initial energy of about 300 MeV/u, these ions induce a C-ratio which is similar to the one induced by X-rays, as can be seen for the 270 MeV/u C-ions in Figure 3.4. The C-ions decelerate on their way through the body and stop in the target volume, where they are expected to induce a high fraction of complex aberrations, as can be seen from the extended Bragg peak C-ion data in Figure 3.4. However, the stopping C-ions are restricted to the target volume, which is small compared to

the volume of irradiated normal tissue in the beam entrance channels. Therefore, in vivo irradiation comprises a mixture of LET values and therefore a mixture of corresponding C-ratios. Although it can be expected from the in vitro experiments that the stopping C-ions induce a high fraction of complex exchanges, this effect is overlaid by the low fraction of complex exchanges induced in the entrance channel. The restriction of the high-LET region to the tumor volume is highly desirable for radiotherapy, but for biological dosimetry in cancer patients the use of the C-ratio as a biomarker for external exposure to densely ionizing radiation is limited.

In contrast to the in vivo exposure to external radiation, where no biomarker for densely ionizing radiation is found, in studies that investigated aberrations in individuals occupationally exposed to plutonium, a α-particle emitter which is inhaled as dust by the exposed individuals, different results were obtained. Hande et al. [2005] reported that complex aberrations have the potential to be a biomarker for exposure to densely ionizing radiation. Anderson et al. [2005] also found that complex aberrations represent a biomarker for α-particles. In contrast, in a study by Tawn et al. [2006] an increased frequency of translocations was found in plutonium workers compared to individuals exposed to γ-rays, but no significant difference in the proportion of complex aberrations. However, as single color FISH was applied in this study complex aberrations may have been misinterpreted as simple ones [Cornforth, 2001].

4.4. Follow-up of radiotherapy - aberration pattern and persistence of aberrations

Transmissible aberrations are of special interest for the monitoring of past radiation exposure, as they persist in individuals for many years after exposure. The aberrations induced in the in vitro experiments and in vivo in the patients undergoing radiotherapy were investigated regarding their transmissibility. The aberrations found one year after the therapy in the irradiated patients were compared to this initial aberration pattern.

4.4.1. Aberration pattern

The aberrations induced in vitro and in vivo in peripheral blood lymphocytes are listed in Tables 3.2 and 3.8. For the simple interchanges the induction rates of transmissible and non-transmissible aberrations are similar, as predicted theoretically by Lucas et al. [1996] (in the present work, 686 translocation and 679 dicentric chromosomes were found after in vitro exposure and 347 translocation and 309 dicentric chromosomes were found in the patients during and at the end of therapy). In contrast, for complex exchanges more non-

transmissible than transmissible types were found after in vitro and in vivo irradiation (again, see Tables 3.2 and 3.8).

In the year after therapy, the ratio of translocations to dicentric chromosomes increased from 1.03 ± 0.09 to 1.73 ± 0.21. A decrease in the aberration yield can easily be explained by the death of some aberrant cells which are replenished by dividing normal cells. A change in aberration pattern towards stable aberrant cells on the other hand is an indicator for dividing aberrant cells, i.e. irradiated bone marrow cells. During radiotherapy of the prostate, bone marrow is exposed to some dose, especially the bone marrow in the hip-bone and in the femur head [Gershkevitsh et al., 1999, 2005]. Bone marrow cells carrying non-transmissible damage will die during the next few divisions, while bone-marrow cells carrying a transmissible damage can pass this damage to their daughter cells. Thus, the results of the present study show that the irradiation of the bone marrow can be detected using cytogenetic methods.

4.4.2. Persistence of aberrations in vivo

Only few publications on the follow-up of cytogenetic damage in radiotherapy patients using mFISH are available. Pouzoulet et al. [2007] analyzed aberrations in two patients with head and neck cancer. Four sampling times were used, the last one four to six months after therapy. In contrast to the method used in the work presented here, the authors scored only those cells carrying stable aberrations, cells with non-transmissible aberrations were excluded from the analysis. Kuechler et al. [2003] reported the yield of aberrations 2–3 years after therapy in 12 patients, but did not analyze blood samples at the end of therapy and all patients had received chemotherapy. Because of these differences, these two studies are not suited for comparison with the data presented here.

However, many studies exist where other staining methods (1–3-color FISH, G-banding) were applied. Mueller et al. [2005] used three-color FISH to investigate the persistence of translocations in eleven patients with testicular seminoma, germinoma and follicular non-Hodgkin's lymphoma. In 9 of 11 cases a decline of translocation frequency was observed during a 36 months period after therapy. In a study by Huber et al. [1999] both dicentrics and translocation yields were scored using single-color FISH in five breast cancer patients. A decline of the aberration yield was observed in two out of five patients during a 14 months period after therapy. Tawn and Whitehouse [2003] reported translocation yields scored by G-banding in 8 patients with different cancers up to 60 months after radiation therapy. Significant decrease was observed in four patients.

In the study presented here, no significant decline in the year after the therapy was observed when the pooled data of the three patient groups were analyzed. When the decline of aberrations in the year after therapy was tested in each patient individually, a statistically significant decrease was found in

two out of 16 patients. These results are in line with the observations reported by Huber et al. [1999], Tawn and Whitehouse [2003] and Mueller et al. [2005], where in similar or longer time intervals a decline in aberration frequency was observed in some patients only. The slow decline in aberration yield is caused by the lifespan of the lymphocytes (lymphocytes consist of several subtypes with lifespans ranging from a few days to several years [Pschyrembel, 2007]) and by the renewal of lymphocytes carrying aberrations by the offspring of irradiated bone marrow cells. As pointed out in the previous section, a part of the bone marrow is irradiated during radiotherapy of the prostate.

Studies exist that describe the presence of aberrations decades after radiotherapy [Kleinerman et al., 1989, 1994]. In these studies blood samples were taken from 96 cervical cancer patients 23 years after therapy and from 34 patients treated for benign gynecological diseases 40 years after therapy. These time intervals are much longer than the mean half-life of blood lymphocytes and the observed aberrant lymphocytes are assumed to be the progenies of bone marrow cells that were exposed during the treatment. As lymphocytes consist of several subpopulations, there are different half-life data published, normally a half life between some weeks and a few years are determined experimentally for the subpopulations [Tough and Sprent, 1995; Mclean and Michie, 1995; McCune et al., 2000; Macallan et al., 2003; Wallace et al., 2004]. The cytogenetically aberrant bone marrow cells contribute to the risk of leukemia as a secondary disease after therapy. Kleinerman found that the aberration level observed long times after therapy is not proportional to the initial dose to the bone marrow and is therefore not a biomarker for radiation dose, but it appears to be a biomarker for the effective risk of the occurrence of leukemia. In that study, the excess leukemia risk was about the same in both groups although the cervical cancer patients received a much higher dose to the bone marrow compared to the patients with benign gynecological diseases. High doses are most likely lethal to the cells and therefore bone marrow cells receiving high doses will die while cells exposed th low doses receive non-lethal damage and survive carrying cytogenetic damage. The volume of bone marrow irradiated during radiotherapy is therefore a major point together with the applied dose when estimating the risk of secondary malignancies.

4.5. Involvement of individual chromosomes

Although it was outside the main purpose of this study, which was to investigate the cytogenetic damage induced by densely ionizing radiation in in vitro experiments and in patients undergoing radiotherapy, an analysis of the involvement of individual chromosomes in aberrations was carried out in parallel to the normal mFISH aberration analysis.

4.5.1. Distribution of breaks in individual chromosomes

The distribution of breakpoints in individual chromosomes was investigated in the in vitro and in vivo experiments and compared to the chromosome length and chromosome surface model (see Section 3.3.1). There was no superiority of one model over the other observed. This is in line with the findings in a recent publication by Lee et al. [2010], where the breakpoint distribution in lymphocytes exposed in vitro to X-rays or 9.5 MeV/u C-ions was investigated. This conclusion was also drawn by Durante et al. [2002]. In other publications contradictory results are reported. Anderson et al. [2006] and Lucas et al. [1992] found that the chromosome length model describes their experimental data better, while Cornforth et al. [2002], Cremer et al. [1996] and Cigarran et al. [1998] favor the chromosome surface model. To draw a definitive conclusion whether one of both models describes the experimental findings accurately, or whether other models must be considered, larger data sets are necessary. The increasing use of mFISH and other whole-genome painting techniques will hopefully lead to more investigations addressing this topic in the future.

4.5.2. Insights in interphase chromosome positioning

Knowledge about chromosome territories in interphase cells is of interest to understand the processes inside the cell nucleus. This includes the question whether chromosome positioning depends on gene density or gene expression [Parada and Misteli, 2002; Kuepper et al., 2007] and whether the chromosome positioning is different for different species [Mora et al., 2006; Neusser et al., 2007]. Laser scanning confocal microscopy and fluorescence microscopy contribute mainly to the progress made in this field (for a overview see Walter et al. [2006]). However, apart from the well-known localization of the acrocentric chromosomes around the nucleoli [Krystosek, 1998; Sullivan et al., 2001; Kalmarova et al., 2007] the positioning of other chromosomes remains unclear.

Another approach to address the positioning of chromosomes in the interphase nucleus is made by the "statistics for chromosome interphase positioning based on interchange data" (SCHIP). If chromosomes are organized within the cell nucleus in territories which form clusters and if misrejoining of double strand breaks occurs mainly between neighboring chromosome territories (i.e. "open ends" do not travel long distances before reconnection to other ends [Jakob et al., 2009]), the chromosomal clusters should be detectable on the basis of interchange data derived from the analysis of radiation-induced aberrations using mFISH or similar whole-genome staining methods.

The data collected during the work presented here were used to create an interchange table (based on about 5200 interchanges) and this was checked for possible clusters using the SCHIP software. As it is known from different publications, that the acrocentric chromosomes are located close to the

nucleoli in the interphase nucleus, this cluster should be detectable using the SCHIP. And indeed, a very low p-value < 0.0001 was found when testing this cluster in the data collected from the work presented here, indicating a highly significant deviation from the random model (see Table 3.9).

The cluster candidates reported in the literature, which are given on the SCHIP homepage, were tested for significant deviation from the random model in the data set obtained here. However, only four of them yielded p-values below 0.05, indicating their spatial proximity. For the others, different reasons for their occurrence may play a role. For example, the translocation between chromosomes 9 and 22, known as the Philadelphia Chromosome found in most chronic myeloid leukemia [Mitelman et al., 2007], shows a p-value of 0.07 in the present data set and 0.66 in the data set published by Arsuaga et al. [2004], indicating that not the spatial proximity of both chromosomes is the reason for their frequent occurrence in leukemia patients, but rather the specific genes affected by the translocation.

In addition to the reported clusters, own candidate clusters were chosen on the basis of the $\Delta(i,j)$ values. These 30 own candidate clusters were tested for significance in the own data set, and all yielded p-values ≤ 0.01 (see Table 3.9). The same candidate clusters were then tested in the largest lymphocytes data set provided at the SCHIP homepage, i.e. the data set published by Arsuaga et al. [2004] (based on about 3700 table entries). From the candidate clusters chosen on the basis of the data presented here, 80% yielded p-values ≤ 0.05 in the independent data set provided by Arsuaga et al. [2004]. This shows that it is possible to idetify chromosome clusters using the method applied by the SCHIP software. Testing the clusters on three other provided data sets (based on data obtained in the experiments described in Loucas and Cornforth [2001]; Cornforth et al. [2002]; Durante et al. [2002]), all of these tables having less entries (between 800 and 1900 table entries), lead to rather disappointing results. Only four of the candidate cluster chosen on the basis of the table reported here yielded p-values below 0.05 in all three other tables (data not shown). The cluster of acrocentric chromosomes was also not significantly different form a random distribution model in any of these tables. This demonstrates that a successful search for clusters can only be performed on very large data sets.

To overcome the subjective choice of candidate cluster and to show the (possible) correlation between the table achieved from the present work and the table published by Arsuaga et al. [2004], the $\Delta(i,j)$ values of the present data set were plotted versus the $\Delta(i,j)$ values of the data set published by Arsuaga et al. [2004]. The resulting Figure 4.2 shows a correlation, chromosomes that exchanged more frequent than expected from the random model in one data set exchanged more frequent in the other data set as well and vice versa. A linear function was fitted to the data (fit parameters $p0 = 0.00 \pm 0.10$ and $p1 = 0.74 \pm 0.08$). However, the large scattering proofs the need for tables

with far more entries.

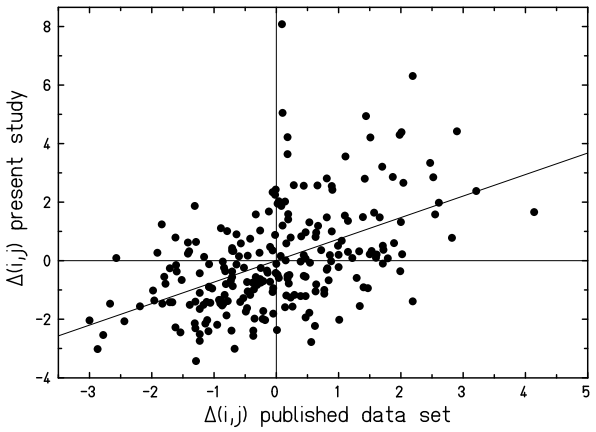

Figure 4.2.: $\Delta(i, j)$ values calculated by the SCHIP software for the table of pairwise exchanges reported here plotted versus those calculated by SCHIP for the data published by Arsuaga et al. [2004].

Altogether, it was demonstrated that clusters of chromosome territories in the interphase nucleus exist, that misrepair of radiation-induced damage between neighboring chromosomes is more frequent than between distant chromosomes and that it is possible to identify chromosome clusters using the SCHIP principle. When large data sets are analyzed, the clustering of the acrocentric chromosomes (which are known to be located in close proximity to each other around the nucleoli in the interphase nucleus) is confirmed. Analysis of tables with less entries fails to confirm this cluster, underlining the importance of large data sets. It was demonstrated that candidate clusters chosen on the basis of one data sets yield statistically significant differences from the random model in an independent data set, as long as sufficiently large data sets are analyzed. For large data sets, a correlation between the $\Delta(i, j)$ values was demonstrated. This shows that the chromosome interphase positioning is not donor-dependent.

An interesting topic for further research would be to compare data sets obtained for other cell types (e.g. human fibroblasts) or other species (e.g. peripheral blood cells from primates). There is also a need for larger data sets for human peripheral blood lymphocytes to confirm the clusters obtained so far and to search for additional ones. As the use of the mFISH method increases, and tables with interchange data can easily be generated in parallel to the normal aberration analysis there will hopefully be more (and larger) interchange data sets published in the future. Then, it may be possible in the future to derive a model of the interphase positioning of all chromosomes, either directly from the mFISH data sets or by combining information achieved from the interchange tables with results from fluorescence microscopy.

5. Summary and Outlook

Protons and C-ion beams are increasingly used in cancer therapy. C-ions are ideally suited for the therapy of deep-seated radioresistant tumors as they show, like all accelerated ions, an inverse depth dose profile compared to photons. In addition, C-ions have the biological advantage of a high relative biological effectiveness in the region of the maximal physical dose deposition.

The purpose of this study was to monitor the cytogenetic damage induced in peripheral blood lymphocytes of prostate-cancer patients treated with C-ion boost plus IMRT or IMRT alone and to perform in vitro experiments with the radiation qualities relevant for the tumor therapy to achieve dose-effect curves for the induction of chromosomal aberrations. The results of the patient study were compared with the in vitro results. For the analysis of the cytogenetic damage, the whole-genome mFISH method was used.

In the in vitro experiments it was found that the relative biological effectiveness of C-ions for the induction of chromosomal damage increases with increasing LET. For the first time, mFISH analysis was applied to measure a set of dose-effect curves of heavy ions (Figures 3.2 and 3.3). The generated data set now allowed determining the RBE for different aberration types. It was found that the RBE for complex aberrations is higher than for simple ones after 100 MeV/u and extended Bragg peak C-ion irradiation (Section 3.1.3). Regarding the spectrum of induced aberrations, an elevated ratio of complex to simple exchanges (C-ratio), which is discussed as a biomarker for densely ionizing radiation (see e.g. Johannes et al. [2004]), was found for high-LET radiation and for high doses (Figure 3.4). Likewise, the complexity of complex exchanges was found to increase with LET and dose (Figure 3.5). The analysis of the completeness of aberrations showed, that the fraction of incomplete exchanges increases with dose, in contrast to the findings by Loucas and Cornforth [2001]. In addition, the fraction of incomplete aberrations seems to increase with increasing LET (Table 3.3).

In the blood samples obtained from prostate-cancer patients undergoing radiotherapy, an increase in aberration yield with therapy course was found (Figure 3.12). This increase was most pronounced in patients treated with a large target volume and hence with a larger volume of irradiated normal tissue. Analysis of the aberration spectrum revealed that mainly simple chromosomal aberrations were induced by the radiotherapy (Figure 3.13). Comparison of blood samples obtained after the C-ion boost and after a comparable dose of IMRT revealed that C-ion boost irradiation induces significantly less aberrations than IMRT. This observation was previously made by Durante et al.

[2000] in esophageal cancer patients treated with C-ion therapy in Japan using 2-color FISH for the aberration analysis and is now confirmed with the mFISH technique. The lower aberration yield found after C-ion boost is caused by the lower integral dose to the normal tissue, compared to IMRT (see Figure 1.9). This underlines the superiority of C-ions for the treatment of deep-seated tumors. Regarding the late effects of radiotherapy, it can be assumed from the lower yield of induced cytogenetic damage that C-ion therapy causes less late effects compared to IMRT. Regarding the presence of a cytogenetic fingerprint of C-ions in vivo, it was found that no statistically significant increased C-ratio was detected in the patients receiving C-ion boost irradiation. In C-ion therapy, the high-LET region is restricted to the target volume. The target volume receives very high doses, which are lethal for the tumor cells. In the surrounding tissue, lower doses are applied and the cells are irradiated with C-ions that have a lower LET. Thus, the induced damages are similar to those caused by X-rays, as shown by the in vitro results of the present study (Section 3.1). As the volume of irradiated normal tissue is larger than the tumor volume (see Figure 1.9), most lymphocytes that float through the irradiation field receive low-LET irradiation rather than high-LET. In addition, cell killing by the high doses in the high-LET region may play a role for the lymphocytes. This explains the results of this study, where no biomarker for high-LET irradiation was found in the patients receiving C-ion boost therapy (Section 3.2.2). In contrast to radiotherapy patients, astronauts receive low doses during space flights, therefore cell killing plays only a minor role. Thus, the cytogenetic damage induced by high-LET exposure should be taken into account for the estimation of the astronauts' health risks [Durante and Cucinotta, 2008].

One year after the therapy, a statistically significant decrease in the aberration yield was found in only two patients. Analysis of the aberration spectrum showed that the fraction of transmissible aberrations increased during the year after therapy (see Table 3.8), indicating that bone marrow cells were exposed to radiation and aberrant bone marrow cells produce progenies carrying transmissible exchanges.

More information about the distribution of DNA damage in individual chromosomes is of basic interest, as well as the exchange frequencies between chromosome pairs after irradiation. The former provide a better understanding of the induced damage and its repair in individual chromosomes (e.g. whether gene-rich chromosomes are more sensitive or resistant to radiation than gene-poor chromosomes). The latter provide information about the chromosome positioning in the interphase cell nucleus, as neighboring chromosomes are assumed to exchange more frequent than distant ones. The mFISH analysis can give information about both, the distribution of breakpoints among individual chromosomes and the exchange frequencies between chromosome pairs. Therefore, albeit this was not the main topic of this study, these were analyzed

in the in vitro and in vivo data. The distribution of breaks among individual chromosomes was compared to the chromosome length and the chromosome surface model. However, there was no superiority of one model over the other observed (Figures 3.16 and 3.18). Therefore, in the future other models should be considered, and larger data sets should be investigated. The distribution of breaks was also compared to the gene density in the individual chromosomes, but no correlation was visible (see Figure 3.17). The frequencies of pairwise exchanges were analyzed using the "statistics for chromosome interphase positioning based on interchange data" software (SCHIP). The method was able to confirm the known cluster of acrocentric chromosomes, indicating that the method is functional and that the data set is sufficiently large to identify chromosome clusters. Own candidate clusters were searched and tested for statistically significant deviations from the random distribution model in the present data set and in a published data set [Arsuaga et al., 2004]. All 30 candidate clusters yielded p-values below 0.01 in the present data set and 80% of the candidate clusters yielded p-values below 0.05 in the published data set. In addition, a correlation between the two data sets was shown (Figure 4.2). These findings indicate that it is worth to spend more efforts in the generation and analysis of interchange tables in the future.

Regarding the in vitro experiments, the complete C-ion energy range relevant for tumor therapy was covered in the present work. Further work could include the application of other staining techniques like multicolor banding (mBand), which provides additional information about the ratio of intra- to interchromosomal rearrangements, another possible biomarker for densely ionizing radiation.

In the future, further research related to the monitoring of the cytogenetic damage induced by radiotherapy in peripheral blood lymphocytes would be useful. Samples from the patients at later times than one year after therapy should be analyzed. When a tumor therapy for prostate cancer applying solely C-ions is performed in the future (in the HIT facility in Heidelberg which started patient therapy recently[1], or in the Partikel-Therapie-Zentrum Marburg which is currently under construction[2]), it would be interesting to compare the aberration yield found in these patients with the patient groups analyzed in the present work. It would be definitely of importance to continue the research on prostate cancer patients solely treated with C-ion irradiation and to confirm the finding that C-ions therapy induces fewer aberrations in the peripheral blood lymphocytes than IMRT.

[1] http://www.klinikum.uni-heidelberg.de/Startseite-HIT.113005.0.html
[2] http://www.rhoen-klinikum-ag.com/rka/cms/ptm/deu/index.html

A. Tables

	Chromosome number										
	1	2	3	4	5	6	7	8	9	10	11
X-rays 1 Gy	17	15	9	13	5	7	10	4	8	13	3
X-rays 2 Gy	22	37	14	14	12	23	12	16	15	11	21
X-rays 3 Gy	20	29	14	29	22	16	21	16	28	27	14
X-rays 4 Gy	61	49	48	52	39	46	42	29	45	39	26
C 270 MeV/u 0.5 Gy	3	4	2	4	7	1	1	3	5	0	3
C 270 MeV/u 1 Gy	8	14	14	13	6	14	6	7	12	6	4
C 270 MeV/u 2 Gy	32	29	30	24	28	13	16	21	21	7	30
C 270 MeV/u 4 Gy	63	57	49	48	42	48	44	41	43	28	28
C 100 MeV/u 1 Gy	19	15	9	22	15	8	22	12	18	9	13
C 100 MeV/u 2 Gy	50	48	43	49	49	42	36	34	37	31	28
C 100 MeV/u 4 Gy	99	72	70	96	74	66	72	55	63	70	54
C ext. Bragg peak 1 Gy	33	32	24	17	32	18	21	17	18	20	18
C ext. Bragg peak 2 Gy	59	53	51	43	47	33	32	32	37	39	36
Sum	486	454	377	424	378	335	335	287	350	300	278
length [Mbp]	247.2	243	199.5	191.3	180.9	170.9	158.8	146.3	140.3	135.4	134.5
Genes	3612	1930	1474	1098	1222	2015	1423	1006	759	1444	1703
Genes/Mbp	14.61	7.94	7.38	5.74	6.76	11.79	8.96	6.88	5.41	10.66	12.66

Table A.1.: Distribution of breakpoints among individual chromosomes. Aberration analysis was performed in peripheral blood lymphocytes irradiated in vitro with X-rays and with C-ions with three different energies. The lower part of the table gives the chromosome length and the number of genes on each chromosome, as published on the homepage of the Ensembl project.

	Chromosome number											
	12	13	14	15	16	17	18	19	20	21	22	X
X-rays 1 Gy	4	4	4	2	7	7	2	2	5	1	2	11
X-rays 2 Gy	13	14	18	14	11	7	11	2	5	2	8	23
X-rays 3 Gy	12	10	8	16	12	14	20	15	16	5	10	38
X-rays 4 Gy	43	25	29	25	27	30	18	18	25	15	12	45
C 270 MeV/u 0.5 Gy	0	0	2	2	6	0	1	0	0	0	2	1
C 270 MeV/u 1 Gy	5	9	8	4	3	4	3	3	5	9	3	13
C 270 MeV/u 2 Gy	14	12	12	11	17	14	13	6	9	7	11	20
C 270 MeV/u 4 Gy	28	43	35	35	29	18	22	15	26	13	19	36
C 100 MeV/u 1 Gy	7	15	10	15	8	9	14	4	1	5	2	9
C 100 MeV/u 2 Gy	33	27	22	21	24	24	23	15	21	16	16	40
C 100 MeV/u 4 Gy	46	44	47	46	54	30	35	19	46	16	30	51
C ext. Bragg peak 1 Gy	11	11	22	11	14	7	16	3	11	13	6	15
C ext. Bragg peak 2 Gy	27	32	41	28	22	23	32	14	19	6	14	30
Sum	243	246	258	230	234	187	210	116	189	108	135	332
length [Mbp]	132.3	114.1	106.4	100.3	88.83	78.77	76.12	63.81	62.44	46.94	49.69	154.9
Genes	1379	759	1026	983	1089	1596	420	1702	902	419	830	1854
Genes/Mbp	10.42	6.65	9.64	9.8	12.26	20.26	5.52	26.67	14.45	8.93	16.70	11.97

Table A.1 continued.

	Chromosome number											
	1	2	3	4	5	6	7	8	9	10	11	12
C+IMRT	61	60	36	49	52	37	43	38	41	51	33	36
IMRT	30	30	30	17	21	17	15	17	29	33	17	12
IMRT*	96	95	57	74	76	57	63	64	51	51	68	60
Sum	187	185	123	140	149	111	121	119	121	135	118	108

	Chromosome number											
	13	14	15	16	17	18	19	20	21	22	X	Y
C+IMRT	24	36	32	25	37	23	18	24	18	19	18	6
IMRT	19	12	13	16	21	15	11	4	7	8	6	7
IMRT*	54	54	54	43	41	39	37	45	25	36	19	13
Sum	97	102	99	84	99	77	66	73	50	63	43	26

Table A.2.: Distribution of breakpoints among individual chromosomes. Aberration analysis was performed in peripheral blood lymphocytes obtained from prostate cancer patients undergoing radiotherapy.

Chr	1	2	3	4	5	6	7	8	9	10	11
22	35	11	13	4	11	11	6	5	25	11	14
21	15	9	4	9	11	9	6	15	16	7	5
20	26	23	14	17	13	9	20	19	32	11	26
19	20	10	7	10	14	10	25	2	10	8	14
18	15	30	15	25	18	13	11	36	31	14	8
17	35	38	35	20	24	17	23	7	17	26	19
16	40	20	24	28	30	17	23	16	45	15	28
15	34	22	22	24	16	13	12	9	25	22	10
14	31	22	20	46	22	22	21	32	31	22	12
13	28	30	25	43	19	31	17	37	27	28	9
12	32	35	27	29	29	30	46	14	11	19	22
11	37	26	24	32	31	27	41	24	24	31	**4.63**
10	51	30	41	48	30	30	32	18	24	**5.2**	1.41
9	63	47	32	42	41	22	31	30	**6.36**	-1.57	-1
8	38	36	24	34	37	29	23	**4.85**	-0.15	-1.44	0.33
7	27	37	32	34	49	20	**5.39**	-0.61	-0.56	0.75	3.21
6	48	33	48	27	34	**5.01**	-1.35	0.96	-1.74	0.78	0.79
5	57	45	28	44	**6.11**	0.62	2.8	1.36	0.35	-0.31	0.51
4	47	45	40	**6.59**	0.59	-1.05	-0.26	0.36	0.01	2.34	0.27
3	58	38	**5.76**	0.32	-1.21	3.56	0.17	-0.75	-0.76	2.02	-0.52
2	53	**6.51**	0.08	0.32	0.83	0.07	0.33	0.79	0.88	-0.66	-0.75
1	**8.17**	-0.02	1.59	-0.94	1.01	1.11	-2.57	-0.26	1.54	1.31	-0.13
Chr	1	2	3	4	5	6	7	8	9	10	11

Table A.3.: Chromosome interchange data obtained form the present study (in vitro experiment data and data from prostate caner patients undergoing radiotherapy are pooled). Upper left part of the table: interchange data $F(i, j)$, number of cells that showed an exchange between chromosomes i and j. Diagonal, in bold letters: single chromosome participation factors g(i). Lower right part: $\Delta(i, j)$ values, deviation from the random model.

12	13	14	15	16	17	18	19	20	21	22	Chr
4	11	14	39	20	12	11	5	24	7	**2.87**	22
3	24	18	15	8	5	8	3	10	**2.01**	0.51	21
13	10	8	22	36	18	10	6	**3.63**	1	4.21	20
27	0	7	7	14	8	3	**2.04**	-0.52	-0.55	-0.36	19
6	34	32	11	24	17	**3.68**	-1.65	-0.91	0.22	0.13	18
27	8	12	13	18	**3.95**	0.64	-0.03	0.97	-1.05	0.19	17
14	12	19	32	**4.83**	-0.25	1.48	1.32	4.42	-0.55	1.64	16
11	16	30	**4.02**	2.86	-0.72	-0.98	-0.42	1.95	2.43	8.08	15
14	28	**4.62**	2.66	-0.7	-1.47	3.64	-0.79	-2.14	2.85	0.2	14
8	**4.43**	1.66	-0.43	-2.03	-2.28	4.39	-3.01	-1.51	5.05	-0.49	13
4.18	-2.45	-1.21	-1.42	-1.38	2.57	-2.39	6.31	-0.56	-1.87	-2.31	12
0.6	-2.54	-2.03	-1.99	1.19	0.16	-2.19	1.48	2.25	-1.42	0.19	11
-0.59	1.03	-0.41	0.24	-2.02	1.2	-1.17	-0.8	-1.81	-1.07	-1.02	10
-3.02	-0.22	0.3	-0.1	2.58	-1.62	1.58	-0.83	1.87	0.9	1.58	9
-1.4	3.34	2.03	-2.37	-1.53	-2.78	4.3	-2.51	0.34	1.68	-2.39	8
4.94	-1.41	-0.78	-2.07	-0.59	0.37	-1.98	4.22	0.1	-1.47	-2.41	7
1.98	1.87	-0.24	-1.59	-1.46	-0.63	-1.26	-0.07	-2.15	-0.34	-0.89	6
0.68	-1.55	-1.17	-1.72	0.09	-0.03	-0.94	0.43	-1.94	-0.37	-1.56	5
0.27	2.55	2.81	-0.48	-0.68	-1.19	0.15	-0.95	-1.41	-1.17	-3.43	4
0.59	-0.11	-1.28	-0.24	-0.73	2.56	-1.34	-1.39	-1.51	-2.23	-0.87	3
1.49	0.22	-1.47	-0.81	-2.04	2.42	1.24	-0.9	-0.12	-1.13	-1.78	2
-0.37	-1.36	-1.1	0.21	0.09	0.47	-2.74	0.81	-0.67	-0.36	2.38	1
12	13	14	15	16	17	18	19	20	21	22	Chr

Table A.3, continued.

Chr	1	2	3	4	5	6	7	8	9	10	11
22	27	15	10	7	4	7	7	8	10	3	11
21	9	13	12	10	7	8	6	7	7	7	3
20	22	12	11	12	16	9	19	9	9	11	12
19	14	7	17	6	7	10	9	4	8	5	10
18	12	8	11	11	13	13	11	17	22	9	8
17	22	24	21	18	19	15	23	16	15	14	15
16	31	8	19	16	8	14	18	12	20	19	19
15	34	26	18	20	19	19	8	16	27	10	16
14	18	9	18	22	15	15	18	15	23	14	15
13	15	29	21	23	25	18	13	25	23	14	5
12	18	30	23	19	25	30	25	11	7	21	25
11	25	24	25	13	30	13	28	24	25	18	**4.31**
10	29	16	23	20	24	31	17	12	21	**3.99**	0.19
9	39	29	26	26	25	21	20	13	**4.97**	0.26	0.77
8	18	25	21	24	26	22	20	**4.08**	-1.61	-1.06	1.53
7	29	24	24	28	31	18	**4.72**	0.18	-0.71	-0.42	1.70
6	26	30	32	27	17	**4.70**	-0.89	0.64	-0.49	2.82	-1.62
5	29	32	31	23	**5.10**	-1.42	1.42	1.15	-0.06	0.81	1.71
4	42	37	21	**5.08**	-0.57	0.63	0.82	0.72	0.15	-0.06	-1.91
3	38	43	**5.60**	-1.40	0.47	1.11	-0.46	-0.38	-0.34	0.14	0.18
2	44	**5.85**	1.79	1.33	0.40	0.47	-0.69	0.23	-0.02	-1.52	-0.25
1	**6.59**	0.88	0.19	1.47	-0.79	-0.89	-0.37	-1.71	1.10	0.53	-0.64
Chr	1	2	3	4	5	6	7	8	9	10	11

Table A.4.: Chromosome interchange data published by Arsuaga et al. [2004]. Upper left part of the table: interchange data $F(i, j)$, number of cells that showed an exchange between chromosomes i and j. Diagonal, in bold letters: single chromosome participation factors g(i). Lower right part: $\Delta(i, j)$ values, deviation from the random model.

12	13	14	15	16	17	18	19	20	21	22	Chr
5	9	11	9	13	10	3	8	10	6	**2.23**	22
5	7	13	7	8	5	9	0	7	**1.80**	0.99	21
10	6	6	11	20	11	11	6	**2.79**	0.89	1.51	20
13	5	2	7	12	4	2	**1.80**	0.44	-1.80	1.99	19
8	16	10	9	15	5	**2.59**	-1.23	1.40	2.02	-1.16	18
16	7	6	13	12	**3.41**	-1.29	-0.86	0.47	-0.46	0.86	17
12	10	13	22	**3.78**	-0.25	1.66	2.00	2.90	0.47	1.57	16
9	10	22	**3.92**	1.87	-0.10	-0.36	-0.01	0.02	-0.01	0.09	15
16	29	**3.65**	2.04	-0.21	-1.83	0.18	-1.78	-1.31	2.52	1.00	14
9	**3.76**	4.14	-1.23	-1.11	-1.62	2.01	-0.67	-1.39	0.10	0.21	13
3.98	-1.54	0.39	-1.67	-0.78	0.66	-0.72	2.19	-0.33	-0.80	-1.30	12
1.89	-2.78	-0.18	-0.22	0.67	0.07	-0.95	0.81	-0.02	-1.71	0.44	11
1.29	-0.26	-0.14	-1.42	1.01	0.10	-0.42	-0.81	-0.05	-0.06	-1.98	10
-2.87	1.00	1.15	1.71	0.28	-0.47	2.55	-0.31	-1.31	-0.64	-0.33	9
-1.30	2.47	0.04	0.01	-0.87	0.56	1.98	-1.23	-0.71	-0.12	-0.37	8
1.44	-1.12	0.20	-2.44	0.04	1.72	-0.35	0.18	1.60	-0.85	-1.09	7
2.61	0.08	-0.52	0.14	-0.90	-0.26	0.23	0.54	-1.14	-0.15	-1.08	6
1.05	1.34	-0.83	-0.21	-2.57	0.39	-0.05	-0.71	0.47	-0.71	-2.19	5
-0.27	0.89	0.81	0.02	-0.73	0.16	-0.60	-1.03	-0.58	0.29	-1.29	4
0.16	0.00	-0.53	-0.84	-0.47	0.44	-0.92	2.19	-1.17	0.62	-0.70	3
1.39	1.50	-2.67	0.64	-3.00	0.90	-1.84	-1.08	-1.08	0.77	0.53	2
-1.60	-1.96	-1.23	1.61	1.22	-0.10	-1.23	0.63	0.84	-0.82	3.21	1
12	13	14	15	16	17	18	19	20	21	22	Chr

Table A.4, continued.

B. List of abbreviated terms

BrdU 5-bromo-2-deoxyuridine

CAB number of chromosomes, number of chromosome arms and number of chromosome breaks involved in a complex aberration

DAPI 4',6-Diamidino-2-phenylindol

DEAC 7-Diethylaminocoumarin-3-carboxylic acid

DNA deoxyribonucleic acid

DSB DNA double strand break

FCS foetal calf serum

FISH fluorescence in situ hybridization

FITC Fluorescein-5-isothiocyanate

FPG Fluorescence plus Giemsa

GS Gleason score

GSI GSI Helmholtzzentrum für Schwerionenforschung GmbH

GTV gross tumor volume

h hours

HIT Heidelberger Ionenstrahl-Therapie, ion beam facility in Heidelberg

HR homologous recombination

IMRT intensity modulated radiotherapy

LET linear energy transfer

M1 first mitosis

Mbp Mega-base-pairs, $1 \cdot 10^6$ base-pairs DNA

mFISH multiplex fluorescence in situ hybridization

min minute(s)

MV mean value

NHEJ non-homologous end-joining

PAINT protocol for aberration identification and nomenclature terminology

PBS phosphate buffered saline

PCC premature chromosome condensation

PSA prostate-specific antigen

PTV planning target volume

RBE relative biological effectiveness

SCHIP Statistics for chromosome interphase positioning based on interchange data

SD standard deviation

SIS heavy ion synchrotron at GSI (Schwerionensynchrotron)

SKY Spectral karyotyping

SpO Spectrum Orange™

SSA single strand annealing

SSC saline-sodium citrate buffer

TR Texas Red®

UV ultra-violett

C. Chemicals and laboratory equipment

C.1. Chemicals

Acetic acid (Merck, Darmstadt)
5-Bromo-2'-deoxyuridine, BrdU (Serva, Heidelberg)
Citric acid (Merck, Darmstadt)
Colcemid, 10 µg/ml (Roche, Mannheim)
Disodium hydrogen phosphate: $Na_2HPO_4 \cdot 12H_2O$ (Merck, Darmstadt)
Ethanol, absolute for analysis (Merck, Darmstadt; Applichem, Darmstadt)
Eukitt (O. Kindler, Freiburg)
Fetal calf serum (Biochrom, Berlin)
Giemsa (Merck, Darmstadt)
Hoechst No.33258 (Sigma, St.Louis, USA)
Hydrochloric acid (Merck, Darmstadt)
Isoton: Casyton (Schaerfe, Reutlingen)
Methanol, GR for analysis (Merck, Darmstadt)
mFISH kit: 24XCyte Human mFISH Probe Kit, (Metasystems, Altlussheim)
Natriumhydroxid NaOH (Sigma Chemie GmbH, Deisenhofen)
PBS without Ca2+ and Mg2+ (Biochrom, Berlin)
Penicillin/Streptomycin, 10000 E/10000 µg/ml (Biochrom, Berlin)
Phytohemagglutinin, PHA (Gibco, Paisley, UK)
Pepsin (Sigma, St. Louis, USA)
Potassium Chloride KCl (Merck, Darmstadt)
Potassium dihydrogen phosphate: KH_2PO_4 (Merck, Darmstadt)
RPMI 1640 medium (Biochrom, Berlin)
Saline-sodium citrate buffer (SSC) 20x (Applichem, Darmstadt)
Tween 20: Polyoxyethylene-sorbitan Monolaurate (Sigma, St.Louis, USA)

C.2. Disposable products

Cell culture flask: 25cm^2 (BD Biosciences Franklin Lakes, USA)
Centrifuge tube: 15 ml (TPP, Trasadingen, Switzerland)
Centrifuge tube: 50 ml (Greiner, Frickenhausen)
Centrifuge tube for cell culture: 10 ml (Nunc, Roskilde, Denmark)

Cover glass: 60 mm x 24 mm and 18 mm x 18 mm (IDL, Nidderau)
Microcentrifuge tubes (Eppendorf, Hamburg)
Pipettes: 2, 5, 10, 25 ml (BD Biosciences Franklin Lakes, USA)
Pasteur pipettes (Roth, Karlsruhe)
Microscope slides: 76 mm x 26 mm (Roth, Karlsruhe)
Tipps: 10, 200, 1000 µl (Brand, Wertheim)
Vacutainer CPT, Cell preparation tube (Becton Dickinson, Franklin Lakes, USA)

C.3. Laboratory equipment

Autoclave: Varioklav-Dampfsterilisator (H+P Labortechnik, Oberschleissheim)
Centrifuge: Megafuge 1.0 (Kendro-Heraeus instruments, Hanau)
Cell counter: Casy 1 model TT (Schaerfe system, Reutlingen)
Clean bench: Hera Safe HSP12 (Kendro-Heraeus instruments, Hanau)
Fluorescence microscope: BX61 (Olympus, Tokyo, Japan)
Hybridization oven: Unitherm oven 6/12 (Kisker, Steinfurt)
Incubator: BBD6220 (Kendro-Heraeus instruments, Hanau)
Pipettes: Eppendorf research (Eppendorf, Hamburg)
Pipette aid: Pipetboy Plus (Integra Bioscience, Fernwald)
Ultrapure water supply-system: Milli-Q Plus (Millipore, Eschborn)
UV lamp (Novodirect, Karlsruhe; Bioblock scientific, Illkirch, France)
Water bath: M12, M20 (Lauda, Lauda-Koenigshofen)
X-ray machine: IV320-12 (Seifert, Ludwigshafen)

Bibliography

Alberts, B., Bray, D., Hopkin, K., Johnson, A., Lewis, J., Raff, M., Ros, K., and Walter, P. (2005). *Lehrbuch der molekularen Zellbiologie*. Wiley-VCH.

Alcobia, I., Dilo, R., and Parreira, L. (2000). Spatial associations of centromeres in the nuclei of hematopoietic cells: evidence for cell-type-specific organizational patterns. *Blood*, 95(5):1608–1615.

Allan, J. M. and Travis, L. B. (2005). Mechanisms of therapy-related carcinogenesis. *Nature Reviews. Cancer*, 5(12):943–955.

Anderson, R. M., Marsden, S. J., Paice, S. J., Bristow, A. E., Kadhim, M. A., Griffin, C. S., and Goodhead, D. T. (2003). Transmissible and nontransmissible complex chromosome aberrations characterized by three-color and mFISH define a biomarker of exposure to high-LET alpha particles. *Radiation Research*, 159(1):40–48.

Anderson, R. M., Marsden, S. J., Wright, E. G., Kadhim, M. A., Goodhead, D. T., and Griffin, C. S. (2000). Complex chromosome aberrations in peripheral blood lymphocytes as a potential biomarker of exposure to high-LET alpha-particles. *International Journal of Radiation Biology*, 76(1):31–42.

Anderson, R. M., Papworth, D. G., Stevens, D. L., Sumption, N. D., and Goodhead, D. T. (2006). Increased complexity of radiation-induced chromosome aberrations consistent with a mechanism of sequential formation. *Cytogenetic and Genome Research*, 112(1-2):35–44.

Anderson, R. M., Tsepenko, V. V., Gasteva, G. N., Molokanov, A. A., Sevan'kaev, A. V., and Goodhead, D. T. (2005). mFISH analysis reveals complexity of chromosome aberrations in individuals occupationally exposed to internal plutonium: a pilot study to assess the relevance of complex aberrations as biomarkers of exposure to high-LET alpha particles. *Radiation Research*, 163(1):26–35.

Ando, K. and Kase, Y. (2009). Biological characteristics of carbon-ion therapy. *International Journal of Radiation Biology*, 85(9):715–728.

Andriole, G. L., Crawford, E. D., Grubb, R. L., Buys, S. S., Chia, D., Church, T. R., Fouad, M. N., Gelmann, E. P., Kvale, P. A., Reding, D. J., Weissfeld,

J. L., Yokochi, L. A., O'Brien, B., Clapp, J. D., Rathmell, J. M., Riley, T. L., Hayes, R. B., Kramer, B. S., Izmirlian, G., Miller, A. B., Pinsky, P. F., Prorok, P. C., Gohagan, J. K., and Berg, C. D. (2009). Mortality results from a randomized prostate-cancer screening trial. *The New England Journal of Medicine*, 360(13):1310–1319.

Arsuaga, J., Greulich-Bode, K. M., Vazquez, M., Bruckner, M., Hahnfeldt, P., Brenner, D. J., Sachs, R., and Hlatky, L. (2004). Chromosome spatial clustering inferred from radiogenic aberrations. *International Journal of Radiation Biology*, 80(7):507–515.

Bailey, N. T. J. (1995). *Statistical Methods in Biology*. Cambridge University Press, 3 edition.

Barendsen, G. W., Beusker, T. L., Vergroesen, A. J., and Budke, L. (1960). Effects of different radiations on human cells in tissue culture. II. biological experiments. *Radiation Research*, 13:841–849.

Barendsen, G. W., Walter, H. M., Fowler, J. F., and Bewley, D. K. (1963). Effects of different ionizing radiations on human cells in tissue culture. III. experiments with cyclotron-accelerated alpha-particles and deuterons. *Radiation Research*, 18:106–119.

Barkas, W. (1963). *Nuclear Research Emulsions*. Academic Press New York.

Bauchinger, M. and Schmid, E. (1998). LET dependence of yield ratios of radiation-induced intra- and interchromosomal aberrations in human lymphocytes. *International Journal of Radiation Biology*, 74(1):17–25.

Borgmann, K., Hoeller, U., Nowack, S., Bernhard, M., Rper, B., Brackrock, S., Petersen, C., Szymczak, S., Ziegler, A., Feyer, P., Alberti, W., and Dikomey, E. (2008). Individual radiosensitivity measured with lymphocytes may predict the risk of acute reaction after radiotherapy. *International Journal of Radiation Oncology, Biology, Physics*, 71(1):256–264.

Bostrom, P. J. and Soloway, M. S. (2007). Secondary cancer after radiotherapy for prostate cancer: should we be more aware of the risk? *European Urology*, 52(4):973–982.

Boyle, S., Gilchrist, S., Bridger, J. M., Mahy, N. L., Ellis, J. A., and Bickmore, W. A. (2001). The spatial organization of human chromosomes within the nuclei of normal and emerin-mutant cells. *Human Molecular Genetics*, 10(3):211–219.

Brenner, D. J., Curtis, R. E., Hall, E. J., and Ron, E. (2000). Second malignancies in prostate carcinoma patients after radiotherapy compared with surgery. *Cancer*, 88(2):398–406.

Brenner, D. J. and Hall, E. J. (2008). Secondary neutrons in clinical proton radiotherapy: a charged issue. *Radiotherapy and Oncology*, 86(2):165–170.

Brenner, D. J., Okladnikova, N., Hande, P., Burak, L., Geard, C. R., and Azizova, T. (2001). Biomarkers specific to densely-ionising (high LET) radiations. *Radiation Protection Dosimetry*, 97(1):69–73.

Brown, A. and Suit, H. (2004). The centenary of the discovery of the bragg peak. *Radiotherapy and Oncology*, 73(3):265–268.

Castro, J. R., Quivey, J. M., Lyman, J. T., Chen, G. T., Phillips, T. L., Tobias, C. A., and Alpen, E. L. (1980). Current status of clinical particle radiotherapy at lawrence berkeley laboratory. *Cancer*, 46(4):633–641.

Christmann, M., Tomicic, M. T., Roos, W. P., and Kaina, B. (2003). Mechanisms of human DNA repair: an update. *Toxicology*, 193(1-2):3–34.

Chun, F. K., Hutterer, G. C., Perrotte, P., Gallina, A., Valiquette, L., Benard, F., McCormack, M., Briganti, A., Ionescu, C., Jeldres, C., Guay, J., Saad, F., and Karakiewicz, P. I. (2007). Distribution of prostate specific antigen (PSA) and percentage free PSA in a contemporary screening cohort with no evidence of prostate cancer. *BJU International*, 100(1):37–41.

Cigarran, S., Barrios, L., Barquinero, J. F., Caballan, M. R., Ribas, M., and Egozcue, J. (1998). Relationship between the DNA content of human chromosomes and their involvement in radiation-induced structural aberrations, analysed by painting. *International Journal of Radiation Biology*, 74(4):449–455.

Combs, S. E., Nikoghosyan, A., Jaekel, O., Karger, C. P., Haberer, T., Mnter, M. W., Huber, P. E., Debus, J., and Schulz-Ertner, D. (2009). Carbon ion radiotherapy for pediatric patients and young adults treated for tumors of the skull base. *Cancer*, 115(6):1348–1355.

Cornforth, M. N. (2001). Analyzing radiation-induced complex chromosome rearrangements by combinatorial painting. *Radiation Research*, 155(5):643–659.

Cornforth, M. N., Greulich-Bode, K. M., Loucas, B. D., Arsuaga, J., Vzquez, M., Sachs, R. K., Brckner, M., Molls, M., Hahnfeldt, P., Hlatky, L., and Brenner, D. J. (2002). Chromosomes are predominantly located randomly with respect to each other in interphase human cells. *The Journal of Cell Biology*, 159(2):237–244.

Cremer, C., Mnkel, C., Granzow, M., Jauch, A., Dietzel, S., Eils, R., Guan, X. Y., Meltzer, P. S., Trent, J. M., Langowski, J., and Cremer, T. (1996). Nuclear architecture and the induction of chromosomal aberrations. *Mutation Research*, 366(2):97–116.

Cremer, M., Kpper, K., Wagler, B., Wizelman, L., von Hase, J., Weiland, Y., Kreja, L., Diebold, J., Speicher, M. R., and Cremer, T. (2003). Inheritance of gene density-related higher order chromatin arrangements in normal and tumor cell nuclei. *The Journal of Cell Biology*, 162(5):809–820.

Cremer, T. and Cremer, C. (2006a). Rise, fall and resurrection of chromosome territories: a historical perspective. part i. the rise of chromosome territories. *European Journal of Histochemistry: EJH*, 50(3):161–176.

Cremer, T. and Cremer, C. (2006b). Rise, fall and resurrection of chromosome territories: a historical perspective. part II. fall and resurrection of chromosome territories during the 1950s to 1980s. part III. chromosome territories and the functional nuclear architecture: experiments and models from the 1990s to the present. *European Journal of Histochemistry: EJH*, 50(4):223–272.

D'Alesio, V., Pacelli, R., Durante, M., Cama, G. C., Cella, L., Gialanella, G., Grossi, G., Pugliese, M., Punzo, G., Sardi, I., Scampoli, P., Solla, R., and Salvatore, M. (2003). Lymph nodes in the irradiated field influence the yield of radiation-induced chromosomal aberrations in lymphocytes from breast cancer patients. *International Journal of Radiation Oncology, Biology, Physics*, 57(3):732–738.

Deng, W., Morrison, D. P., Gale, K. L., and Lucas, J. N. (2000). A comparative study on potential cytogenetic fingerprints for radiation LET in human lymphocytes. *International Journal of Radiation Biology*, 76(12):1589–1598.

Dickerman, J. D. (2007). The late effects of childhood cancer therapy. *Pediatrics*, 119(3):554–568.

Durante, M., Ando, K., Furusawa, Y., Obe, G., George, K., and Cucinotta, F. A. (2004). Complex chromosomal rearrangements induced in vivo by heavy ions. *Cytogenetic and Genome Research*, 104(1-4):240–244.

Durante, M. and Cucinotta, F. A. (2008). Heavy ion carcinogenesis and human space exploration. *Nature Reviews. Cancer*, 8(6):465–472.

Durante, M., George, K., and Cucinotta, F. A. (2006). Chromosomes lacking telomeres are present in the progeny of human lymphocytes exposed to heavy ions. *Radiation Research*, 165(1):51–58.

Durante, M., George, K., Wu, H., and Cucinotta, F. A. (2002). Karyotypes of human lymphocytes exposed to high-energy iron ions. *Radiation Research*, 158(5):581–590.

Durante, M., Kraft, G., O'Neill, P., Reitz, G., Sabatier, L., and Schneider, U. (2007). Preparatory study of a ground-based space radiobiology program in europe. *Advances in Space Research*, 39(6):1082–1086.

Durante, M. and Loeffler, J. S. (2010). Charged particles in radiation oncology. *Nature Reviews. Clinical Oncology*, 7(1):37–43.

Durante, M., Yamada, S., Ando, K., Furusawa, Y., Kawata, T., Majima, H., Nakano, T., and Tsujii, H. (1999). Measurements of the equivalent whole-body dose during radiation therapy by cytogenetic methods. *Physics in Medicine and Biology*, 44(5):1289–1298.

Durante, M., Yamada, S., Ando, K., Furusawa, Y., Kawata, T., Majima, H., Nakano, T., and Tsujii, H. (2000). X-rays vs. carbon-ion tumor therapy: cytogenetic damage in lymphocytes. *International Journal of Radiation Oncology, Biology, Physics*, 47(3):793–798.

Edwards, A. A., Lindholm, C., Darroudi, F., Stephan, G., Romm, H., Barquinero, J., Barrios, L., Caballin, M. R., Roy, L., Whitehouse, C. A., Tawn, E. J., Moquet, J., Lloyd, D. C., and Voisin, P. (2005). Review of translocations detected by FISH for retrospective biological dosimetry applications. *Radiation Protection Dosimetry*, 113(4):396–402.

Efstathiou, J. A., Trofimov, A. V., and Zietman, A. L. (2009). Life, liberty, and the pursuit of protons: an evidence-based review of the role of particle therapy in the treatment of prostate cancer. *Cancer Journal (Sudbury, Mass.)*, 15(4):312–318.

Gatti, R. A. (2001). The inherited basis of human radiosensitivity. *Acta Oncologica (Stockholm, Sweden)*, 40(6):702–711.

George, K., Durante, M., Willingham, V., Wu, H., Yang, T. C., and Cucinotta, F. A. (2003a). Biological effectiveness of accelerated particles for the induction of chromosome damage measured in metaphase and interphase human lymphocytes. *Radiation Research*, 160(4):425–435.

George, K., Durante, M., Wu, H., Willingham, V., and Cucinotta, F. A. (2003b). In vivo and in vitro measurements of complex-type chromosomal exchanges induced by heavy ions. *Advances in Space Research: The Official Journal of the Committee on Space Research (COSPAR)*, 31(6):1525–1535.

George, K., Wu, H., Willingham, V., Furusawa, Y., Kawata, T., and Cucinotta, F. A. (2001). High- and low-LET induced chromosome damage in human lymphocytes: a time-course of aberrations in metaphase and interphase. *International Journal of Radiation Biology*, 77(2):175–183.

Gershkevitsh, E., Clark, C. H., Staffurth, J., Dearnaley, D. P., and Trott, K. (2005). Dose to bone marrow using IMRT techniques in prostate cancer patients. *Strahlentherapie und Onkologie*, 181(3):172–178.

Gershkevitsh, E., Hildebrandt, G., Wolf, U., Kamprad, F., Realo, E., and Trott, K. (2002). Chromosomal aberration in peripheral lymphocytes and doses to the active bone marrow in radiotherapy of prostate cancer. *Strahlentherapie und Onkologie*, 178(1):36–42.

Gershkevitsh, E., Rosenberg, I., Dearnaley, D. P., and Trott, K. R. (1999). Bone marrow doses and leukaemia risk in radiotherapy of prostate cancer. *Radiotherapy and Oncology*, 53(3):189–197.

Gudowska-Nowak, E., Kleczkowski, A., Nasonova, E., Scholz, M., and Ritter, S. (2005). Correlation between mitotic delay and aberration burden, and their role for the analysis of chromosomal damage. *International Journal of Radiation Biology*, 81(1):23–32.

Gudowska-Nowak, E., Lee, R., Nasonova, E., Ritter, S., and Scholz, M. (2007). Effect of let and track structure on the statistical distribution of chromosome aberrations. *Advances in Space Research*, 39(6):1070 – 1075.

Haberer, T., Becher, W., Schardt, D., and Kraft, G. (1993). Magnetic scanning system for heavy ion therapy. *Nuclear Instruments and Methods in Physics Research Section A: Accelerators, Spectrometers, Detectors and Associated Equipment*, 330(1-2):296–305.

Hall, E. J. (1988). *Radiobiology for the Radiologist*. J.B. Lippincott Company, third edition edition.

Hall, E. J. (2006). Intensity-modulated radiation therapy, protons, and the risk of second cancers. *International Journal of Radiation Oncology, Biology, Physics*, 65(1):1–7.

Hall, E. J. and Wuu, C. (2003). Radiation-induced second cancers: the impact of 3D-CRT and IMRT. *International Journal of Radiation Oncology, Biology, Physics*, 56(1):83–88.

Hande, M. P., Azizova, T. V., Burak, L. E., Khokhryakov, V. F., Geard, C. R., and Brenner, D. J. (2005). Complex chromosome aberrations persist in individuals many years after occupational exposure to densely ionizing radiation: an mFISH study. *Genes, Chromosomes & Cancer*, 44(1):1–9.

Harper, P. S. (2006). The discovery of the human chromosome number in lund, 1955-1956. *Human Genetics*, 119(1-2):226–232.

Hartel, C., Nikoghosyan, A., Durante, M., Sommer, S., Nasonova, E., Fournier, C., Lee, R., Debus, J., Schulz-Ertner, D., and Ritter, S. (2010). Chromosomal aberrations in peripheral blood lymphocytes of prostate cancer patients treated with IMRT and carbon ions. *Radiotherapy and Oncology*, in press, corrected proof.

Hernandez, J. and Thompson, I. M. (2004). Prostate-specific antigen: a review of the validation of the most commonly used cancer biomarker. *Cancer*, 101(5):894–904.

Hill, M. A. (2004). The variation in biological effectiveness of x-rays and gamma rays with energy. *Radiation Protection Dosimetry*, 112(4):471–481.

Huber, R., Braselmann, H., Kulka, U., Schumacher-Georgiadou, V., Bayerl, A., Molls, M., and Bauchinger, M. (1999). Follow-up analysis of translocation and dicentric frequencies, measured by FISH-chromosome painting in breast cancer patients after partial-body radiotherapy with little bone marrow exposure. *Mutation Research*, 446(1):103–109.

ICRU (1970). Linear energy transfer. ICRU Report 16, International Comission on Radiation Units and Measurements, Washington D.C., ICRU Publications P.O. Box 4869 Washington D.C. 20008 U.S.A.

International Atomic Energy Agency (2001). Cytogenetic analysis for radiation dose assessment - a manual. Technical Report Series 405, International Atomic Energy Agency, Vienna, Austria.

Ishikawa, H., Tsuji, H., Kamada, T., Hirasawa, N., Yanagi, T., Mizoe, J., Akakura, K., Suzuki, H., Shimazaki, J., and Tsujii, H. (2006). Risk factors of late rectal bleeding after carbon ion therapy for prostate cancer. *International Journal of Radiation Oncology, Biology, Physics*, 66(4):1084–1091.

Ito, K., Kubota, Y., Yamamoto, T., Suzuki, K., Fukabori, Y., Kurokawa, K., and Yamanaka, H. (2001). Long term follow-up of mass screening for prostate carcinoma in men with initial prostate specific antigen levels of 4.0 ng/ml or less. *Cancer*, 91(4):744–751.

Jakob, B., Splinter, J., Durante, M., and Taucher-Scholz, G. (2009). Live cell microscopy analysis of radiation-induced DNA double-strand break motion. *Proceedings of the National Academy of Sciences of the United States of America*, 106(9):3172–3177.

Johannes, C., Horstmann, M., Durante, M., Chudoba, I., and Obe, G. (2004). Chromosome intrachanges and interchanges detected by multicolor banding in lymphocytes: searching for clastogen signatures in the human genome. *Radiation Research*, 161(5):540–548.

Kalmarova, M., Smirnov, E., Masata, M., Koberna, K., Ligasova, A., Popov, A., and Raska, I. (2007). Positioning of NORs and NOR-bearing chromosomes in relation to nucleoli. *Journal of Structural Biology*, 160(1):49–56.

Kearney, L. (2006). Multiplex-FISH (M-FISH): technique, developments and applications. *Cytogenetic and Genome Research*, 114(3-4):189–198.

Kiefer, J. (1999). Radiation risk in manned space flights. *Mutation Research*, 430(2):307–313.

Kiefer, J. and Straaten, H. (1986). A model of ion track structure based on classical collision dynamics. *Physics in Medicine and Biology*, 31(11):1201–1209.

Kleinerman, R. A., Littlefield, L. G., Tarone, R. E., Machado, S. G., Blettner, M., Peters, L. J., and Boice, J. D. (1989). Chromosome aberrations in peripheral lymphocytes and radiation dose to active bone marrow in patients treated for cancer of the cervix. *Radiation Research*, 119(1):176–190.

Kleinerman, R. A., Littlefield, L. G., Tarone, R. E., Sayer, A. M., Cookfair, D. L., Wactawski-Wende, J., Inskip, P. D., Block, A., Ramesh, K. H., and Boice, J. D. (1994). Chromosome aberrations in lymphocytes from women irradiated for benign and malignant gynecological disease. *Radiation Research*, 139(1):40–46.

Kobayashi, J., Iwabuchi, K., Miyagawa, K., Sonoda, E., Suzuki, K., Takata, M., and Tauchi, H. (2008). Current topics in DNA double-strand break repair. *Journal of Radiation Research*, 49(2):93–103.

Kraemer, M., Jaekel, O., Haberer, T., Kraft, G., Schardt, D., and Weber, U. (2000). Treatment planning for heavy-ion radiotherapy: physical beam model and dose optimization. *Physics in Medicine and Biology*, 45(11):3299–3317.

Kraemer, M. and Scholz, M. (2000). Treatment planning for heavy-ion radiotherapy: calculation and optimization of biologically effective dose. *Physics in Medicine and Biology*, 45(11):3319–3330.

Kraemer, M., Weyrather, W. K., and Scholz, M. (2003). The increased biological effectiveness of heavy charged particles: from radiobiology to treatment planning. *Technology in Cancer Research & Treatment*, 2(5):427–436.

Kraft, G. (1999). RBE and its interpretation. *Strahlentherapie und Onkologie*, 175 Suppl 2:44–47.

Kraft, G. (2000a). Tumor therapy with heavy charged particles. *Progress in Particle and Nuclear Physics*, 45(Supplement 2):S473–S544.

Kraft, G. (2000b). Tumortherapy with ion beams. *Nuclear Instruments and Methods in Physics Research Section A: Accelerators, Spectrometers, Detectors and Associated Equipment*, 454(1):1–10.

Kraft, G., Kraemer, M., and Scholz, M. (1992). LET, track structure and models. a review. *Radiation and Environmental Biophysics*, 31(3):161–180.

Kraft, G. and Kraft, S. D. (2009). Research needed for improving heavy-ion therapy. *New Journal of Physics*, 11(2):025001.

Krystosek, A. (1998). Repositioning of human interphase chromosomes by nucleolar dynamics in the reverse transformation of HT1080 fibrosarcoma cells. *Experimental Cell Research*, 241(1):202–209.

Kuechler, A., Dreidax, M., Pigorsch, S. U., Liehr, T., Claussen, U., Wendt, T. G., and Dunst, J. (2003). Residual chromosomal damage after radiochemotherapy with and without amifostine detected by 24-color FISH. *Strahlentherapie und Onkologie*, 179(7):493–498.

Kuepper, K., Koelbl, A., Biener, D., Dittrich, S., von Hase, J., Thormeyer, T., Fiegler, H., Carter, N. P., Speicher, M. R., Cremer, T., and Cremer, M. (2007). Radial chromatin positioning is shaped by local gene density, not by gene expression. *Chromosoma*, 116(3):285–306.

Lazutka, J. R. (1996). Chromosome aberrations and rogue cells in lymphocytes of chernobyl clean-up workers. *Mutation Research*, 350(2):315–329.

Lee, R. (2006). *Chromosome aberrations in human lymphocytes irradiated with heavy ions*. PhD thesis, Technische Universitaet Darmstadt.

Lee, R., Nasonova, E., and Ritter, S. (2005). Chromosome aberration yields and apoptosis in human lymphocytes irradiated with fe-ions of differing LET. *Advances in Space Research: The Official Journal of the Committee on Space Research (COSPAR)*, 35(2):268–275.

Lee, R., Sommer, S., Hartel, C., Nasonova, E., Durante, M., and Ritter, S. (2010). Complex exchanges determine the effectiveness of carbon ions at the first post-irradiation mitosis. *Mutation Research*, in press.

Lee, R., Yamada, S., Yamamoto, N., Miyamoto, T., Ando, K., Durante, M., and Tsujii, H. (2004). Chromosomal aberrations in lymphocytes of lung cancer patients treated with carbon ions. *Journal of Radiation Research*, 45(2):195–199.

Loucas, B. D. and Cornforth, M. N. (2001). Complex chromosome exchanges induced by gamma rays in human lymphocytes: an mFISH study. *Radiation Research*, 155(5):660–671.

Lucas, J. N., Awa, A., Straume, T., Poggensee, M., Kodama, Y., Nakano, M., Ohtaki, K., Weier, H. U., Pinkel, D., and Gray, J. (1992). Rapid translocation frequency analysis in humans decades after exposure to ionizing radiation. *International Journal of Radiation Biology*, 62(1):53–63.

Lucas, J. N., Chen, A. M., and Sachs, R. K. (1996). Theoretical predictions on the equality of radiation-produced dicentrics and translocations detected by chromosome painting. *International Journal of Radiation Biology*, 69(2):145–153.

Lukasova, E., Kozubek, S., Kozubek, M., Kroha, V., Mareckova, A., Skalnikova, M., Bartova, E., and Slotova, J. (1999). Chromosomes participating in translocations typical of malignant hemoblastoses are also involved in exchange aberrations induced by fast neutrons. *Radiation Research*, 151(4):375–384.

Macallan, D. C., Asquith, B., Irvine, A. J., Wallace, D. L., Worth, A., Ghattas, H., Zhang, Y., Griffin, G. E., Tough, D. F., and Beverley, P. C. (2003). Measurement and modeling of human t cell kinetics. *European Journal of Immunology*, 33(8):2316–2326.

McCune, J. M., Hanley, M. B., Cesar, D., Halvorsen, R., Hoh, R., Schmidt, D., Wieder, E., Deeks, S., Siler, S., Neese, R., and Hellerstein, M. (2000). Factors influencing t-cell turnover in HIV-1-seropositive patients. *The Journal of Clinical Investigation*, 105(5):R1–8.

Mclean, A. R. and Michie, C. A. (1995). In vivo estimates of division and death rates of human t lymphocytes. *Proceedings of the National Academy of Sciences of the United States of America*, 92(9):3707–3711.

Mitelman, F., Johansson, B., and Mertens, F. (2007). The impact of translocations and gene fusions on cancer causation. *Nature Reviews. Cancer*, 7(4):233–245.

M'kacher, R., Girinsky, T., Koscielny, S., Dossou, J., Violot, D., Bron-Gaillard, N., Ribrag, V., Bourhis, J., Bernheim, A., Parmentier, C., and Carde, P. (2003). Baseline and treatment-induced chromosomal abnormalities in peripheral blood lymphocytes of hodgkin's lymphoma patients. *International Journal of Radiation Oncology, Biology, Physics*, 57(2):321–326.

Monobe, M. and Ando, K. (2002). Drinking beer reduces radiation-induced chromosome aberrations in human lymphocytes. *Journal of Radiation Research*, 43(3):237–245.

Mora, L., Snchez, I., Garcia, M., and Pons, M. (2006). Chromosome territory positioning of conserved homologous chromosomes in different primate species. *Chromosoma*, 115(5):367–375.

Mueller, A., Ganswindt, U., Bamberg, M., and Belka, C. (2007). Risk of second malignancies after prostate irradiation? *Strahlentherapie und Onkologie*, 183(11):605–609.

Mueller, I., Geinitz, H., Braselmann, H., Baumgartner, A., Fasan, A., Thamm, R., Molls, M., Meineke, V., and Zitzelsberger, H. (2005). Time-course of radiation-induced chromosomal aberrations in tumor patients after radiotherapy. *International Journal of Radiation Oncology, Biology, Physics*, 63(4):1214–1220.

Munro, T. R. (1970). The relative radiosensitivity of the nucleus and cytoplasm of chinese hamster fibroblasts. *Radiation Research*, 42(3):451–470.

Mustonen, R., Lindholm, C., Tawn, E. J., Sabatier, L., and Salomaa, S. (1998). The incidence of cytogenetically abnormal rogue cells in peripheral blood. *International Journal of Radiation Biology*, 74(6):781–785.

Nagele, R. G., Freeman, T., McMorrow, L., Thomson, Z., Kitson-Wind, K., and y Lee, H. (1999). Chromosomes exhibit preferential positioning in nuclei of quiescent human cells. *Journal of Cell Science*, 112 (Pt 4):525–535.

Nasonova, E. and Ritter, S. (2004). Cytogenetic effects of densely ionising radiation in human lymphocytes: impact of cell cycle delays. *Cytogenetic and Genome Research*, 104(1-4):216–220.

Neel, J. V. (1998). An association, in adult japanese, between the occurrence of rogue cells among cultured lymphocytes (JC virus activity) and the frequency of "simple" chromosomal damage among the lymphocytes of persons exhibiting these rogue cells. *American Journal of Human Genetics*, 63(2):489–497.

Neusser, M., Schubel, V., Koch, A., Cremer, T., and Mller, S. (2007). Evolutionarily conserved, cell type and species-specific higher order chromatin arrangements in interphase nuclei of primates. *Chromosoma*, 116(3):307–320.

Neves, H., Ramos, C., da Silva, M. G., Parreira, A., and Parreira, L. (1999). The nuclear topography of ABL, BCR, PML, and RARalpha genes: evidence for gene proximity in specific phases of the cell cycle and stages of hematopoietic differentiation. *Blood*, 93(4):1197–1207.

Neyman, J. (1939). On a new class of "contagious" distributions, applicable in entomology and bacteriology. *The Annals of Mathematical Statistics.*, 10:35–57.

Nikoghosyan, A., Schulz-Ertner, D., Didinger, B., Jkel, O., Zuna, I., Hss, A., Wannenmacher, M., and Debus, J. (2004). Evaluation of therapeutic potential of heavy ion therapy for patients with locally advanced prostate cancer. *International Journal of Radiation Oncology, Biology, Physics*, 58(1):89–97.

Obe, G. and Vijayalaxmi (2007). *Chromosomal Alterations: Methods, Results and Importance in Human Health*. Springer, Berlin, 1 edition.

Parada, L. and Misteli, T. (2002). Chromosome positioning in the interphase nucleus. *Trends in Cell Biology*, 12(9):425–432.

Perry, P. and Wolff, S. (1974). New giemsa method for the differential staining of sister chromatids. *Nature*, 251(5471):156–158.

Pfeiffer, P., Goedecke, W., Kuhfittig-Kulle, S., and Obe, G. (2004). Pathways of DNA double-strand break repair and their impact on the prevention and formation of chromosomal aberrations. *Cytogenetic and Genome Research*, 104(1-4):7–13.

Pfeiffer, P., Goedecke, W., and Obe, G. (2000). Mechanisms of DNA double-strand break repair and their potential to induce chromosomal aberrations. *Mutagenesis*, 15(4):289–302.

Pignalosa, D., Bertucci, A., Gialanella, G., Grossi, G., Manti, L., Pugliese, M., Scampolia, P., and Durante, M. (2008). Chromosome inter- and intrachanges detected by arm-specific DNA probes in the progeny of human lymphocytes exposed to energetic heavy ions. *Radiation Research*, 170(4):458–466.

Pombo, A., Cuello, P., Schul, W., Yoon, J. B., Roeder, R. G., Cook, P. R., and Murphy, S. (1998). Regional and temporal specialization in the nucleus: a transcriptionally-active nuclear domain rich in PTF, oct1 and PIKA antigens associates with specific chromosomes early in the cell cycle. *The EMBO Journal*, 17(6):1768–1778.

Pouzoulet, F., Roch-Lefvre, S., Giraudet, A. L., Vaurijoux, A., Voisin, P., Buard, V., Delbos, M., Bourhis, J., Voisin, P., and Roy, L. (2007). Monitoring translocations by M-FISH and three-color FISH painting techniques: a study of two radiotherapy patients. *Journal of Radiation Research*, 48(5):425–434.

Pschyrembel, W. (2007). *Pschyrembel Klinisches Woerterbuch*. de Gruyter, 261. edition.

Ramsey, M. J., Moore, D. H., Briner, J. F., Lee, D. A., a Olsen, L., Senft, J. R., and Tucker, J. D. (1995). The effects of age and lifestyle factors on the accumulation of cytogenetic damage as measured by chromosome painting. *Mutation Research*, 338(1-6):95–106.

Rithidech, K. N., Honikel, L., and Whorton, E. B. (2007). mFISH analysis of chromosomal damage in bone marrow cells collected from CBA/CaJ mice following whole body exposure to heavy ions (56Fe ions). *Radiation and Environmental Biophysics*, 46(2):137–145.

Ritter, S., Nasonova, E., Furusawa, Y., and Ando, K. (2002a). Relationship between aberration yield and mitotic delay in human lymphocytes exposed to 200 MeV/u fe-ions or x-rays. *Journal of Radiation Research*, 43 Suppl:S175–179.

Ritter, S., Nasonova, E., and Gudowska-Novak, E. (2002b). Effect of LET on the yield and quality of chromosomal damage in metaphase cells: a time-course study. *International Journal of Radiation Biology*, 78(3):191–202.

Ritter, S., Nasonova, E., Gudowska-Nowak, E., Scholz, M., and Kraft, G. (2000). High-LET-induced chromosome aberrations in v79 cells analysed in first and second post-irradiation metaphases. *International Journal of Radiation Biology*, 76(2):149–161.

Ritter, S., Nasonova, E., Scholz, M., Kraft-Weyrather, W., and Kraft, G. (1996). Comparison of chromosomal damage induced by x-rays and ar ions with an LET of 1840 keV/micrometer in g1 v79 cells. *International Journal of Radiation Biology*, 69(2):155–166.

Sancar, A., Lindsey-Boltz, L. A., Unsal-Kamaz, K., and Linn, S. (2004). Molecular mechanisms of mammalian DNA repair and the DNA damage checkpoints. *Annual Review of Biochemistry*, 73:39–85.

Sasaki, M. S. (2009). Advances in the biophysical and molecular bases of radiation cytogenetics. *International Journal of Radiation Biology*, 85(1):26–47.

Savage, J. R. and Simpson, P. J. (1994). FISH "painting" patterns resulting from complex exchanges. *Mutation Research*, 312(1):51–60.

Schardt, D. (2007). Tumor therapy with high-energy carbon ion beams. *Nuclear Physics A*, 787(1-4):633 – 641.

Schardt, D., Schall, I., Geissel, H., Irnich, H., Kraft, G., Magel, A., Mohar, M. F., Munzenberg, G., Nickel, F., Scheidenberger, C., Schwab, W., and Sihver, L. (1996). Nuclear fragmentation of high-energy heavy-ion beams in water. *Advances in Space Research: The Official Journal of the Committee on Space Research (COSPAR)*, 17(2):87–94.

Schimmerling, W., Cucinotta, F. A., and Wilson, J. W. (2003). Radiation risk and human space exploration. *Advances in Space Research: The Official Journal of the Committee on Space Research (COSPAR)*, 31(1):27–34.

Scholz, M., Kraft-Weyrather, W., Ritter, S., and Kraft, G. (1994). Cell cycle delays induced by heavy ion irradiation of synchronous mammalian cells. *International Journal of Radiation Biology*, 66(1):59–75.

Scholz, M., Ritter, S., and Kraft, G. (1998). Analysis of chromosome damage based on the time course of aberrations. *International Journal of Radiation Biology*, 74(3):325–331.

Schroeder, F. H., Hugosson, J., Roobol, M. J., Tammela, T. L. J., Ciatto, S., Nelen, V., Kwiatkowski, M., Lujan, M., Lilja, H., Zappa, M., Denis, L. J., Recker, F., Berenguer, A., Mttnen, L., Bangma, C. H., Aus, G., Villers, A., Rebillard, X., van der Kwast, T., Blijenberg, B. G., Moss, S. M., de Koning, H. J., and Auvinen, A. (2009). Screening and prostate-cancer mortality in a randomized european study. *The New England Journal of Medicine*, 360(13):1320–1328.

Schulz-Ertner, D. (2009). The clinical experience with particle therapy in adults. *Cancer Journal (Sudbury, Mass.)*, 15(4):306–311.

Schulz-Ertner, D., Karger, C. P., Feuerhake, A., Nikoghosyan, A., Combs, S. E., Jaekel, O., Edler, L., Scholz, M., and Debus, J. (2007a). Effectiveness of carbon ion radiotherapy in the treatment of skull-base chordomas. *International Journal of Radiation Oncology, Biology, Physics*, 68(2):449–457.

Schulz-Ertner, D., Nikoghosyan, A., Hof, H., Didinger, B., Combs, S. E., Jaekel, O., Karger, C. P., Edler, L., and Debus, J. (2007b). Carbon ion radiotherapy of skull base chondrosarcomas. *International Journal of Radiation Oncology, Biology, Physics*, 67(1):171–177.

Schulz-Ertner, D., Nikoghosyan, A., Jaekel, O., Haberer, T., Kraft, G., Scholz, M., Wannenmacher, M., and Debus, J. (2003). Feasibility and toxicity of combined photon and carbon ion radiotherapy for locally advanced adenoid cystic carcinomas. *International Journal of Radiation Oncology, Biology, Physics*, 56(2):391–398.

Schulz-Ertner, D., Nikoghosyan, A., Thilmann, C., Haberer, T., Jaekel, O., Karger, C., Kraft, G., Wannenmacher, M., and Debus, J. (2004). Results of carbon ion radiotherapy in 152 patients. *International Journal of Radiation Oncology, Biology, Physics*, 58(2):631–640.

Shipley, W. U., Tepper, J. E., Prout, G. R., Verhey, L. J., Mendiondo, O. A., Goitein, M., Koehler, A. M., and Suit, H. D. (1979). Proton radiation as boost therapy for localized prostatic carcinoma. *JAMA: The Journal of the American Medical Association*, 241(18):1912–1915.

Skarsgard, L. D. (1998). Radiobiology with heavy charged particles: a historical review. *Physica Medica*, 14 Suppl 1:1–19.

Skarsgard, L. D., Kihlman, B. A., Parker, L., Pujara, C. M., and Richardson, S. (1967). Survival, chromosome abnormalities, and recovery in heavy-ion and x-irradiated mammalian cells. *Radiation Research. Supplement*, 7:208–221.

Sorokine-Durm, I., Whitehouse, C., and Edwards, A. (2000). The variability of translocation yields amongst control populations. *Radiat Prot Dosimetry*, 88(1):93–99.

Speicher, M. R., Ballard, S. G., and Ward, D. C. (1996). Karyotyping human chromosomes by combinatorial multi-fluor FISH. *Nature Genetics*, 12(4):368–375.

Stenman, U., Finne, P., Zhang, W., and Leinonen, J. (2000). Prostate-specific antigen and other prostate cancer markers. *Urology*, 56(6):893–898.

Suit, H., Goldberg, S., Niemierko, A., Ancukiewicz, M., Hall, E., Goitein, M., Wong, W., and Paganetti, H. (2007). Secondary carcinogenesis in patients treated with radiation: a review of data on radiation-induced cancers in human, non-human primate, canine and rodent subjects. *Radiation Research*, 167(1):12–42.

Sullivan, G. J., Bridger, J. M., Cuthbert, A. P., Newbold, R. F., Bickmore, W. A., and McStay, B. (2001). Human acrocentric chromosomes with transcriptionally silent nucleolar organizer regions associate with nucleoli. *The EMBO Journal*, 20(11):2867–2874.

Tawn, E. J. and Whitehouse, C. A. (2001). Frequencies of chromosome aberrations in a control population determined by g banding. *Mutation Research*, 490(2):171–177.

Tawn, E. J. and Whitehouse, C. A. (2003). Persistence of translocation frequencies in blood lymphocytes following radiotherapy: implications for retrospective radiation biodosimetry. *Journal of Radiological Protection: Official Journal of the Society for Radiological Protection*, 23(4):423–430.

Tawn, E. J., Whitehouse, C. A., and Riddell, A. E. (2006). FISH chromosome analysis of plutonium workers from the sellafield nuclear facility. *Radiation Research*, 165(5):592–597.

Tenhumberg, S., Gudowska-Nowak, E., Nasonova, E., and Ritter, S. (2007). Cell cycle arrest and aberration yield in normal human fibroblasts. II: effects of 11 MeV u-1 c ions and 9.9 MeV u-1 ni ions. *International Journal of Radiation Biology*, 83(8):501–513.

Testard, I., Dutrillaux, B., and Sabatier, L. (1997). Chromosomal aberrations induced in human lymphocytes by high-LET irradiation. *International Journal of Radiation Biology*, 72(4):423–433.

Tough, D. F. and Sprent, J. (1995). Life span of naive and memory t cells. *Stem Cells (Dayton, Ohio)*, 13(3):242–249.

Tsujii, H., Kamada, T., Baba, M., Tsuji, H., Kato, H., Kato, S., Yamada, S., Yasuda, S., Yanagi, T., Kato, H., Hara, R., Yamamoto, N., and Mizoe, J. (2008). Clinical advantages of carbon-ion radiotherapy. *New Journal of Physics*, 10(7):075009.

Tsujii, H., Mizoe, J., Kamada, T., Baba, M., Tsuji, H., Kato, H., Kato, S., Yamada, S., Yasuda, S., Ohno, T., Yanagi, T., Imai, R., Kagei, K., Kato, H., Hara, R., Hasegawa, A., Nakajima, M., Sugane, N., Tamaki, N., Takagi, R., Kandatsu, S., Yoshikawa, K., Kishimoto, R., and Miyamoto, T. (2007). Clinical results of carbon ion radiotherapy at NIRS. *Journal of Radiation Research*, 48 Suppl A:A1–A13.

Tucker, J. D., Morgan, W. F., Awa, A. A., Bauchinger, M., Blakey, D., Cornforth, M. N., Littlefield, L. G., Natarajan, A. T., and Shasserre, C. (1995). A proposed system for scoring structural aberrations detected by chromosome painting. *Cytogenetics and Cell Genetics*, 68(3-4):211–221.

Virsik, R. P. and Harder, D. (1981). Statistical interpretation of the overdispersed distribution of radiation-induced dicentric chromosome aberrations at high LET. *Radiation Research*, 85(1):13–23.

Vives, S., Loucas, B., Vazquez, M., Brenner, D. J., Sachs, R. K., Hlatky, L., Cornforth, M., and Arsuaga, J. (2005). SCHIP: statistics for chromosome interphase positioning based on interchange data. *Bioinformatics (Oxford, England)*, 21(14):3181–3182.

Vorobtsova, I., Semenov, A., Timofeyeva, N., Kanayeva, A., and Zvereva, I. (2001). An investigation of the age-dependency of chromosome abnormalities in human populations exposed to low-dose ionising radiation. *Mechanisms of Ageing and Development*, 122(13):1373–1382.

Wahab, M. A., Nickless, E. M., Najar-M'kacher, R., Parmentier, C., Podd, J. V., and Rowland, R. E. (2008). Elevated chromosome translocation frequencies in new zealand nuclear test veterans. *Cytogenetic and Genome Research*, 121(2):79–87.

Wakatsuki, M., Tsuji, H., Ishikawa, H., Yanagi, T., Kamada, T., Nakano, T., Suzuki, H., Akakura, K., Shimazaki, J., and Tsujii, H. (2008). Quality of life in men treated with carbon ion therapy for prostate cancer. *International Journal of Radiation Oncology, Biology, Physics*, 72(4):1010–1015.

Wallace, D. L., Zhang, Y., Ghattas, H., Worth, A., Irvine, A., Bennett, A. R., Griffin, G. E., Beverley, P. C. L., Tough, D. F., and Macallan, D. C. (2004). Direct measurement of t cell subset kinetics in vivo in elderly men and women. *Journal of Immunology (Baltimore, Md.: 1950)*, 173(3):1787–1794.

Walter, J., Joffe, B., Bolzer, A., Albiez, H., Benedetti, P. A., Mller, S., Speicher, M. R., Cremer, T., Cremer, M., and Solovei, I. (2006). Towards many colors in FISH on 3D-preserved interphase nuclei. *Cytogenetic and Genome Research*, 114(3-4):367–378.

Watson, J. D. and Crick, F. H. (1953). Molecular structure of nucleic acids; a structure for deoxyribose nucleic acid. *Nature*, 171(4356):737–738.

Weber, U. and Kraft, G. (2009). Comparison of carbon ions versus protons. *Cancer Journal (Sudbury, Mass.)*, 15(4):325–332.

Whitehouse, C. A., Edwards, A. A., Tawn, E. J., Stephan, G., Oestreicher, U., Moquet, J. E., Lloyd, D. C., Roy, L., Voisin, P., Lindholm, C., Barquinero, J., Barrios, L., Caballin, M. R., Darroudi, F., and Fomina, J. (2005). Translocation yields in peripheral blood lymphocytes from control populations. *International Journal of Radiation Biology*, 81(2):139–145.

Wu, H., Durante, M., Furusawa, Y., George, K., Kawata, T., and Cucinotta, F. A. (2003). Truly incomplete and complex exchanges in prematurely condensed chromosomes of human fibroblasts exposed in vitro to energetic heavy ions. *Radiation Research*, 160(4):418–424.

Wyman, C. and Kanaar, R. (2006). DNA double-strand break repair: all's well that ends well. *Annual Review of Genetics*, 40:363–383.

Yamada, S., Durante, M., Ando, K., Furusawa, Y., Kawata, T., Majima, H., and Tsujii, H. (2000). Complex-type chromosomal exchanges in blood lymphocytes during radiation therapy correlate with acute toxicity. *Cancer Letters*, 150(2):215–221.

Acknowledgments

This is the place where I want to say "thank you" to everybody who supported me during my PhD work.

First, I want to express my gratitude to Prof. Dr. Marco Durante, the supervisor of my work. His enthusiasm for biophysics is unique. I am also deeply thankful to Prof. Dr. Gerhard Kraft. He encouraged me to continue my research at GSI after I finished my diploma and he always took interest in my work. I am specially grateful to Dr. Sylvia Ritter, my tutor and a constant help. She was always willing to discuss results, give advice, have a look at the most special chromosomal aberrations and spend the night in the lab during the irradiation experiments. I thank Petra Hessel for her skillful help in the laboratory, taking blood samples, preparing and staining chromosome slides and analyzing cells—and for the good atmosphere in our office. I thank Dr. Elena Nasonova (JINR, Russia), the chromosome expert who was able to "rescue" bad chromosome spreading and who spend weeks and weeks at the microscope analyzing FPG stained slides. I also thank Dr. Sylwester Sommer who introduced me to the mFISH hybridization technique and the aberration analysis of mFISH stained metaphases. Special thanks to Dr. Ryonfa Lee, who was always willing to have a look at the complex aberrations I found and to discuss them with me. I also thank Dr. Claudia Fournier for fruitful discussions and good suggestions. I am grateful to Prof. Dr. Ewa Gudowska-Nowak (Jagellonian University, Poland) for her advice and for interesting discussions regarding the analysis of break distributions and the SCHIP data. I also thank Annabelle Becker and Dido Szypowsky for their help. I thank everybody from the "Chromo-group" for the good discussions during our meetings. Special thanks to the participants of the "Blut-Rufbereitschaft" who spend the weekends in the lab when a blood sample had arrived. I also particularly appreciate the blood donor volunteers from GSI. For the technical support during the beam times, I thank the "irradiation team" from the biophysics group and the accelerator operating team. I am specially grateful to my fellow PhD students Dr. Cläre von Neubeck and Daniela Becker for good interdisciplinary discussions as well as for nice lunch hours, help and encouragement. I thank all current and former biophysics group members for the nice time in good atmosphere and, of course, for having great "cake-meetings" in the corridor. I really liked working in this interdisciplinary group, I always found someone who helped me to adjust the microscope, solved computer problems, told me how to work with the chemicals, answered mathematical or physical questions or who explained biological processes to me.

I thank the team from the Heidelberg University Hospital, especially Mrs. Renate Haselmann, Dr. Anna Nikoghosyan, Prof. Dr. Daniela Schulz-Ertner and Prof. Dr. Dr. Jürgen Debus for the good collaboration, for providing the blood samples and data concerning the characterization of the patients.

This work would not have been possible without the funding of the federal ministry of education and research, Bonn, Germany (contract numbers 02S8203 and 02S8497).

I am very thankful to my family who always supported me during my PhD work. Special thanks to my husband Philipp Hartel for his patience, his encouragement and for being the "Fels in der Brandung".

Curriculum vitae

Personal data

Name:	Carola Sabine Hartel geb. Gübitz
Date of Birth:	30.04.1980
Place of birth:	Frankfurt am Main
Marital status:	Married
Nationality:	German

Education and qualifications

1986 – 1999	Freie Waldorfschule Frankfurt am Main
6/1999	Abitur
1999 – 2006	Studies of Physics at Technische Universität Darmstadt
2/2005 – 4/2006	Diploma student in the Biophysics Group at the GSI Helmholtzzentrum für Schwerionenforschung (GSI) Title of thesis: Strahlenbiologische und physikalische Messungen für die Bestrahlungsplanung mit leichten Ionen
7/2006	Diploma in Physics
since 12/2006	PhD student in the Biophysics Group at the GSI Helmholtzzentrum für Schwerionenforschung (GSI)

Eidesstattliche Erklärung

Hiermit erkläre ich an Eides statt, daß ich die vorliegende Dissertation ohne Hilfe Dritter und nur unter Verwendung der angegebenen Quellen und Hilfsmittel angefertigt habe. Desweiteren erkläre ich, zu keinem früheren Zeitpunkt bereits einen Promotionsversuch unternommen zu haben.

Darmstadt, den 9.2.2010

Carola Hartel